University of Thessaly
School of Engineering
Department of Mechanical Engineering

Diploma Thesis

SHAPE MEMORY ALLOYS

Microstructure and Mechanical Properties

by

Chatzimpaloglou Kyrillos

Submitted in Partial Fulfillment of the Requirements for the
Diploma in Mechanical Engineering

2016

Εγκρίθηκε από τα Μέλη της Τριμελούς Εξεταστικής Επιτροπής

Πρώτος Εξεταστής	Δρ. Α. Ζερβάκη
(Επιβλέπων)	Τμήμα Μηχανολόγων Μηχανικών
	Πανεπιστήμιο Θεσσαλίας
Δεύτερος Εξεταστής	Δρ. Γρ. Χαϊδεμενόπουλος
	Καθηγητής,
	Τμήμα Μηχανολόγων Μηχανικών,
	Πανεπιστήμιο Θεσσαλίας.
Τρίτος Εξεταστής	Δρ. Α. Κερμανίδης
	Επίκουρος Καθηγητής,
	Τμήμα Μηχανολόγων Μηχανικών,
	Πανεπιστήμιο Θεσσαλίας.

Certified by the member of the Thesis Committee

First member (Supervisor)

Dr. A. Zervaki
Department of Mechanical Engineering
University of Thessaly

Second member

Dr. G. Haidemenopoulos
Professor
Department of Mechanical Engineering
University of Thessaly

Third member

Dr. A. Kermanidis
Assistant Professor
Department of Mechanical Engineering
University of Thessaly

Acknowledgments

First of all I would like to thank the supervisor of my diploma thesis Dr. Anna Zervaki for the help and guidance that she provided me during my work. Moreover i am thankful to the other members of the selection board of the dissertation, Dr. Haidemenopoulos and Dr. Kermanidis for their participation and the careful read of this diploma thesis. Last but not least I would like to thank my family and my friends for their support and patience during the whole five years course of the Diploma in Mechanical of Engineering.

Chatzimpaloglou Kyrillos

Abstract

Shape Memory Alloys (SMAs) have been on the forefront of research for the last decades because of their unique properties of Shape Memory effect (SME) and Super Elasticity (SE). They have been used for a wide variety of applications in various fields ranging from medical devices (stents, guide wires, filtration devices) to engineering applications (actuators, fasteners, couplings) in various industrial sectors.

The present diploma thesis constitutes an initial approach to the shape memory alloys, through the experimental study of the microstructure, the determination of the basic mechanical properties (microhardness and modulus of elasticity), as well as the determination of the characteristic transformation temperatures. A NiTiCu SMA actuator was used in the study either in spring shape or in its deployed condition as wire.

The constituents of the microstructure were identified by Optical Microscopy and SEM/EDX analysis. The Vickers and Knoop microhardness were measured, while the Modulus of Elasticity was determined via the Marshall method. DSC measurements were also carried out and allowed the determination of As, Af, Ms and Mf temperatures.

The results are in good agreement with the reported values in the literature, and provide a basis for further studies with this specific material.

Περίληψη

Τα κράματα μνήμης σχήματος (SMA) είναι γνωστά για την ιδιότητα τους να θυμούνται το αρχικό τους σχήμα και να επανακάμπτουν σε αυτό μετά από μεγάλες φορτίσεις χωρίς μόνιμη παραμόρφωση. Εχουν βρει πολύ μεγάλη εφαρμογή σε πολλούς τομείς της βιομηχανίας (αυτοκινητοβιομηχανία, αεροπορική βιομηχανία, καταναλωτικά προϊόντα, ηλεκτρονικά) καθώς και στη Ιατρική (stents, ορθοδοντικά σύρματα)

Η παρούσα διπλωματική εργασία αποτελεί μια αρχική πειραματική προσέγγιση στα κράματα μνήμηςσχήματος (SMA) τα οποία ανήκουν στην ευρύτερη οικογένεια των έξυπνων υλικών, που έχουν την ιδιότητα να αναγνωρίζουν εξωτερικά μη μηχανικά φορτία και να αντιδρούν σε αυτά μέσω της κύρια ιδιότητας τους, του φαινομένου της μνήμης σχήματος (shape memory effect).

Ειδικότερα, κύριο αντικείμενο αποτελεί η μελέτη της μικροδομής, των θερμοκρασιών μετασχηματισμού και των βασικών μηχανικών ιδιοτήτων (σκληρότητα, μέτρο ελαστικότητας) του κράματος μνήμηςNi44Ti7Cu. Η μελέτη πραγματοποιήθηκε σε δύο δείγματα που προέρχονται απο ενεργοποιητή (actuator), το πρώτο σε σχήμα ΄΄ελατηρίου΄΄ που αντιστοιχεί στην ωστενιτική φάση ενώ το δεύτερο σε σχήμα ΄΄σύρματος΄΄ αντιστοιχεί στην μαρτενσιτική. Αρχικά τα δείγματα προσβλήθηκαν χημικά, έγινε παρατήρηση σε οπτικό μικροσκόπιο και στη συνέχεια πραγματοποιήθηκε ανάλυση με SEM/EDX. Πραγματοποιήθηκαν μικροσκληρομετρήσεις με εντυπωτή Vickers και KNOOP ενώ η μέθοδος Knoορχρησιμοποιήθηκε για τον υπολογισμό του μέτρου ελαστικότητας, με βάση τη μέθοδο Marshall. Προσδιορίστηκαν επίσης οι χαρακτηριστικές θερμοκρασίες μετασχηματισμού ωστενίτη/μαρτενσίτη (As, Af, Ms και Mf) με τη μέθοδο DSC.

Τα αποτελέσματα ευρίσκονται σε ικανοποιητική συμφωνία με τα δημοσιευμένα στην ανοιχτή διεθνή βιβλιογραφία, και μπορούν να αποτελέσουν βάση για την αναλυτικότερη μελέτη του συγκεκριμένου υλικού σε επόμενη φάση.

Contents

List of Figures

List of Tables

Chapter 1 Introduction

1.1 Overview of Smart Materials

Classical materials like metals and alloys have played a significant role as structural materials for many centuries. Engineers have designed components and selected alloys by employing the classical engineering approach of understanding the macroscopic properties of the material and selecting the appropriate one to match the desired functionality based on the application [1]. With advancements in science and technology, and a deeper understanding of the effects of microstructure and processing techniques on the material behavior, the field of material science has radically improved through the past decades [2].

The everlasting goal for engineers in many cases is to improve product efficiency and reduce its weight without comprising on either its cost or performance. To achieve this goal, replacing multi-component and multi-material systems with fewer multifunctional light weights, high performing materials has been an attractive alternative. The capability to engineer different material properties (mechanical, thermal, electrical, etc.) for a variety of applications has enabled the development of new alloys and composites. The demand for lighter, stronger materials with tailored properties that address both stringent structural requirements and provide additional engineering functionality (e.g., sensing, actuation, electromagnetic shielding) has spawned a new branch of materials called active or multifunctional materials.

Active materials are a subgroup of such multifunctional materials that show a capability of recognizing non-mechanical external stimuli from its surrounding environment and reversibly respond to the same. Such materials can judge the magnitude of this external stimuli (signal) and react with an optimal response by either changing its physical or mechanical properties (generally macroscopic shape change) [1].

1.2 Shape Memory Alloys - A Brief History

The discovery of martensite in steels in the 1890s by Adolf Martens was a major step toward the eventual discovery of shape memory alloys. The martensitic transformation, as observed in the Fe-C system, was established as an irreversible process [2].

The reversible martensitic transformation and the alloys that exhibited them remained unutilized until 1963. The breakthrough for engineering applications occurred with the discovery of NiTi by Buehler and coworkers while investigating materials useful for heat shielding [3]. It was noticed that in addition to its good mechanical properties, comparable to some common engineering metals, the material also possessed a shape recovery capability. A Shape Memory Alloy (SMA) is able to memorize and recover its original shape, after it has been deformed by heating over its transformation temperature. This unique effect of returning to an original geometry after a large inelastic deformation (near 10%) is known as the Shape Memory Effect (SME) [5]. Following this observation, the term "NiTinol" was coined for this NiTi material in honor of its discovery at the Naval Ordnance Laboratory (NOL) [4].

Moving on the research about NiTi, studies revealed that the addition of a third element, like Co or Fe, in the binary NiTi system caused a decrease in the SMA transformation temperatures. Also in 1978 studies showed that the ternary NiTiCu system had a narrowed stress hysteresis and an improved fatigue life compared to the binary one while the low cost, associated with this material system, made it suitable for a wide variety of engineering applications.

1.2.1 NiTi – Based Alloys

Shape memory alloys can be classified based on a wide variety of categories: primary alloying elements, mode of actuation (magnetic, thermal), operating temperature, or desired behavior.

Of the known SMA compositions, the NiTi alloy system has been studied most extensively and is used in the greatest number of commercial applications. This alloy exhibits strong SME, TWSME, and pseudoelastic behavior under the right conditions, which makes this material ideal for a variety of applications. It also exhibits resistance to corrosion and is biocompatible, making it suitable for use in biomedical applications.

- *NiTi:* Decreasing the Ni atomic percentage (at.%) from the equiatomic composition does not change the transformation temperatures. If the composition of nickel is increased above 50 at.%, the transformation temperature begins to decrease, with A_f becoming as low as −40 ^{o}C for 51 at.% nickel. NiTi alloys exhibit fully recoverable transformation strains of up to 8% and can be commercially obtained in various forms (e.g., wires, strips, rods, tubes and plates).
  Recent studies have also investigated 55 at.% NiTi composition. This composition exhibits transformation temperatures in the range of −10 ^{o}C to 60 ^{o}C. The 55 at.% NiTi alloy has been proven to show superior corrosion resistance as compared to stainless steels in harsh environments such as a salt water bath or salt fog.

- *NiTiCu:* The addition of Cu to NiTi preferentially replaces Ni to form NiTiCu alloys. The unique property of these alloys is that addition of Cu reduces the hysteresis of the SMA response. However, this also results in a decrease in the transformation strain. The addition of Cu also reduces the pseudoelastic hysteresis, it also greatly reduces the sensitivity of the martensitic start temperature to composition The small hysteresis associated with the transformation makes TiNiCu an ideal choice for actuators. Among the different compositions of TiNiCu, 5.0at.% ≤ Cu ≤ 10.0at.% is most preferred.

- *NiTiNb:* The requirement from the material to show minimal response to wide temperature changes can be achieved by widening the hysteresis of binary

NiTi. The alloying element that facilitates this characteristic is Niobium. It is noted that one consequence of adding Nb to NiTi is the widening of the thermal hysteresis. The wide hysteresis has important practical use in the field of SMAs, facilitating the engineering of material properties for which room temperature lies within the regions of the hysteresis. This allows the material to be deformed at low temperatures and yet be safely transported at ambient temperatures.

- *NiTiX (X= Pd , Pt, Hf, Zr) :* Applications involving high operating temperatures, such as in the core region of an aircraft engine or down hole applications in the oil industry require SMAs with high transformation temperatures and stable material properties. This demand for SMAs with high transformation temperatures has led to the development of a new class of SMAs known as High Temperature Shape Memory Alloys (HTSMAs). HTSMAs are a unique class of SMAs that have transformation temperatures greater than 100 ^{o}C and are capable of actuating under high temperature conditions. The transformation temperatures can be shifted anywhere in the range of 100–800 ^{o}C.

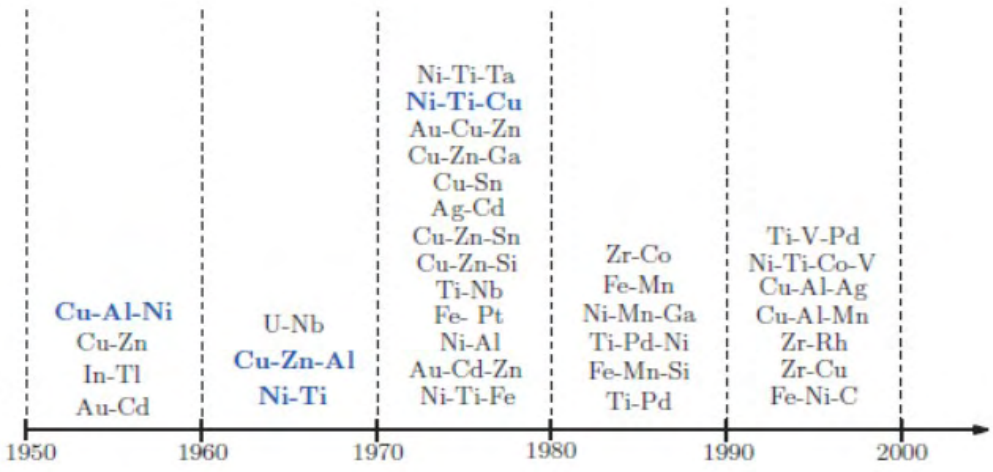

Fig.1.1: Various shape memory alloys discovered over the second half of 20th century. The most important commercially used alloys are highlighted in blue [1].

1.3 Actuators – Background

Microelectromechanical and intelligent materials systems have received much attention because of their great scientific significance and promising potential applications in automation, micromanipulation, and medical technology. However, most applications require a source of mechanical power, micro scale motors and actuators that provide the effect of "muscles" to make things happen [6].

An actuator is a type of motor, a mechanism, that is responsible for moving or controlling a system upon an environment. Several different physical mechanisms such as electrostatic and magnetostatic forces, phase changes (shape memory alloys and electrorheological fluids), piezoelectric/electrostrictive strains, magnetostriction, and thermal stresses have been explored as potential actuation sources. Each kind of actuator has its own advantages and drawbacks, so their selection and optimization should be determined by the requirements of the application [6].

1.3.1 Basic Type of SMA- Based Actuators

Traditionally, there have been two methods to deploy a structure: Controlled Deployment and Unconstrained Deployment (or Free Deployment). The first method is to deploy the structure by means of actuators or cables which are linked to electrical motors. The second method uses the elastic strain energy stored in the folded structure to drive deployment. The most important difference between the two methods is that controlled deployment is often reversible while unconstrained deployment is usually irreversible, because it requires an external agent to initiate the folding procedure and to put strain energy back into the system.

Instead of traditional actuator, cable or folded structure, SMA can be used in these deployment schemes with very smooth motion due to its inherent damping properties. SMA based deployable structure can be folded easily by large deformation of SMA. During deployment, SMA is heated to above its transformation temperature to recover its original shape. This is exactly the idea of unconstrained deployable.

Furthermore, reversible deployment can also be achieved by using two sets of SMA elements in the form of one against another, i.e. the structure is deployed by heating one set of SMA element and retracted by heating another set.

Both one-way SMA and two-way SMA may be used for deployable structures. Although two-way SMA can perform in two directions due to its two-way shape memory mechanism, transformation strain associated with it is normally only half of that in one-way SMA [5].

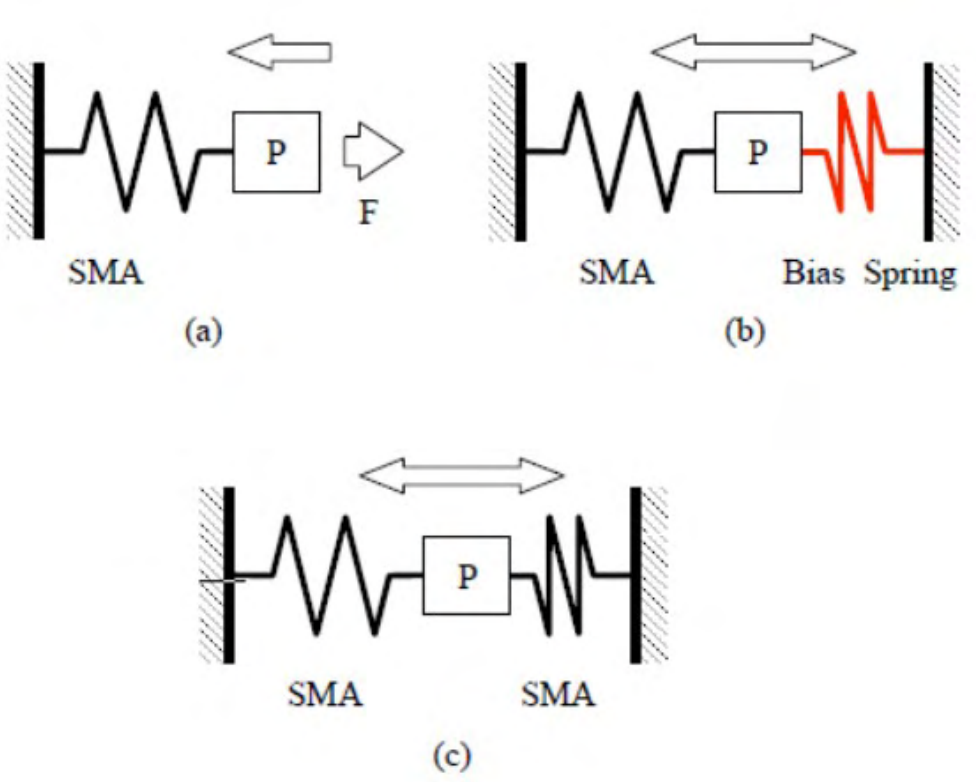

Fig.1.2: Basic types of SMA actuators. (a) One Way Actuator; (b) Biased Actuator; (c) Two Way Actuator.[5]

- **One Way Actuator:** The SMA element is elongated initially, at low temperature, and then is heated above its transformation temperature to regain its initial form and move element P in the direction of the arrow.

- **Biased Actuator:** The SMA element is deformed at low temperature, before being connected to the spring. When is heated, the recovery force which is generated pulls the spring, thus storing energy in it. When the SMA element is cooled, the energy stored in the spring is released and the SMA element deforms back.

- **Two Way Actuator:** Includes two SMA elements. Two SMA elements are used. Any motion can be obtained by cooling or heating the two SMA elements.

1.4 Shape Memory Alloys Applications

Active materials are quickly gaining the attention of engineers and scientists worldwide as more emphasis is placed on both reliability and multifunctionality. For the past several decades, engineers and other designers in many fields have been developing ways to convert thermal energy into mechanical work through the use of SMAs and apply these solutions to real-world applications [2]. The ability of SMA to reversibly respond to external temperature changes and change their physical/mechanical properties has enabled them to find many applications. In a thermomechanical system, SMAs can be used as combined sensors and actuators where they can sense the changes in external stimuli and monitor certain desired functions [1].

Although medical applications for shape memory alloys now dominate in today's market, there are many applications in the industrial sector which have reached large volume production that far surpass the material usage in the medical fields. In the early growth of shape memory alloy technology the most important

applications were for fasteners and couplings, mainly in the military sector. With the maturing of the technology, and the broader availability of alloys, industrial applications appear in a wide spectrum of commerce [7]. A review of mane SMA devices in use across many engineering applications is detailed in the following sections.

1.4.1 Medical Applications

The shape memory and pseudoelastic characteristics coupled with the biocompatibility of NiTi make them an attractive candidate for medical applications. The combination of these unique characteristics has led to the development of various applications such as stents, filters, orthodontic wires as well as devices for minimally invasive surgery (MIS).

An important requirement for an SMA, or any other material to be used in the human body, is that it be biocompatible. Biocompatibility is a property of the material to remain nontoxic through its functional period inside the human body. A biocompatible material can not produce any allergic reaction or inflammatory response in the host. The other requirement for the material is its biofunctionality, which is the ability to function desirably for its expected service life in the human body environment. These two requirements are crucial for the application of SMAs in the medical industry [2].

In most of these biomedical applications, transformation temperatures of the SMA are programmed such that the A_f is below the body temperature. The superelastic SMA components are cooled to their martensitic state (i.e., below Mf) and deformed to a temporary shape for easy insertion. Upon deployment at the right location in the body, the SMA device is heated above A_f (i.e., austenitic state) where the NiTi component recovers back to its original shape and performs the necessary function as desired. Some specific examples are discussed below to illustrate this point [1].

- *Cardiovascular Applications*: Self expanding stents named in the honor of dentist C.T. Stent find applications in cardiovascular applications with the goal of preventing collapse of blood vessels. NiTinol Stents are shape set in their deployed configuration (generally expanded diameter in its austenitic state) and then compressed into a catheter at lower temperatures below M_f. Stents employed in arteries may be subjected to continuously varying external pressures and collapsing or crushing of deployed stents could result in serious medical complications. SMA stents with their superior flexibility and spring back properties prevent the stents from collapsing when compared to its counterparts.

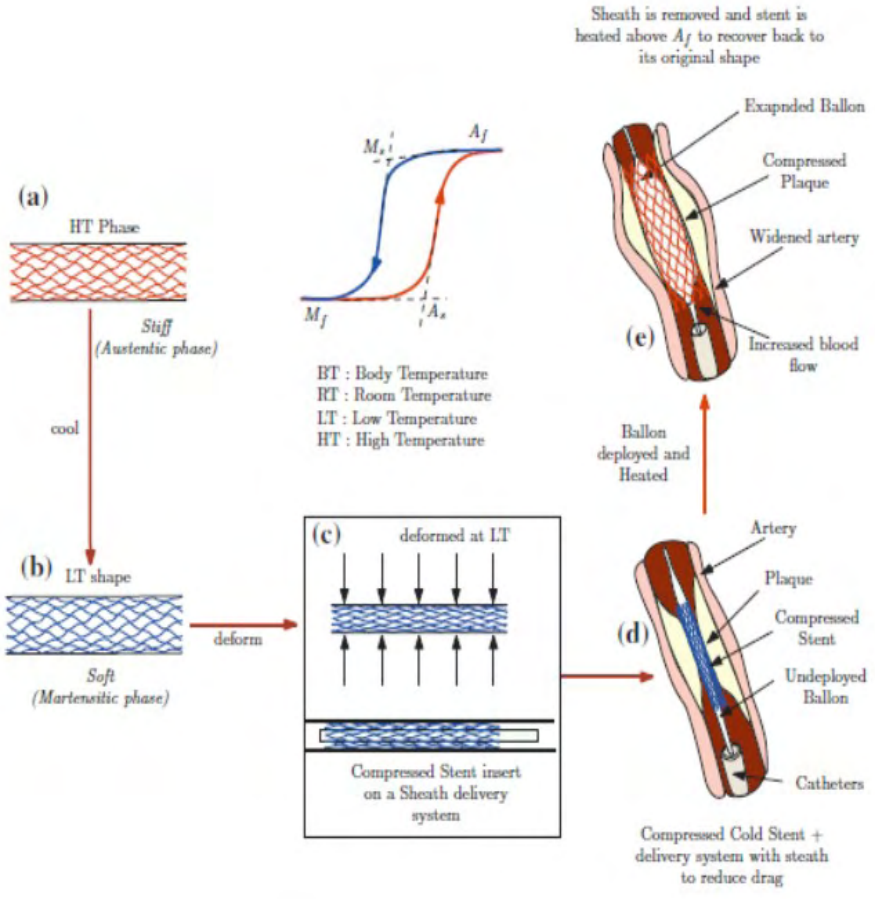

Fig.1.3: Self expanding NiTinol stents find applications in cardiovascular applications with the goal of preventing collapse of blood vessels.[1]

- *Orthodontic Applications*: Nitinol orthodontic archwires have been used since the 1970s, and are more effective than other alternative materials. In a linear elastic material like stainless steel, there is a large increment in stress, for a small increment in strain which results in a large amount of force on the tooth for a small amount of corrective motion. The advantage of pseudoelastic arch wires is the ability to operate in the pseudoelastic plateau, during which the material has a near-zero stress change over a large strain increment. As a result, they provide a nearly constant, moderate force to actively move the teeth over a longer period of time compared with stainless steel. Further, the material composition and processing can be engineered to produce different levels of optimal force.

Fig.1.4: Shape Memory Alloy based Archwire.

1.4.2 Aerospace Applications

Noise produced by airplanes has a great impact on the human community. The early jets were noisy - extremely so. Apart from heavy construction plant, unsuppressed motor-cycles and emergency service sirens, they were the loudest source of noise in the community. Moreover, the noise of the jet drew attention to the rapidly increasing numbers of aircraft. Engine noise has become a serious concern for many airports and surrounding communities. Without noise-reducing technologies, the Federal Government, airline companies, and nearby schools must spend millions of dollars on soundproofing installments to avoid the negative impacts of jet noise on schools and neighborhood communities around airports [8].

To reduce this noise, some designers are installing chevrons onto engines to mix the flow of exhaust gases and reduce engine noise. Research is being performed into methods by which SMA beam components can be embedded inside chevrons. The SMA beams bend the chevrons into the flow during low-altitude flight or low speed flight, thereby increasing mixing and reducing noise. During high-altitude, high speed flight, these SMA beam components will cool into martensite, thereby straightening the chevrons and increasing engine performance [2].

Fig.1.5: Flight test hardware for Variable Geometry SMA Chevrons[2]

1.4.3 Civil Engineering Applications

Smart systems for civil structures are described as systems that can automatically adjust structural characteristics in response to external disturbances and/or unexpected severe loading toward structural safety, extension of the structure's life time, and serviceability [9].

- *Damping Elements* :In many civil engineering applications, large SMA wires, ropes, springs and beams are being used as damping elements in bridges, buildings and also in seismic resisting systems due to their excellent energy dissipation and recentering capability.

- *Smart - Self Healing Structures :* If a SMA reinforcement in its martensitic form is deformed (also referred to as pre-tensioning) and embedded in concrete and then electrically activated such that it reaches temperatures above A_f, sufficient constraining forces can be generated as the SMA tries to recover back to its original shape. The extent of prestressing can be increased or decreased by controlling the amount of initial deformation of SMA [1].

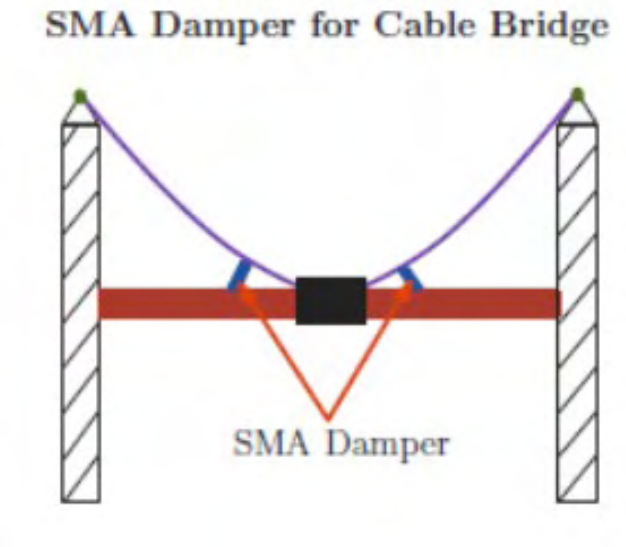

Fig.1.6: SMA Damper for Cable Bridge.[1]

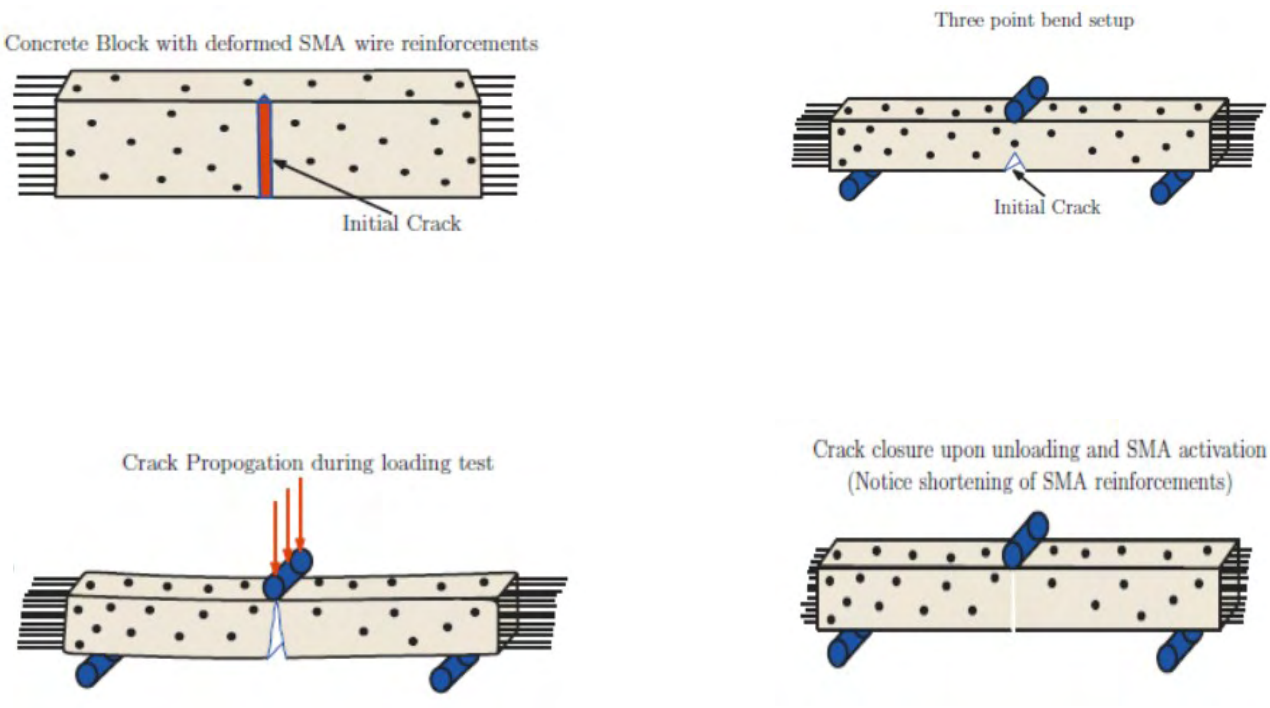

Fig.1.7: Smart Concrete Structure that can potentially ‘’Self Heal’’ [1]

1.4.4 Actuator Applications

Various SMA actuators such as wire, compression and tension springs and cantilever had been used in both electrical and thermal actuation systems

Thermal actuators of SMA are used as both sensors and actuators. An example now in production is a NiTiCu spring for controlling the opening of the door in a self-cleaning oven. For a period the Daimler Benz company used a similar spring to control the flow of transmission fluid in an automatic transmission during the period of initial warm up. SMA thermal actuators are also used in domestic safety devices. One of the most frequent causes of injury in the household and in hospitality buildings such as hotels is excessively hot water in the sink, tub and shower. An antiscald valve is now being produced which employs a small cantilever NiTiCu element which, when heated to 48°C, the temperature above which scalding will occur, closes the valve. The valve automatically reopens when the water temperature is safe [7].

Fig.1.8: NiTiCu cantilever actuators used in antiscald safety valves.[7]

Fig.1.9: Antiscald shower valve.[7]

The oil and gas industry uses many hydraulic and electro-hydraulic systems along with additional signal conditioning components which makes the overall system quite bulky. Many SMA components along with bias systems have been considered to replace these traditional hydraulic and electro-hydraulic systems. A combination of SMA and steel bias springs is usually employed to actuate pistons in "blowout preventer's" that either block or unblock drill pipes [1].

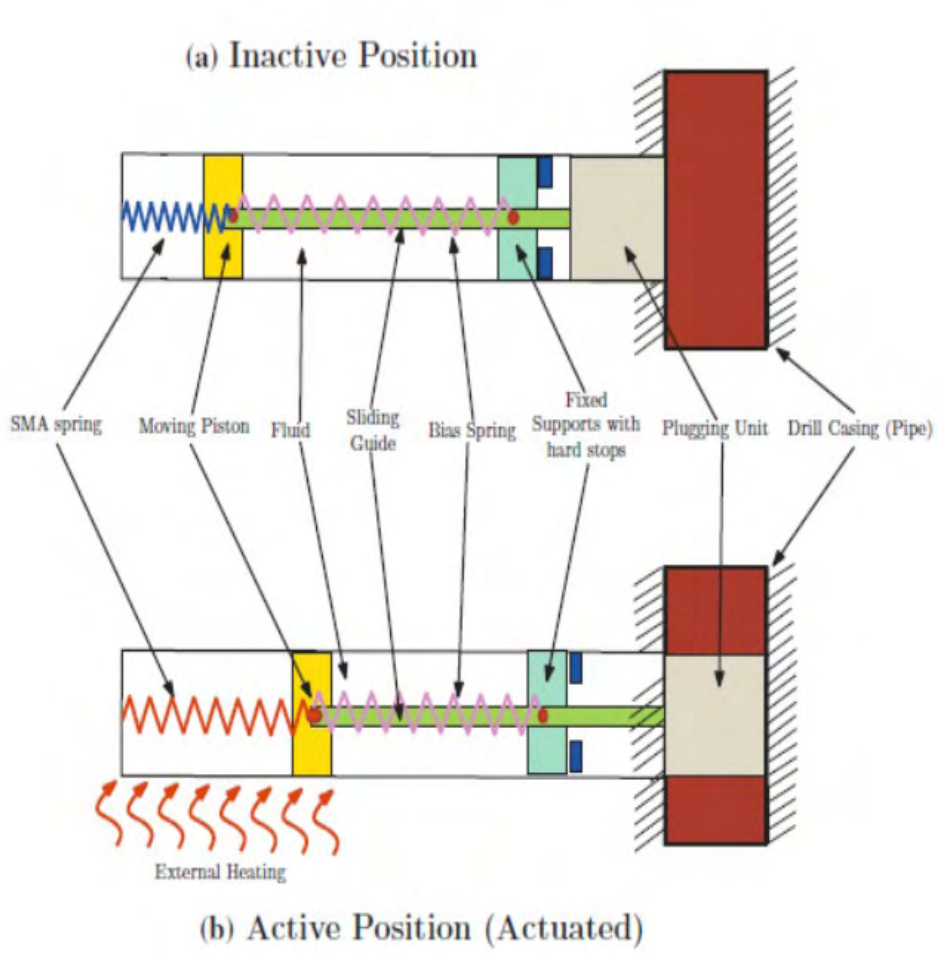

Fig.1.10: SMA and bias springs are employed to actuate pistons in ''blowout preventer's". [1]

Chapter 2 Literature Review

More than 60 years have passed since SMAs were first identified. The changes in micro-structure related to the phase transformation are now well understood, although the underlying microscopic mechanisms are still a research topic in materials science area, the connection between microscopic and macroscopic behavior is still under investigation, and existing micro-structural thermo mechanic models can describe the behavior of SMAs only qualitatively. An understanding of the micromechanical behavior of SMA is necessary to understand their macroscopic behavior [5].

2.1 Temperature Induced Phase Transformations

In thermally responsive SMAs, the reversible solid-solid, diffusionless thermoelastic phase transformations between a stable high temperature austenitic phase and low temperature martensitic phase are responsible for them to demonstrate interesting phenomenon like shape memory effect (SME) and superelasticity (SE).Their capability to return to a predetermined shape on heating is referred to as the shape memory effect (SME). Their ability to recover large strains (8%) and associated large stress–strain hysteresis due to mechanical loading–unloading under isothermal conditions is referred to as superelasticity/pseudoelasticity (SE) [1].

SMAs have two phases, each with a different crystal structure and therefore different properties. One is the high temperature phase called austenite (A) and the other is the low temperature phase called martensite (M). Austenite (generally cubic B2) has a different crystal structure from martensite (tetragonal, orthorhombic or monoclinic B19′).

The transformation from one structure to the other does not occur by diffusion of atoms, but rather by shear lattice distortion. Such a transformation is known as martensitic transformation. Each martensitic crystal formed can have a different orientation direction, called a variant. The assembly of martensitic variants can exist in two forms: *twinned martensite (Mt)*, which is formed by a combination of "*self-*

accommodated" martensitic variants, and *detwinned (Md)* or *reoriented martensite* in which a specific variant is dominant *"single variant martensite"*. The reversible phase transformation from austenite (parent phase) to martensite (product phase) and vice versa forms the basis for the unique behavior of SMAs.

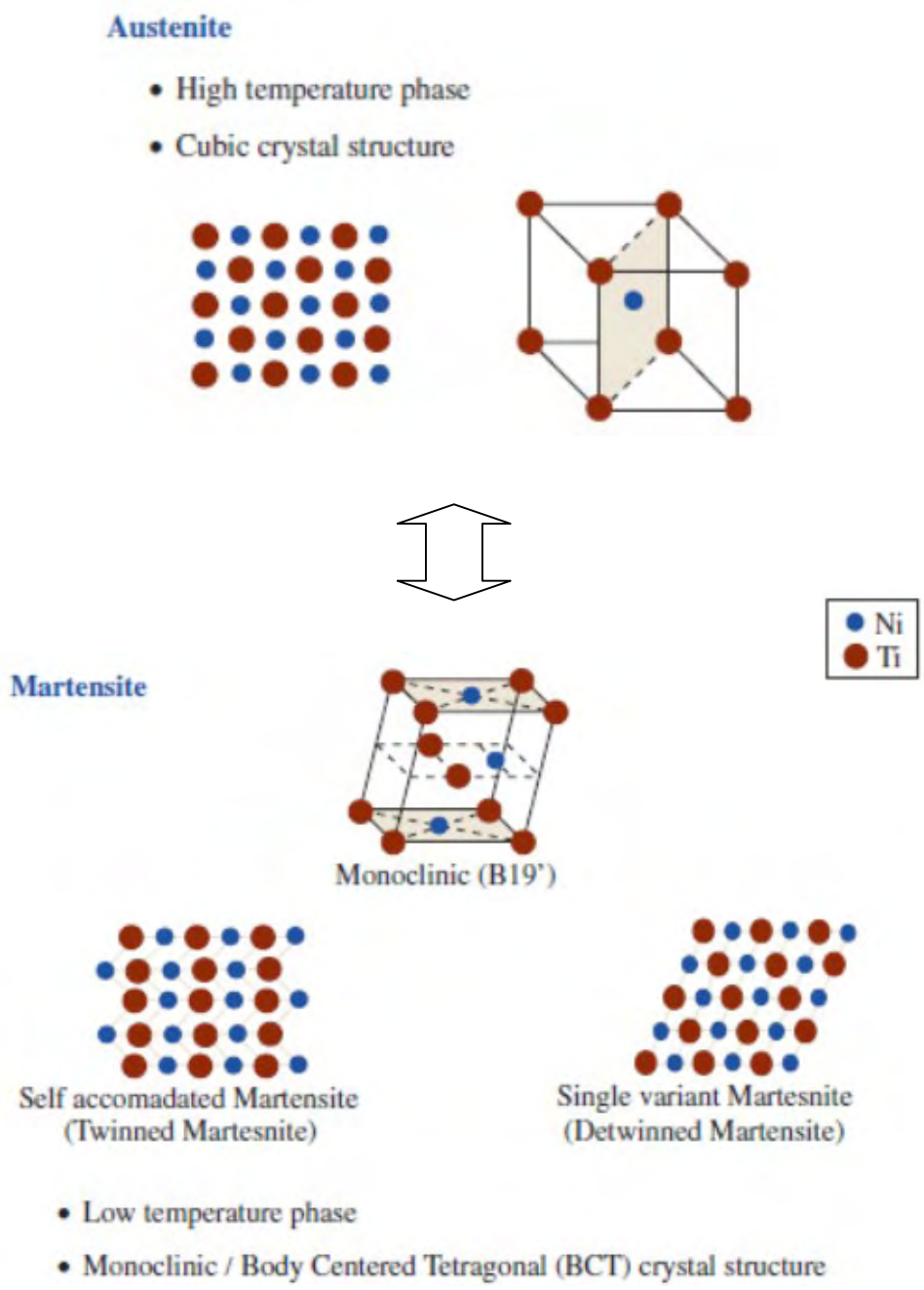

Fig.2.1: Microstructural changes in SMA, cubic structure of austenite and different variants of martensite. [1]

2.1.1 Characteristic Temperatures

There are four characteristic temperatures associated with the phase transformation. During the forward transformation, austenite, under zero load, begins to transform to twinned martensite at the martensitic start temperature (Ms) and completes transformation to martensite at the martensitic finish temperature (Mf). At this stage, the transformation is complete and the material is fully in the twinned martensitic phase [2].

Similarly, when the material is heated from the martensitic phase, the crystal structure begins to transform back to austenite, at the austenitic start temperature (As). The transformation is completed at the austenitic finish temperature (Af), this transition is called reverse transformation during which there is no associated shape change.

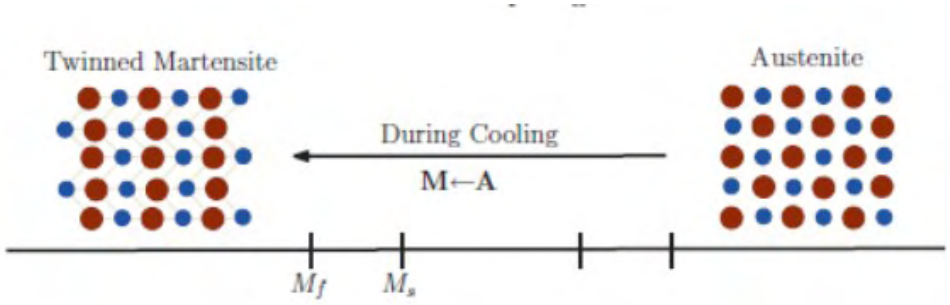

Fig.2.2: Forward Transformation

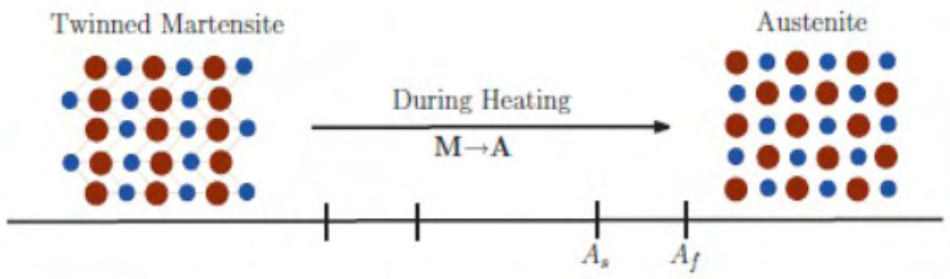

Fig.2.3: Reverse Transformation [1]

2.1.2 Differential Scanning Calorimetry

The four characteristic SMA temperatures are measured via Differential Scanning Calorimetry or DSC. DSC is a thermoanalytical technique in which the difference in the amount of heat required to increase the temperature of a sample and reference is measured as a function of temperature. Both the sample and reference are maintained at nearly the same temperature throughout the experiment. The basic principle underlying this technique is that when the sample undergoes a physical transformation such as phase transitions, more or less heat will need to flow to it than the reference to maintain both at the same temperature. Whether less or more heat must flow to the sample depends on whether the process is exothermic or endothermic.

The DSC setup is automatically capable of heating and cooling the samples up to 10°C/min while recording the differential energy inputs between the specimen and the reference by monitoring the heat flow rates. Finally it generates a heat flow (J/gk) versus temperature.

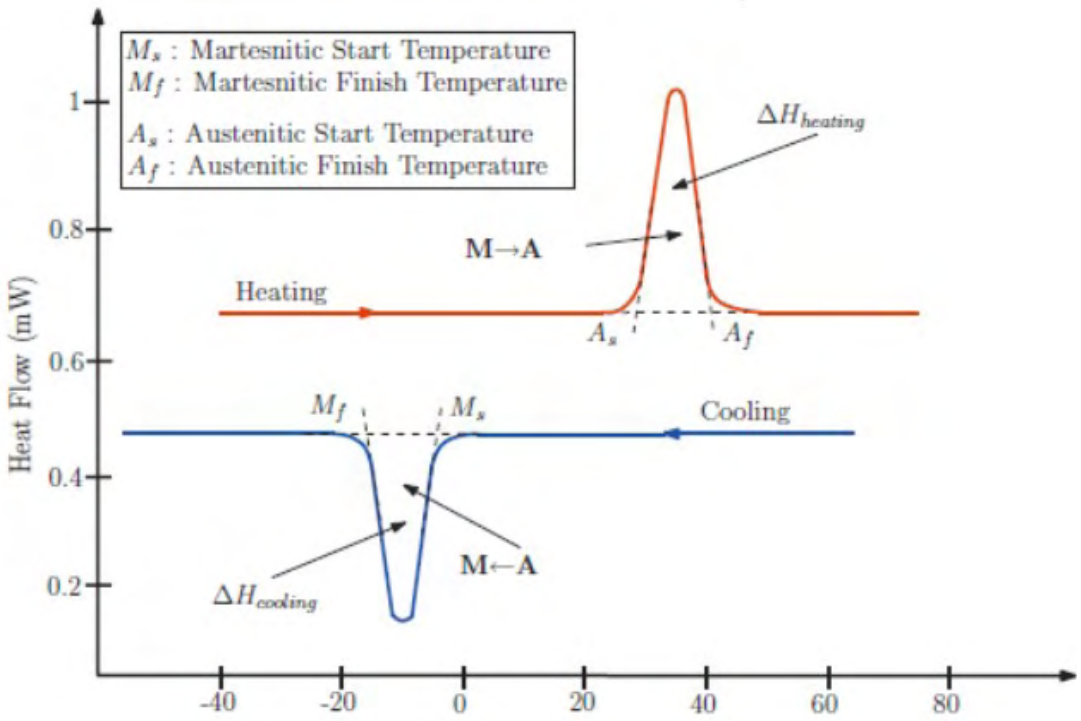

Fig.2.4: Ideal DSC plot [1]

2.2 Shape Memory Alloy – Abilities

2.2.1 Shape Memory Effect

The ability of SMA to return to a predetermined shape on heating above the characteristic transformation temperature A_f is referred to as the shape memory effect (SME). A SMA exhibits the shape memory effect (SME) when it is deformed while in the twinned martensitic phase and then unloaded while at a temperature below As. When it is subsequently heated above A_f, the SMA will regain its original shape by transforming back into the parent austenitic phase. The nature of the SME can be better understood by following the thermomechanical loading path in a combined stress-strain-temperature space as shown in **Fig.2.5**

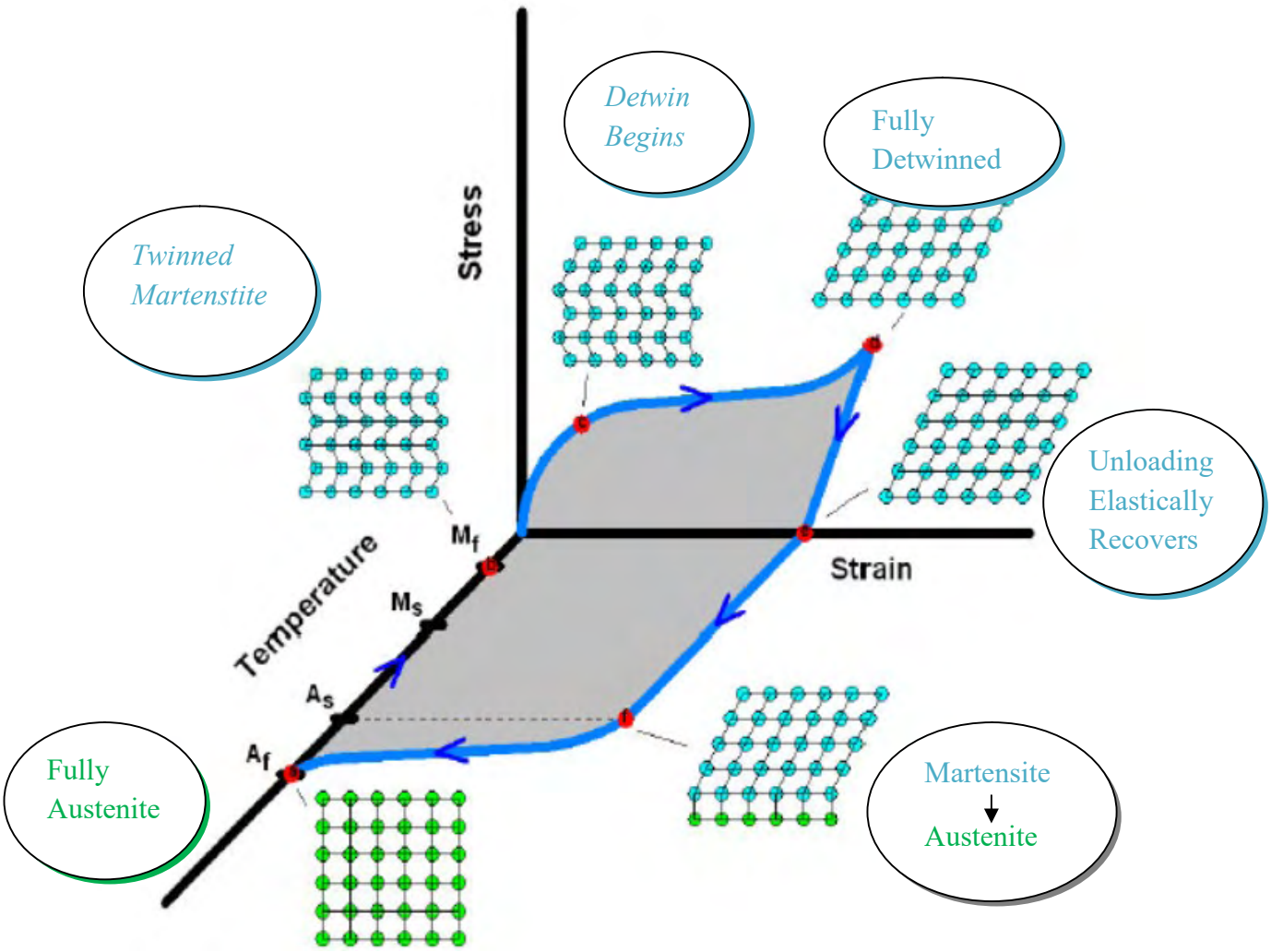

Fig.2.5 [10]: Stress-Strain-Temperature data exhibiting the Shape Memory Effect for a typical SMA [2]

- Starting from the parent phase (point a), the stress-free cooling of austenite below the forward transformation temperatures (M_s and M_f) results in the formation of twinned martensite (point b).

- When the twinned martensite is subjected to an applied stress that exceeds the start stress level (σ_s point c), the reorientation process is initiated, resulting in the growth of certain favorably oriented martensitic variants that grow at the expense of other less favorable variants. The stress level for reorientation of the variants is far lower than the permanent plastic yield stress of martensite.

- The detwinning process is completed at a stress level, $\sigma_{f\,(}$at4% strain), that is characterized by the end of the plateau in the σ-ε diagram.

- The material is then elastically unloaded from d to e and the detwinned martensitic state is retained.

- Upon heating in the absence of stress, the reverse transformation initiates as the temperature reaches A_s, (at point f) and is completed at temperature A_f (point a), above which only the parent austenitic phase exists.

- In the absence of permanent plastic strain generated during detwinning, the original shape of the SMA is regained.

- The above described phenomenon is called one-way shape memory effect, or simply SME, because the shape recovery is achieved only during heating after the material has been detwinned by an applied mechanical load.

2.2.2 Superelasticity/Pseudoelasticity

On the other hand, these martensitic transformations can be induced purely due to mechanical loading–unloading in the austenitic phase with SMA. The ability of SMA to recover large strains (~8%) with associated stress–strain hysteresis due to mechanical loading–unloading under isothermal conditions is referred to as superelastic/pseudoelastic effect (SE) [1]. The pseudoelastic behavior of SMAs is associated with stress-induced transformation, which leads to strain generation during loading and subsequent strain recovery upon unloading at temperatures above A_f. The nature of the SE can be better understood by following the thermomechanical loading path in a stress - strain diagram as shown in **Fig.2.6**.

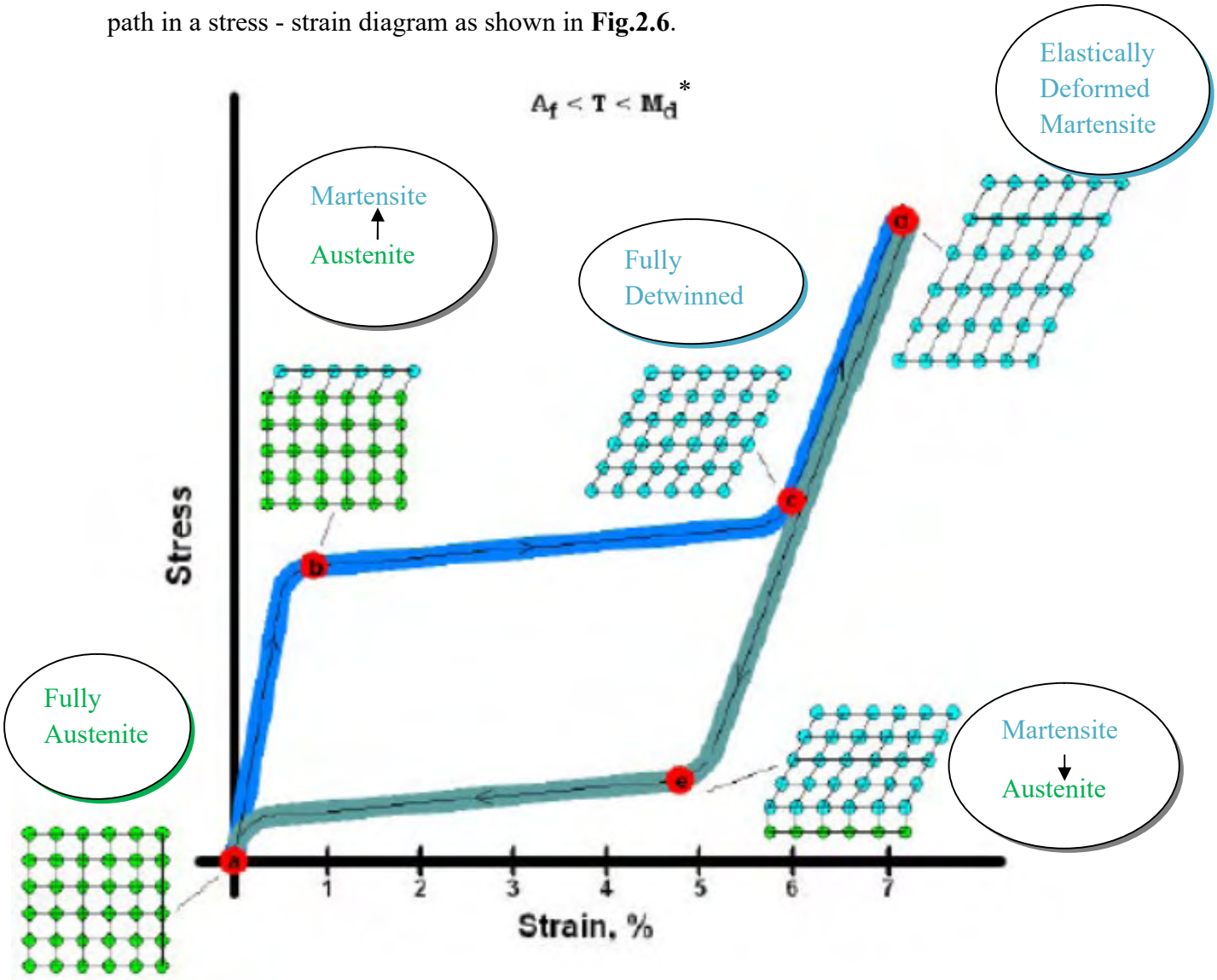

Fig.2.6: Stress – Strain diagram exhibiting Superelasticity effect for a typical SMA [2]

- Above A_f the material is fully austenite under moderate external loads the austenite elastically deforms, something that looks like a classic elastic deformation of metal or alloy specimen (a).

- Upon continued loading at some critical stress, it is thermodynamically stable for austenite to start transforming to a single variant martensite (stress induced martensite SIM, to differentiate this martensite variant form that formed due to twinning in SME).Transformation to martensite occurs. The martensite forms in twins and instantaneously detwins due to high applied stresses (b).

- Further loading fully transforms the material to martensite (c).

- Upon complete transformation, if loaded further this results in elastic deformation of SIM. However, higher loads can cause plastic deformation of SIM and they cannot be recovered back completely. In real world applications, this part of the response is rarely used in designing SMA components due to poor fatigue life and thus the maximum strains in SMA's are restricted to about 6% strains (d).

- Unloading back through point (c) recovers the elastic strains in the martensite.

- Continued unloading to (e) forces the onset of the reverse transformation, because its thermodynamically stable for the SIM to transform back to austenite.

- Full reverse transformation upon complete unloading to (a).

*At temperatures below the martensite finish temperature, Mf, the martensite is stable and a transformation cannot occur by the addition of stress. Additionally, if temperatures exceed the so-called martensite deformation temperature, Md, the energy (in the form of applied stress) required to form SIM exceeds the energy to plastically deform the austenite (via dislocation mobility), thereby making the structure a stable, non transforming austenite phase. Only within temperatures between the austenite finish, Af, and the Md can a stress-induced phase transformation occur.

2.2.3 Shape Memory Effect and Superelasticity

The SMA abilities of Shape Memory Effect and Superelasticity are represented together in **Fig.2.7.** The description of these effects was discussed in previous sections (2.2.2-2.2.3).

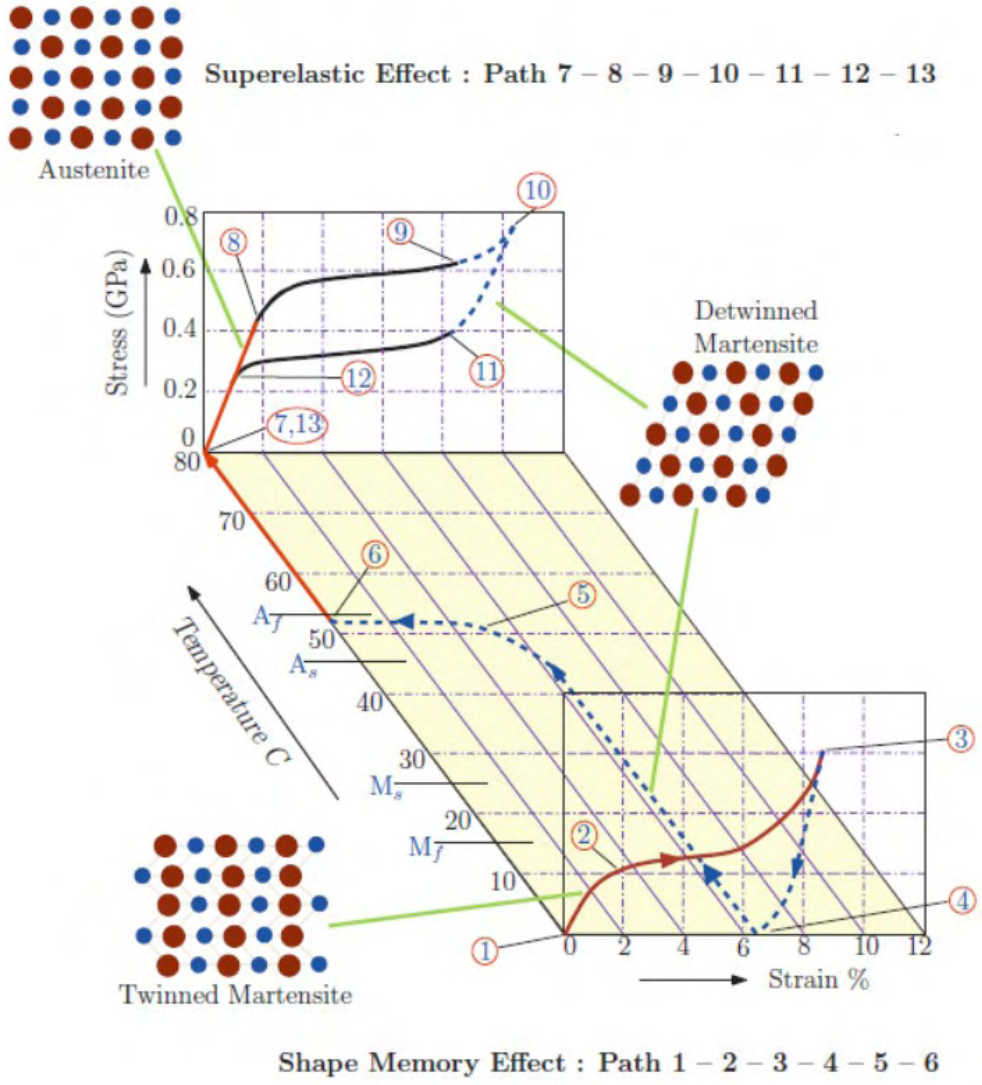

Fig.2.7: A three-dimensional stress-strain-temperature plot. Describes the thermomechanical experiment showing both shame memory effect (path 1-6) and superelastic effect (path 7-13) [1]

2.3 Determination of Mechanical Properties

The determination of materials' mechanical properties requires the application of some specialized methods. In this section a brief description of Vickers, Knoop and Marshall methods for the determination of microhardness and modulus of elasticity is given.

2.3.1 Vickers Hardness Test Method

The Vickers hardness test can be performed on both the micro and macro scales (some Vickers testers have a maximum test load of up to 50 kilograms). Like Knoop microhardness testing, these tests are also performed by applying controlled pressure for a standard length of time, but with a square-based diamond pyramid indenter. The diagonal of the resulting indention is measured under a microscope, then this measurement and the test load are used in a specific formula to calculate the Vickers hardness value [11].

$$HV = \frac{0.01819F(N)}{d^{2}\,(mm)} \tag{2.1}$$

2.3.2 Knoop Hardness Test Method

The Knoop hardness is a property of a material used for small parts, thin sections and is defined via a microhardness test. A pyramidal diamond indenter is pressed into the polished surface of the test material with a known load, for a specified dwell time, and the resulting imprint's main diagonal is measured using a microscope.

The geometry of this indenter is an extended pyramid with the length to width ratio being 7:1 and respective face angles are 172 degrees for the long edge and 130 degrees for the short edge. The depth of the indentation can be approximated as 1/30 of the long dimension [12].

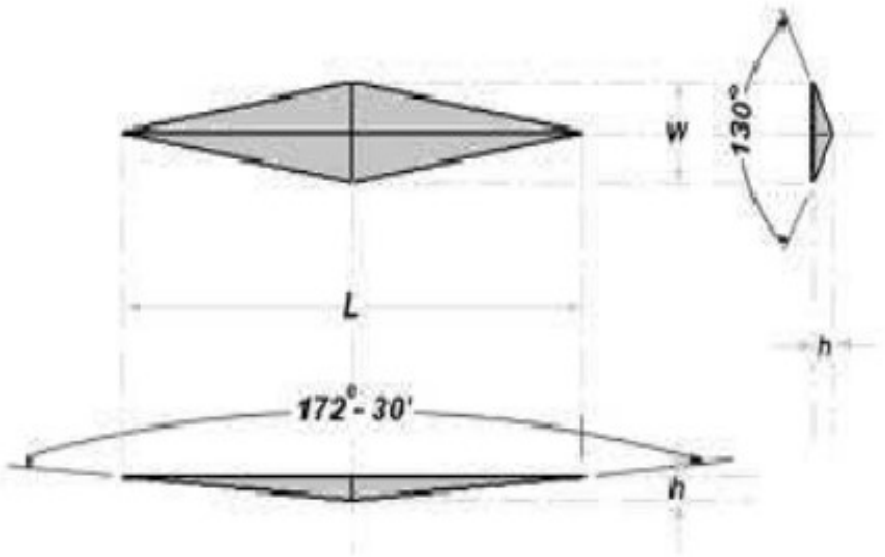

Fig.2.8: Geometry of a Knoop hardness test indenter

The Knoop hardness HK or KHN is then given by the formula:

$$\frac{Projected\ area}{Longitudinal\ diagonal^{2}} = conversion\ factor C$$

$$HK = KHN = \frac{P}{Cl^{2}} = \frac{14.286P}{l_1^2} \qquad (2.2)$$

Where, HK: Knoop Hardness

P: Load (Kg)

I_l: length of indentation along its long axis (mm)

Cp: Correction factor related to the shape of the indenter, ideally 0.070279

The transformation of Knoop Hardness (kgf/mm^2) to GPa:

$$\frac{1kgf}{mm^2} = \frac{9.807N}{(10^{-3})^2 m^2} = 9.807*10^6 \frac{N}{m^2} = 9.807*10^6 Pa = 9.807*10^6 *10^{-9} GPa = 0.009807 GPa$$

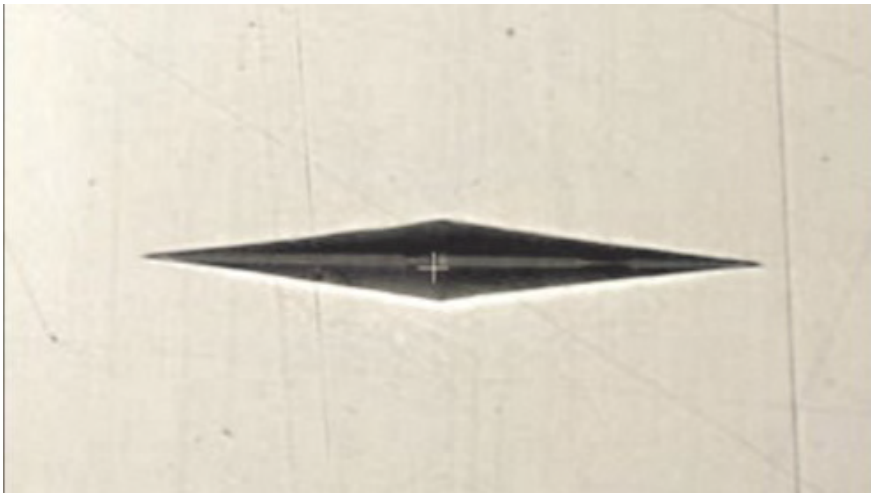

Fig.2.9: Knoop indentation on a smoothly polished surface

2.3.3 Determination of Elastic Modulus- Marshall Method

The method is based on the measurement of elastic recovery of the in-surface dimensions of Knoop indentations. In the fully loaded state, the ratio of the diagonal dimensions, a and b, of the Knoop contact area is defined by the indenter geometry, a/b =7.11. However, on unloading, elastic recovery reduces the length of the shorter indentation diagonal (as well as the indentation depth), whereas the longer diagonal remains relatively unaffected.

The extent of recovery depends on the hardness-to-modulus ratio; recovery is largest in highly elastic materials (high H/E) and zero in rigidiplastic materials (low H/E). Therefore, the distortion of the residual impression, characterized by the ratio of its dimensions, b′ / a′, provides a measure of H/E [13].

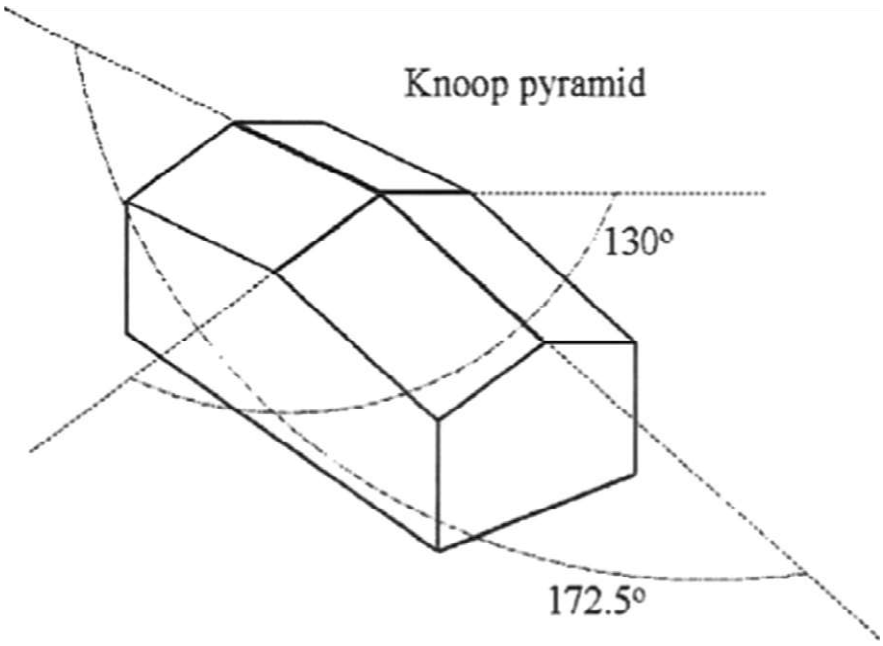

(a)

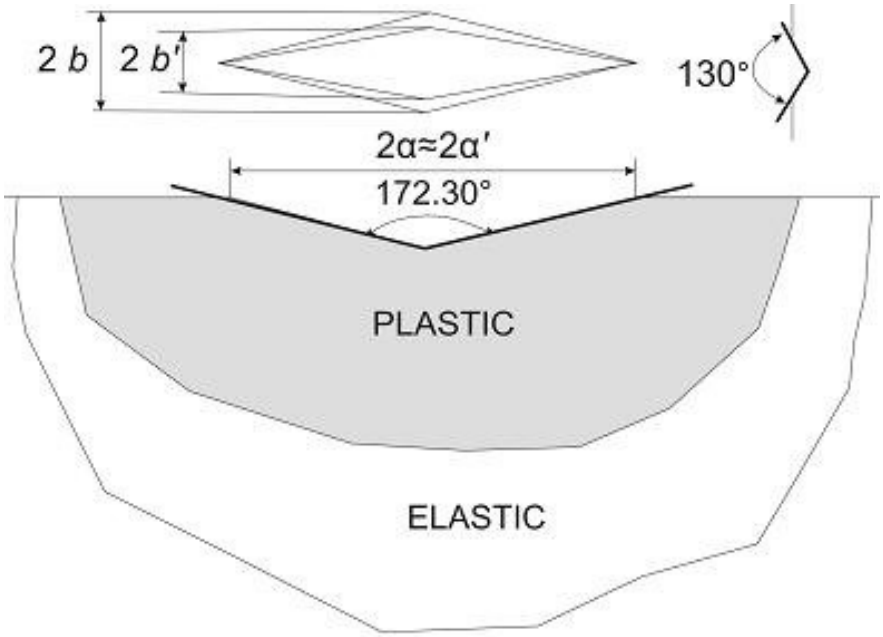

(b)

Fig.2.10: (a) Knoop Indenter, (b) Description of Knoop indentation, 2b=small diagonal, 2b´=small diagonal after the indentation, $2\alpha \approx 2\alpha$ mean diagonal before and after the indentation

The Modulus of Elasticity is then given by the formula:

$$E = \frac{\alpha \cdot HK}{\left(\frac{b}{a} - \frac{b'}{a'} \right)} \qquad (2.2)$$

Where, HK: Knoop Hardness

b/α: ~ 1/7 (defined by the indenter geometry)

b′/α′: ratio of the diagonal dimensions after unloading

α=α′

α= 1,5 Marshall's theoretical value
or
0.45 Marshall's experimental value (usually gives better results)
or
0.34 Watts experimental value

Chapter 3: Experimental Procedure

The aim of this chapter, is to describe the experimental procedures, carried out in the laboratory, in order to identify the microstructure, the microhardness, the modulus of Elasticity as well as the critical transformation temperatures (A_s, A_f, M_s, M_f) of a NiTiCu spring actuators, deliverd by AMSF, Leuven. The processing stages of the actuator spring are presented in **Fig.3.1,** while the chemical analysis is given in **Table.1.** The spring was heat treated after coiling to memorize shape.

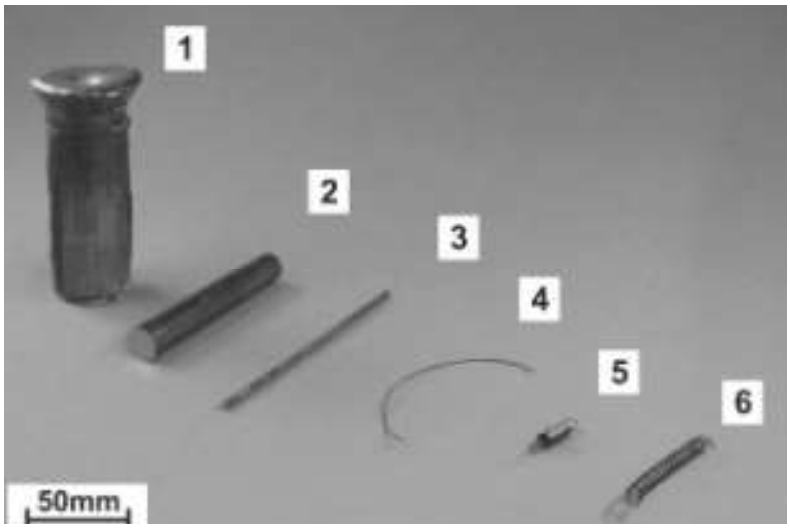

Fig.3.1 Photograph showing different stages of actuator spring processing (1– 5). (1) As cast ingot (2) Swaged rod. (3) Rolled cylinder (4) Drawn wire. (5) after coiling

Table.1. Chemical Analysis of spring (wt %)

Ni	Ti	Cu
49	44	7

3.1 Specimen Preparation

3.1.1 Sampling and cutting

The samples were studied in two different shape conditions**.** In **Fig.3.1** the actuator in its spring shape is shown and its geometrical characteristics are provided. In Fig.3.2 the relevant sample when the actuator is fully deployed, as a wire, is given. From each sample both transverse and longitudinal sections were prepared and studied

Fig.3.2: Sample 1, "spring" shape

Inner Diameter: 10mm

Fig.3.3: Sample 2, "wire" shape

Diameter: 1,5mm

3.1.2 Mounting

For the specimen mounting acrylic resin (Acryfix) was used, with a mixing ration volume: 1 part of liquid and 2 parts of powder. With and average mixing time of 30sec and curing time about 10 min.

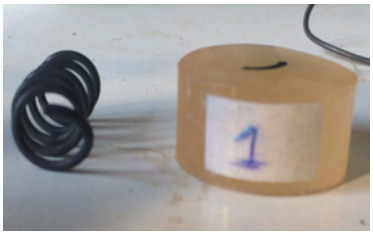

Fig.3.4: Sample 1, "spring" shape, after mounting, longitudinal section

Fig.3.5: Sample 2, "wire" shape, after mounting, longitudinal section

3.1.3 Grinding – Polishing

Each specimen was grinded with 120, 180, 220, 320, 500, 800, 1000 and 2000 grit of SiC papers followed by polishing with diamond paste of a 3μm grain size and then with alumina powder of a 0.05μm grain size

3.1.4 Etching

Etching procedure was very difficult since several etchants –found- in the literature didn't work in this specific material. Finally the microstructure was revealed, by immersing the metallographic specimens in the solution 3.2% HF, 14.6%HNO_3, balance deionized water, for 270sec. Then the specimens were etched again with the same etchant for 150sec.

3.2 Optical Microscopy

The examination of the metallographic specimens was carried out on an Optical Metallographic Microscope, Leitz ''Aristomet'' at magnifications 50x –1000x

3.3 SEM/EDX analysis

SEM/EDX analysis was conducted on both specimens (spring/wire). The purpose was to identify the composition of the phases observed in the microstructure. A SEM JEOL JSM- 840A combined with EDS analysis was employed for the analyses.

\

3.4 Microhardness Measurements

The microhardness measurements were performed both on Vickers and Knoop scale, and for that purpose the microhardness tester WolpertGroup (type402MVD) was employed. The tester was setup with the hardness measurement of a certified test block with known hardness. The loads applied varied between 50g, 200g, and 500g. For the determination of the Modulus of Elasticity the imprints measurements were performed with the aim of optical microscope installed in the tester.

3.5 Differential Scanning Calorimetry

DSC analysis was conducted on both samples (1 & 2) so as to determine the transformation and reverse transformation temperatures, i.e.: A_s, A_f, M_s, M_f.

The temperature protocol followed for both samples was:
393K [5min] → 173K [5min] → 393K with a heating/cooling rate of 10K/min.
The mass of each sample was:

Specimen #1 (spring): m_1=43.56mg
Specimen #2)wire): m_2=48.56mg.

The equipment employed for the DSC analysis was a Perkin Elmer Pyris 6 .

Chapter 4: Results

In this chapter, the results of the diploma thesis are represented

4.1 Metallography

4.1.1 Specimen 1: “Spring shape”

The specimen, when in the spring shape, corresponds to the austenitic phase according to the literature. The microstructure is consisted from elongated phases uniformly dispersed in the matrix (**Fig.4.1-4.3**). Their cross section is given in **Figs.4.4-4.6**

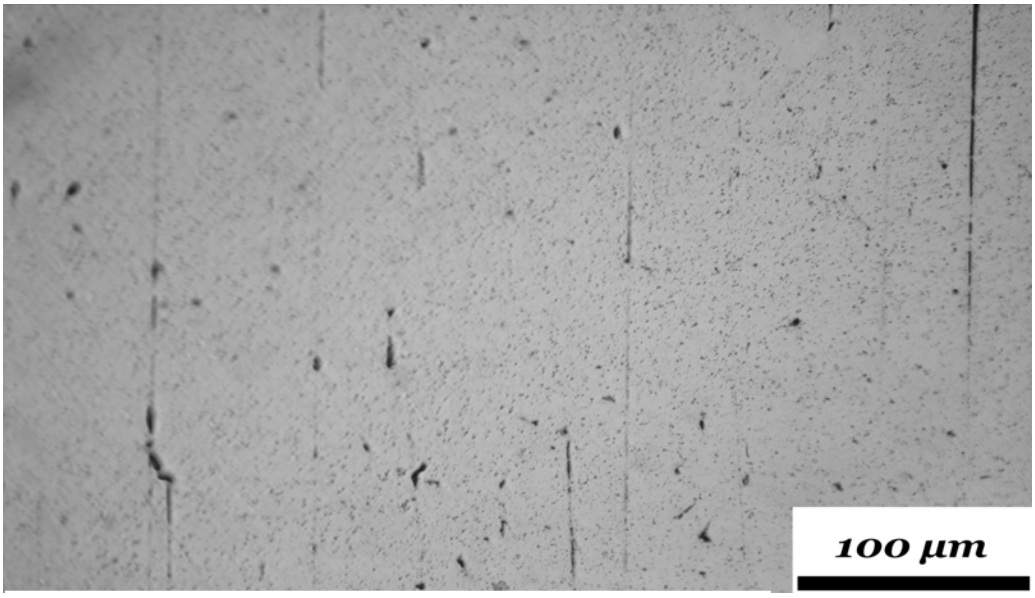

Fig.4.1 Optical photograph, unetched (200X)

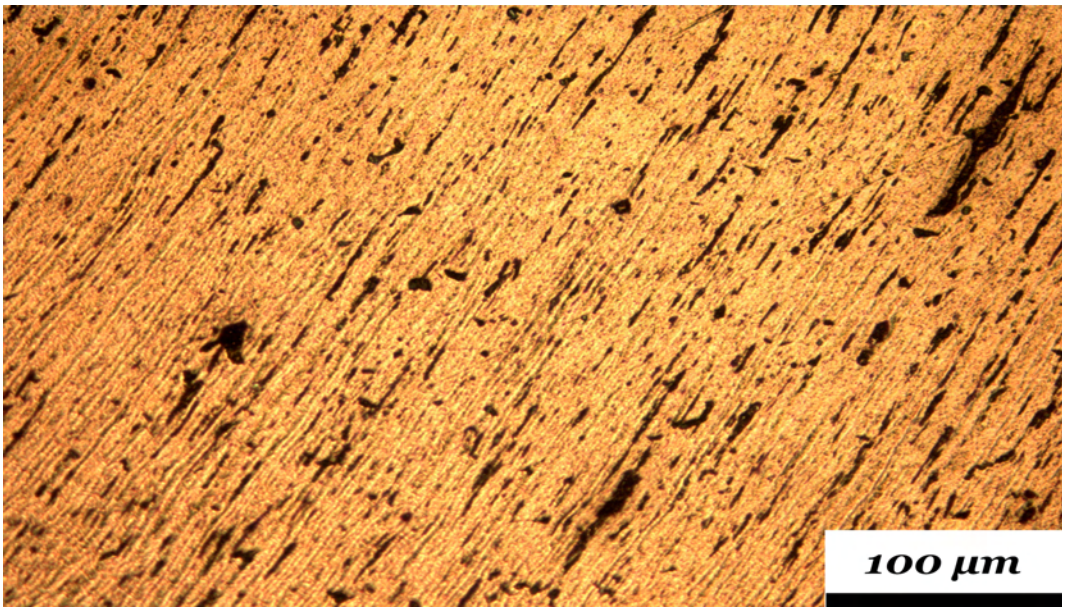

Fig.4.2 Optical photograph, longitudinal section (etched 200X)

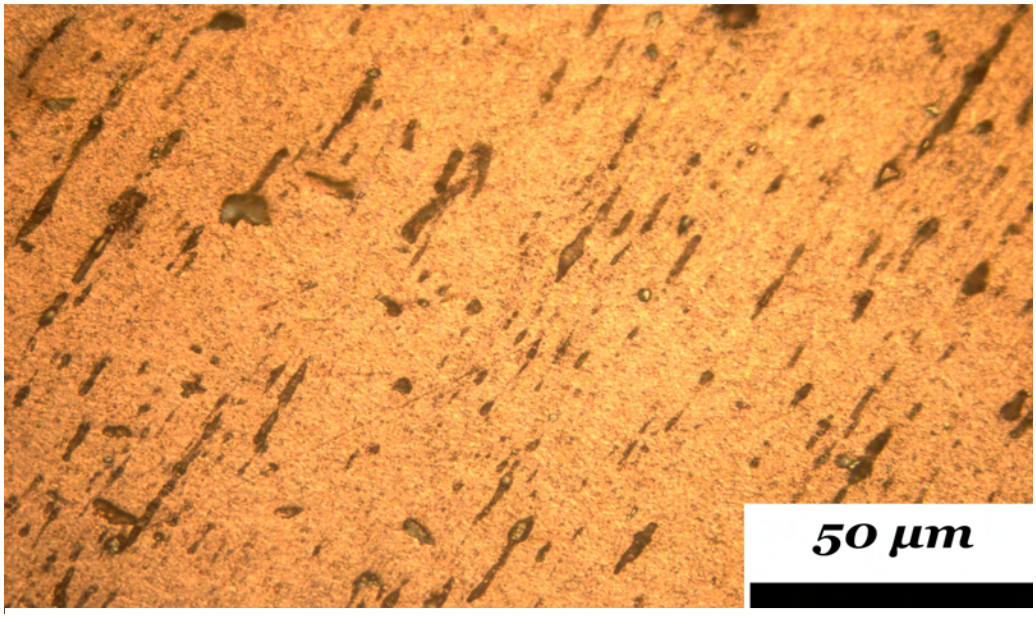

Fig.4.3 Optical photograph, longitudinal section (etched 500X)

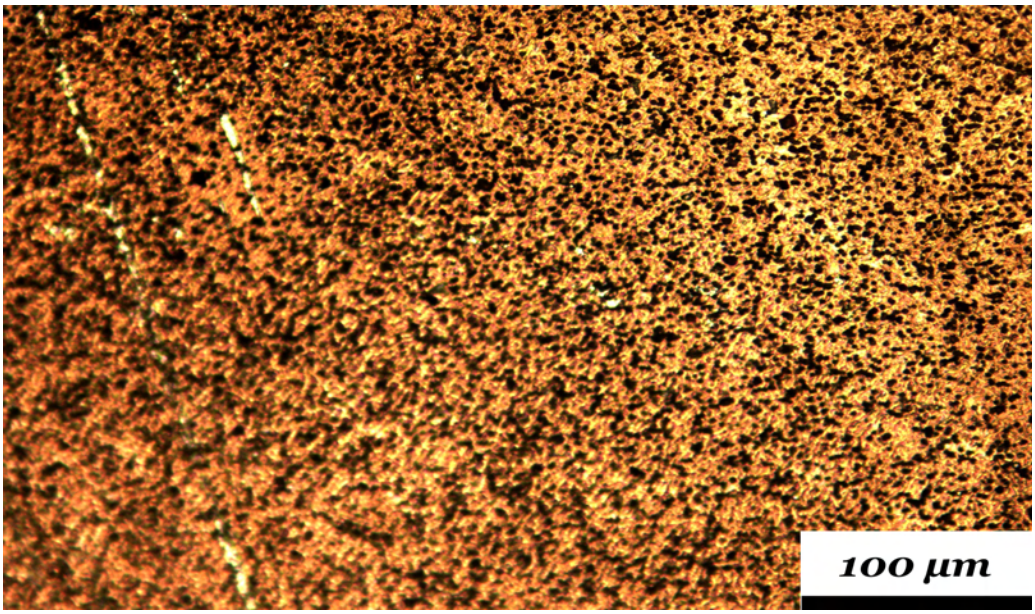

Fig.4.4 Optical photograph, transverse section (etched 200X)

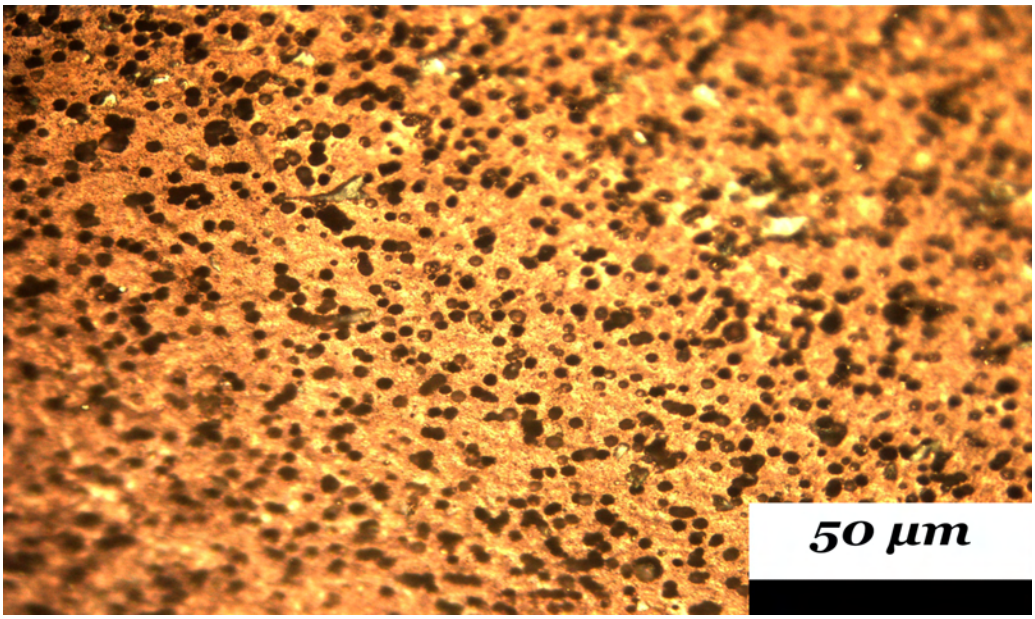

Fig.4.5 Optical photograph, transverse section (etched 500X)

4.1.2 Specimen 2: “Wire shape”

The specimen, when in the wire shape, corresponds to the martensitic phase according to the literature. The results are presented in **Figs.4.6-4.10** below. There are simularities with the microstructure observed in the “spring” shape, while there are specific areas in the specimen where are a needle shape microstructure can benn seen (**Figs.4.9,4.10)**

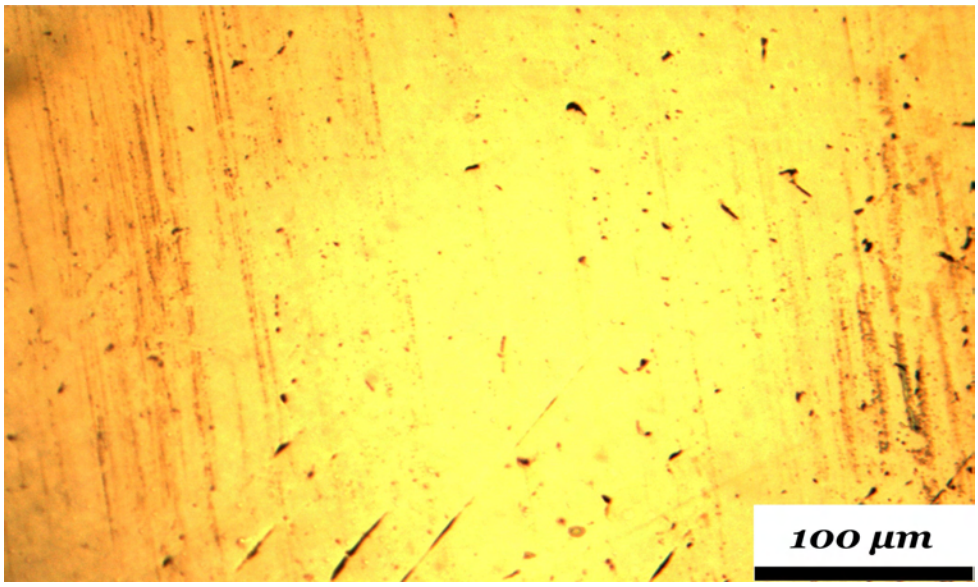

Fig.4.6 Optical photograph, unetched (200X)

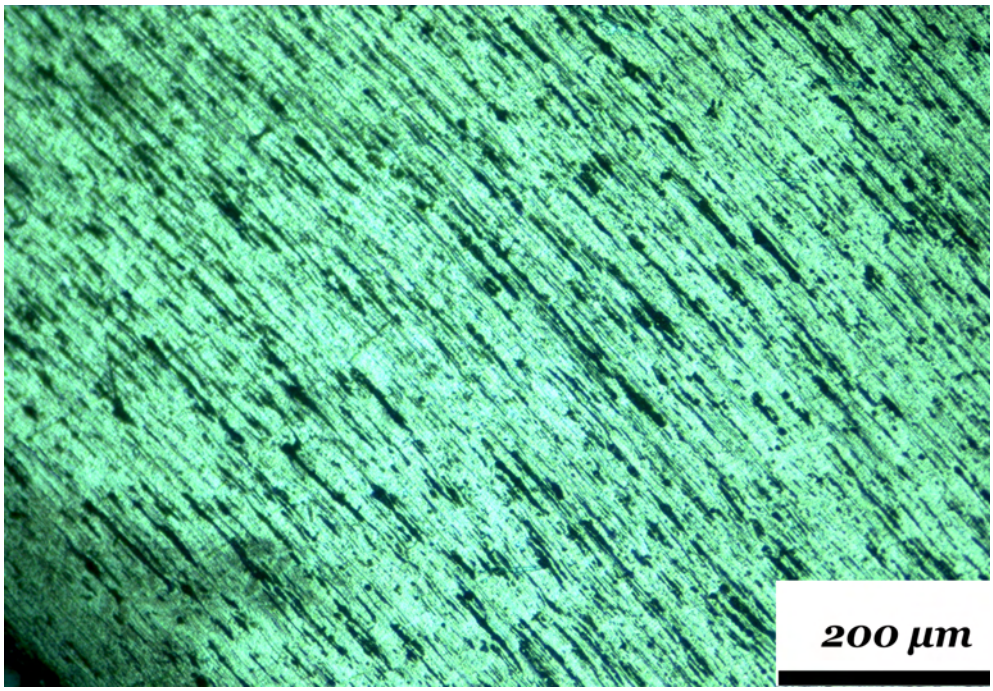

Fig.4.7: Optical photograph, longitudinal section etched (200X)

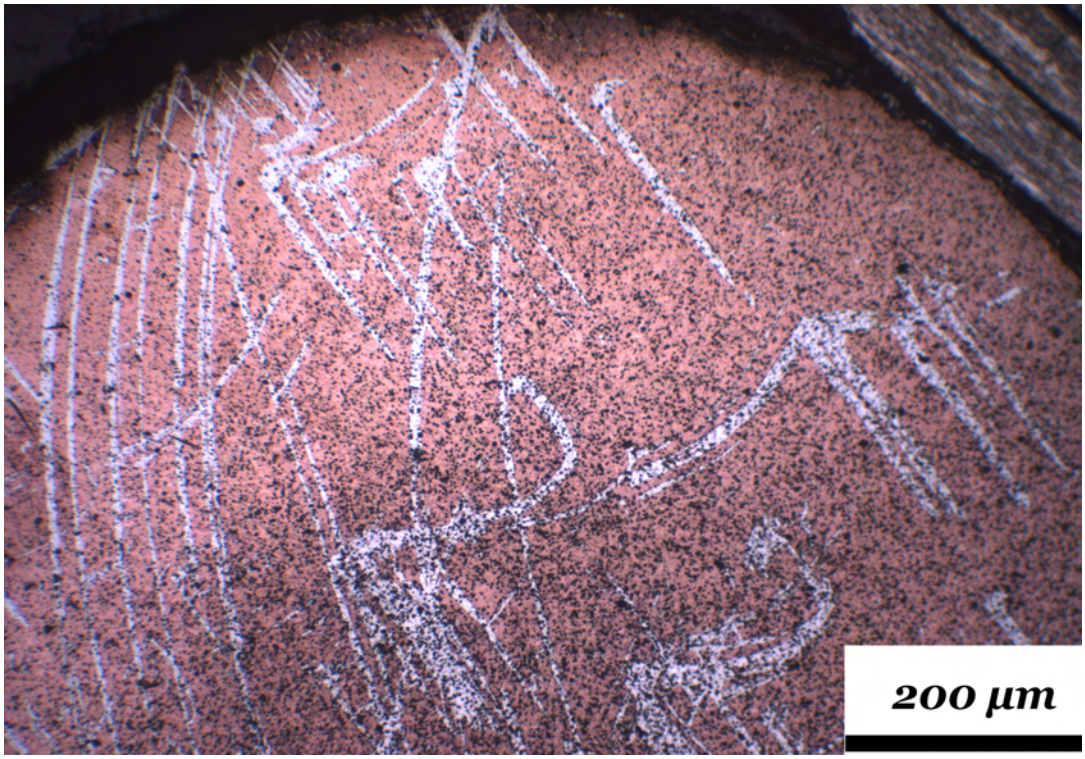

Fig.4.8: Optical photograph, transverse section (etched, 100X)

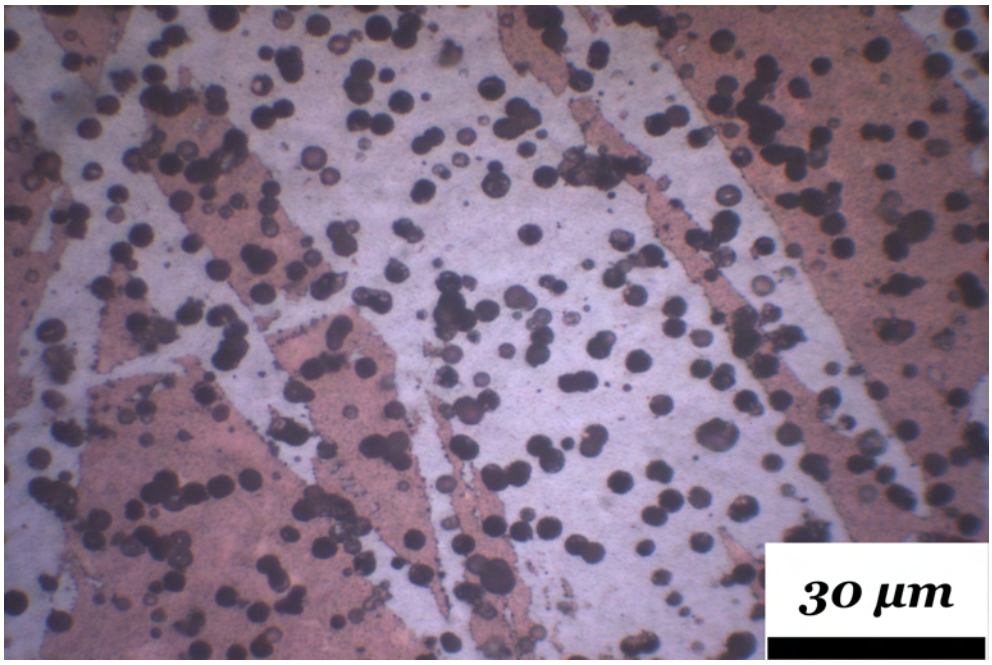

Fig.4.9 Optical photograph,transvesre section (etched, 1000X)

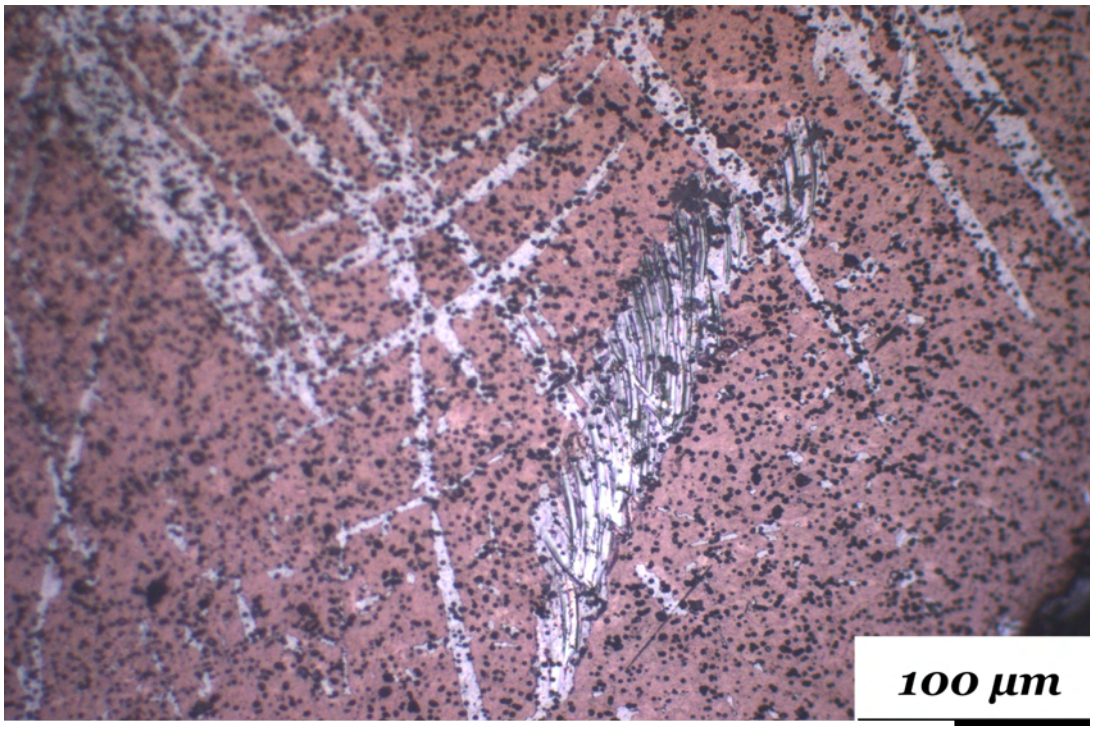

Fig.4.10 Optical photograph, transverse section (etched 200X)

4.2 EDX Analysis

The results from SEM/EDX analysis conducted on selected areas of the metallographic specimens are given in the next paragraphs.

4.2.1 Specimen 1: “Spring” shape – transverse

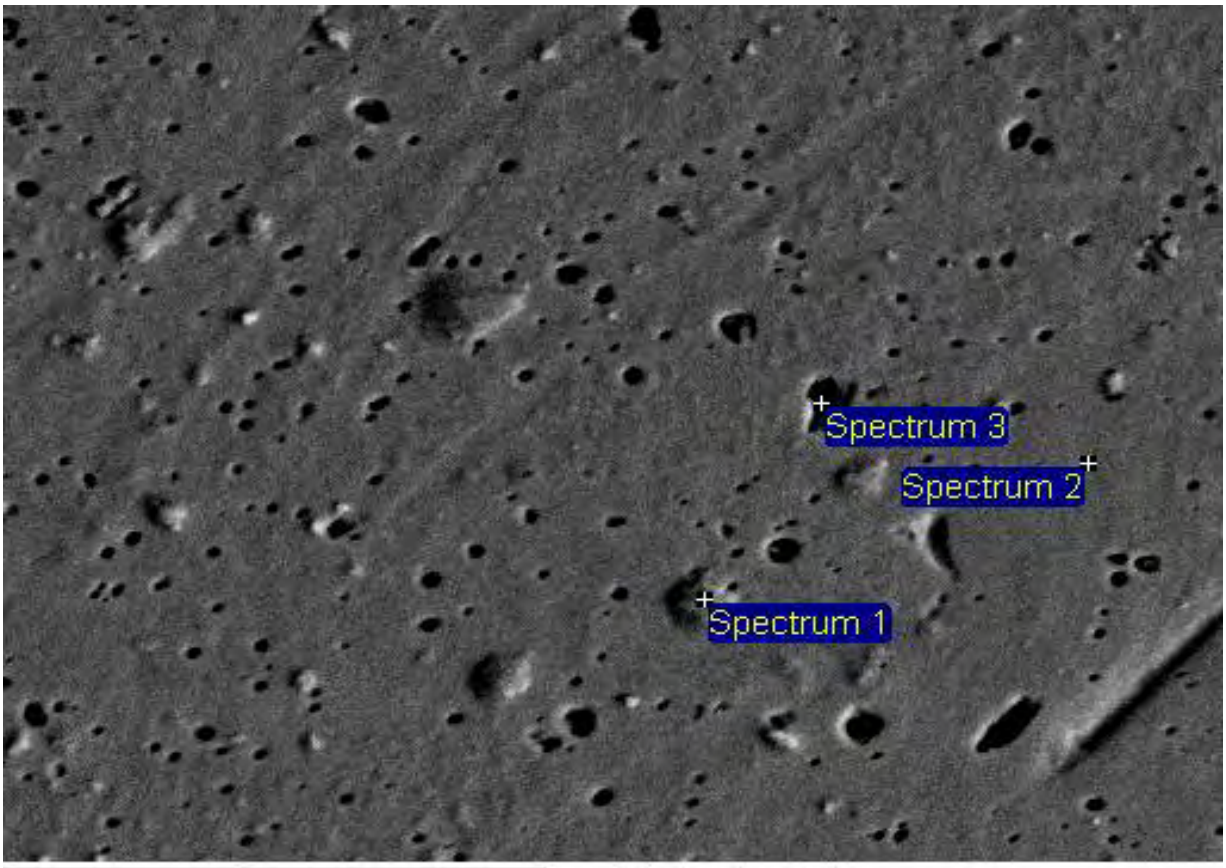

Spectrum	In stats.	Ti	Ni	Cu
Spectrum 1	Yes	34.67	26.96	38.37
Spectrum 2	Yes	50.63	44.17	5.20

Fig.4.11. Secondary Electron image – EDX Quantitative spot analysis on selected phases indicating by the cross.

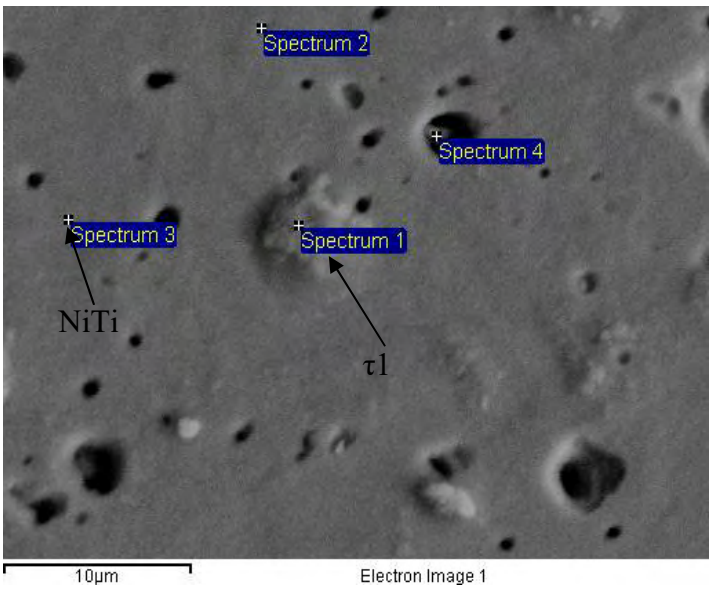

Spectrum	In stats.	Ti	Ni	Cu
Spectrum 1	Yes	25.69	18.81	55.50
Spectrum 2	Yes	49.03	45.15	5.81
Spectrum 3	Yes	48.70	46.08	5.22
Spectrum 4	Yes	52.34	39.07	8.59

Fig.4.12. Secondary Electron image – EDX Quantitative spot analysis on selected phases indicating by the cross.

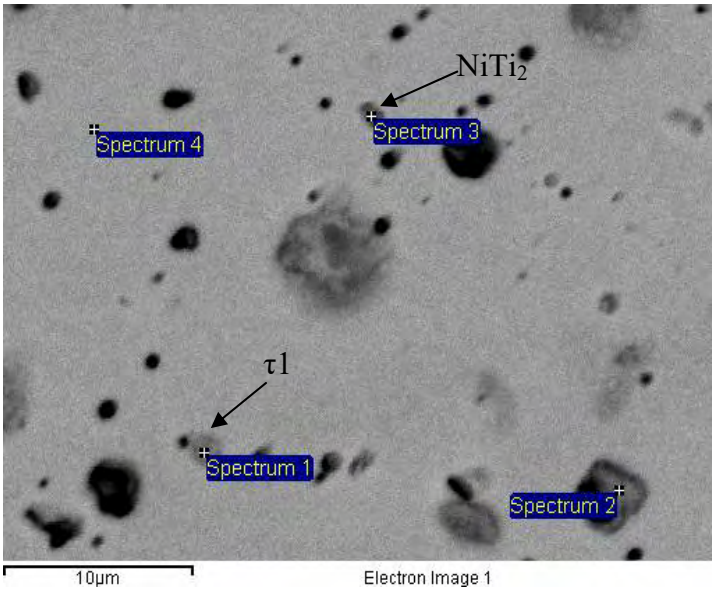

Spectrum	In stats.	Ti	Ni	Cu
Spectrum 1	Yes	35.24	26.25	38.51
Spectrum 2	Yes	48.15	41.74	10.10
Spectrum 3	Yes	55.78	38.30	5.92
Spectrum 4	Yes	50.13	45.37	4.50

Fig.4.13. Backscattered Electron image – EDX Quantitative spot analysis on selected phases

Table.2: The Ni-Ti-Cu solid phases considered in this work for specimen 1. [14]

Phase		Molecular Weight	at % Ti	at % Ni	at % Cu	Composition Range
Bcc_B2, NiTi		106.4	44.9	55	-	Dissolves 43-50.5 at%Ti
$NiTi_2$	**$(Cu_xNi_{1-x})Ti_2$, x=0**	154.2	62	38	-	x=0-0.15, dissolves ~6%atCu
	$(Cu_xNi_{1-x})Ti_2$, x=0.15	155	61.6	32	6	
τ1	**$(Cu_xNi_{1-x})_2Ti$, x=0.23**	167.2	28.5	53.9	17.4	x=0.20-0.82, dissolves 13-55at%Cu
	$(Cu_xNi_{1-x})_2Ti$, x=0.75	157.4	30.36	18.61	60.55	

4.2.2 Specimen 2: “Wire” shape – transverse

The results from SEM/EDX analysis conducted on the wire shape are presented in **Figs. 4.14-4.29**

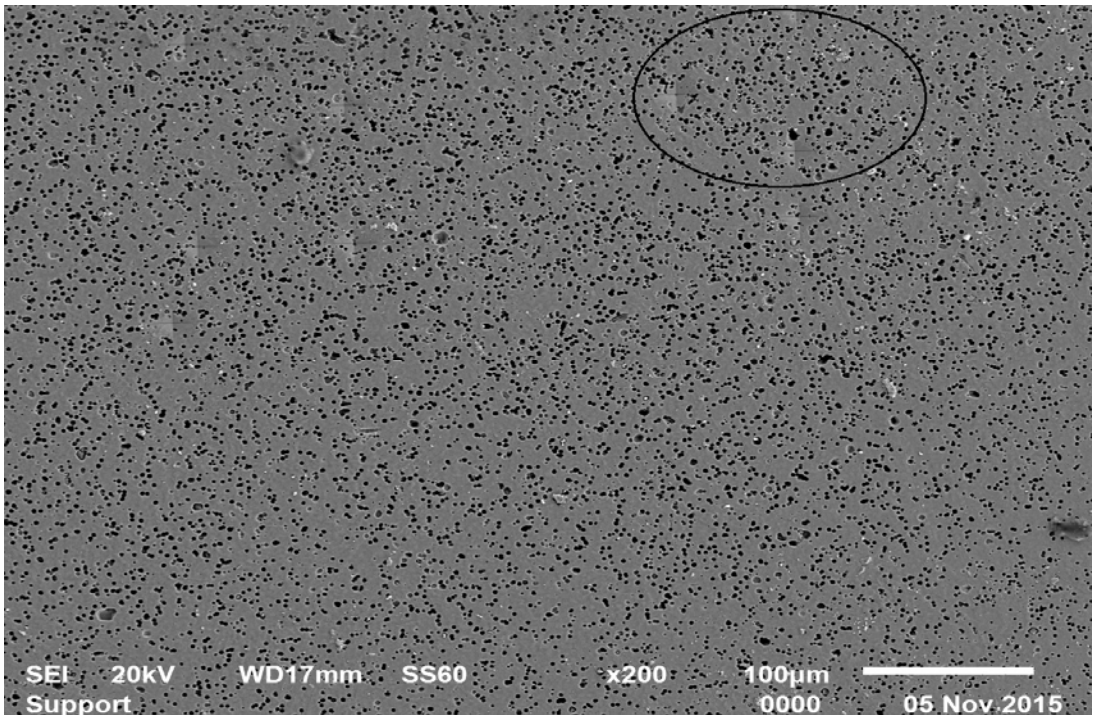

Fig.4.14. Microstructure as observed in SEM

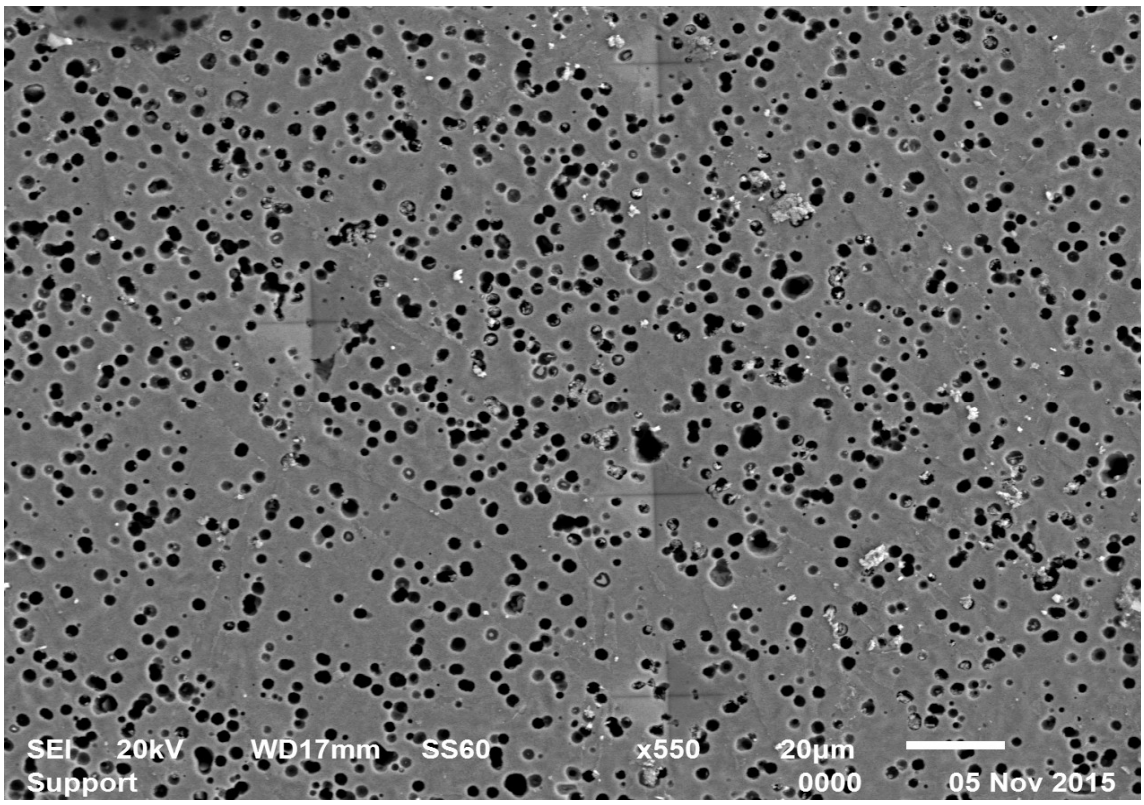

Fig.4.15. Microstructure at higher magnification. A phase with almost round shape is uniformly distributed within the matrix.

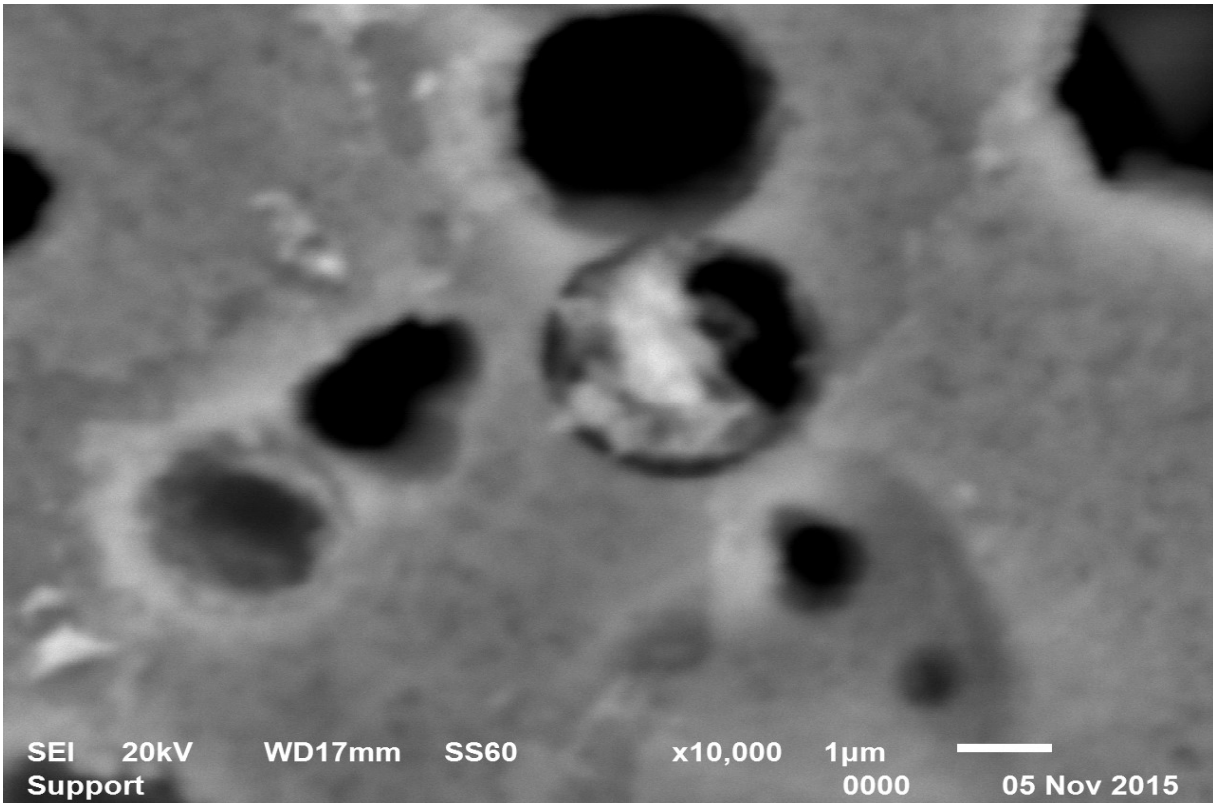

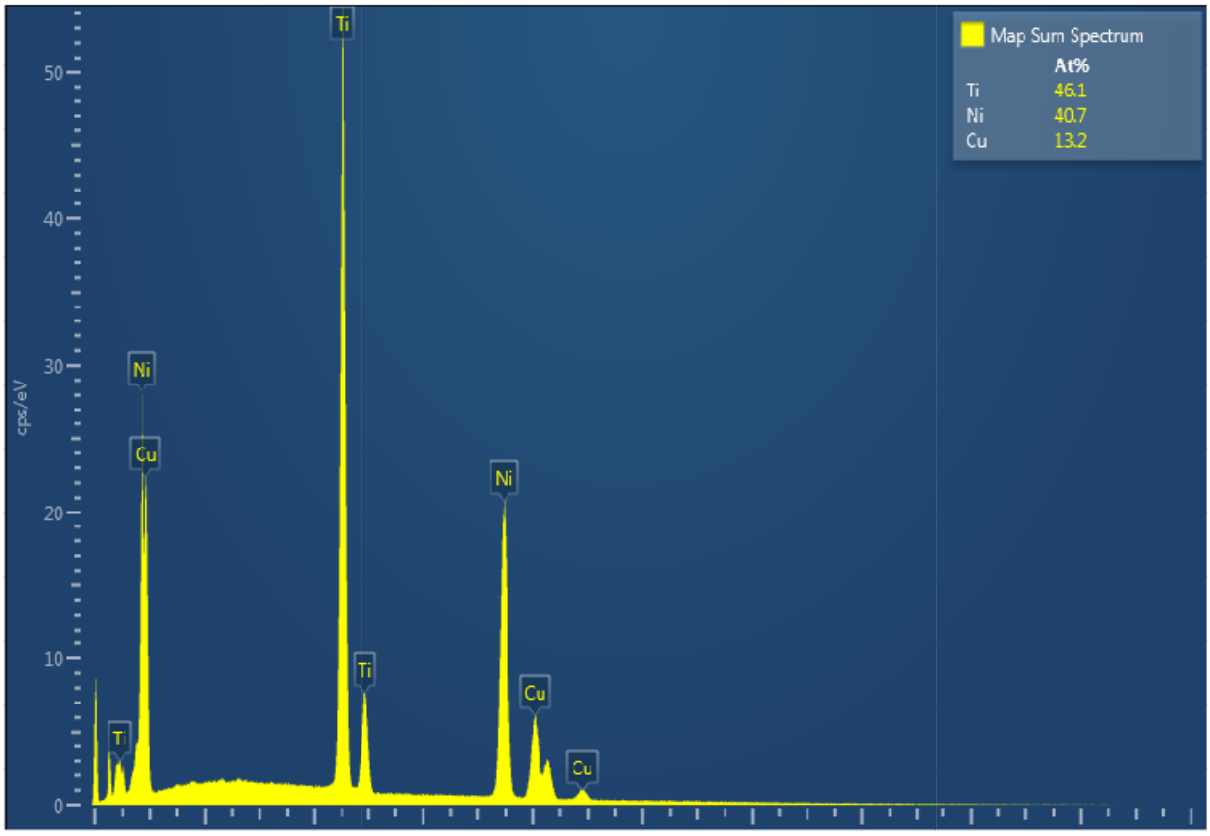

Fig.4.16. Microstructure at higher magnification: Besides the round shape phase, a finer phase seems to be present. The overall EDX analysis of the whole area is provided.

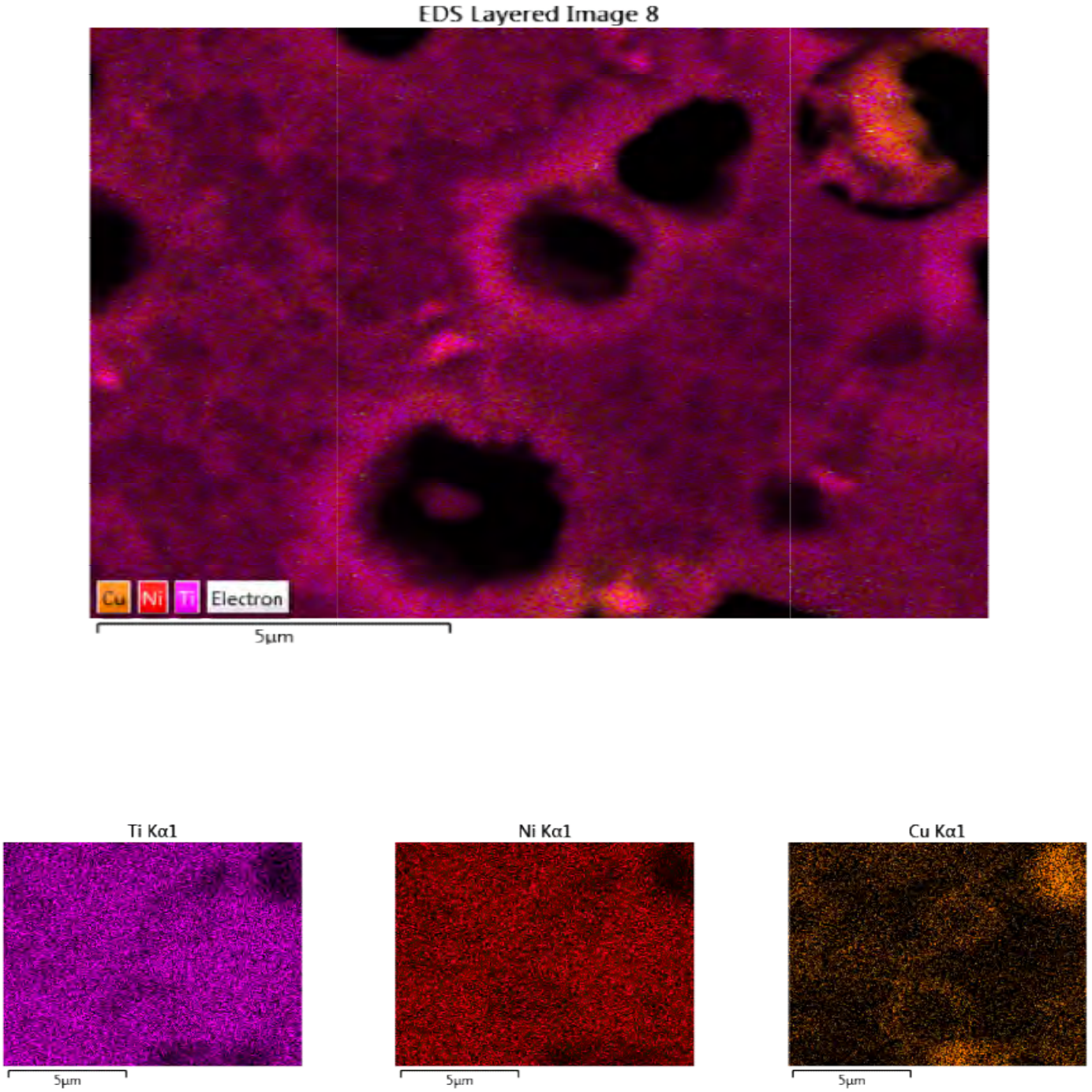

Fig.4.17. X-ray mapping, corresponds to Fig.4.16. Higher Cu concentration associated with the round shaped phases.

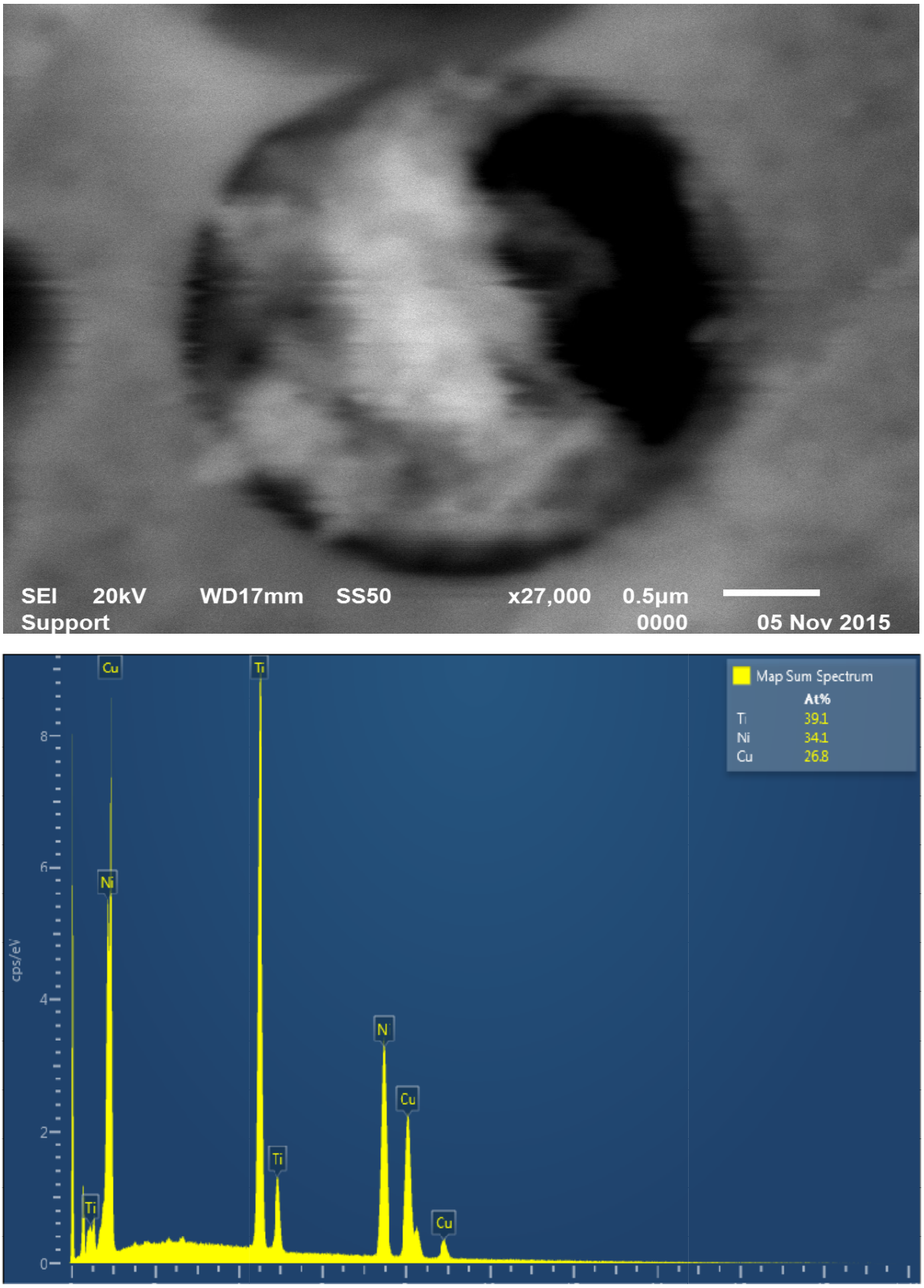

Fig.4.18. Higher magnification of the area around the round particles. The EDX analysis indicates Cu-rich phase.

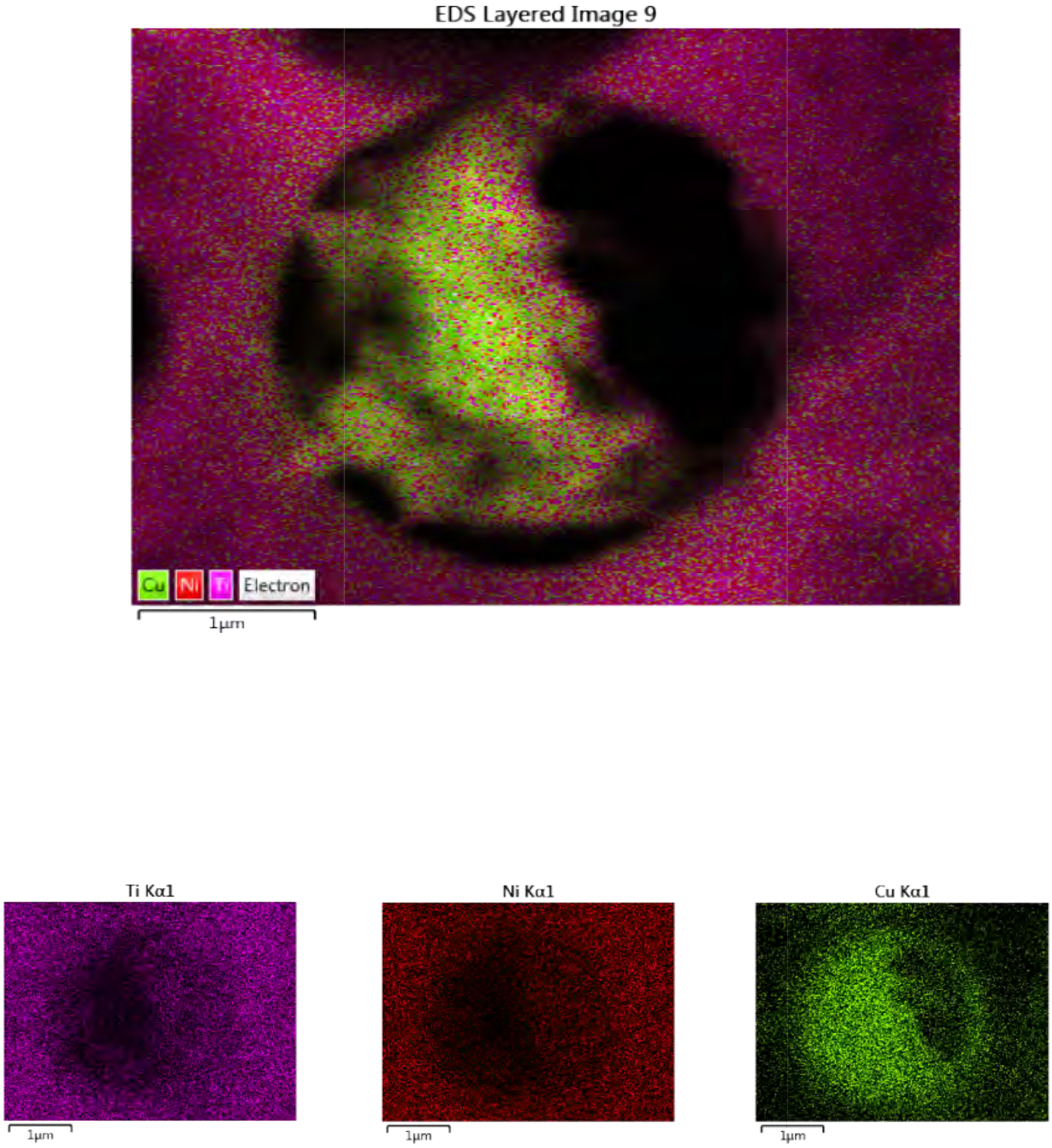

Fig.4.19. X -ray mapping of Fig.4.18. Cu -rich phase at the center of the image.

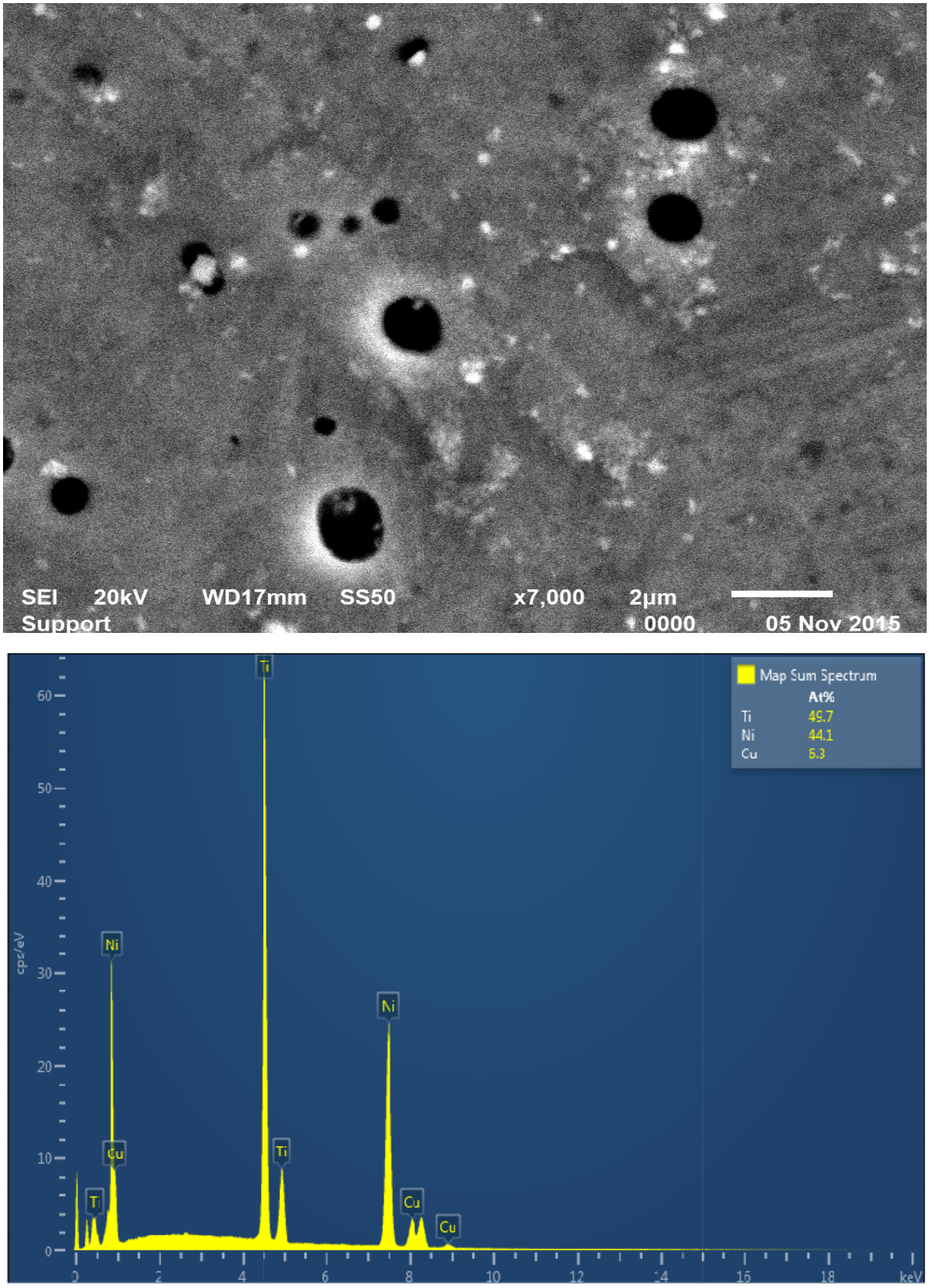

Fig.4.20. Microstructure alongside with overall EDX analysis

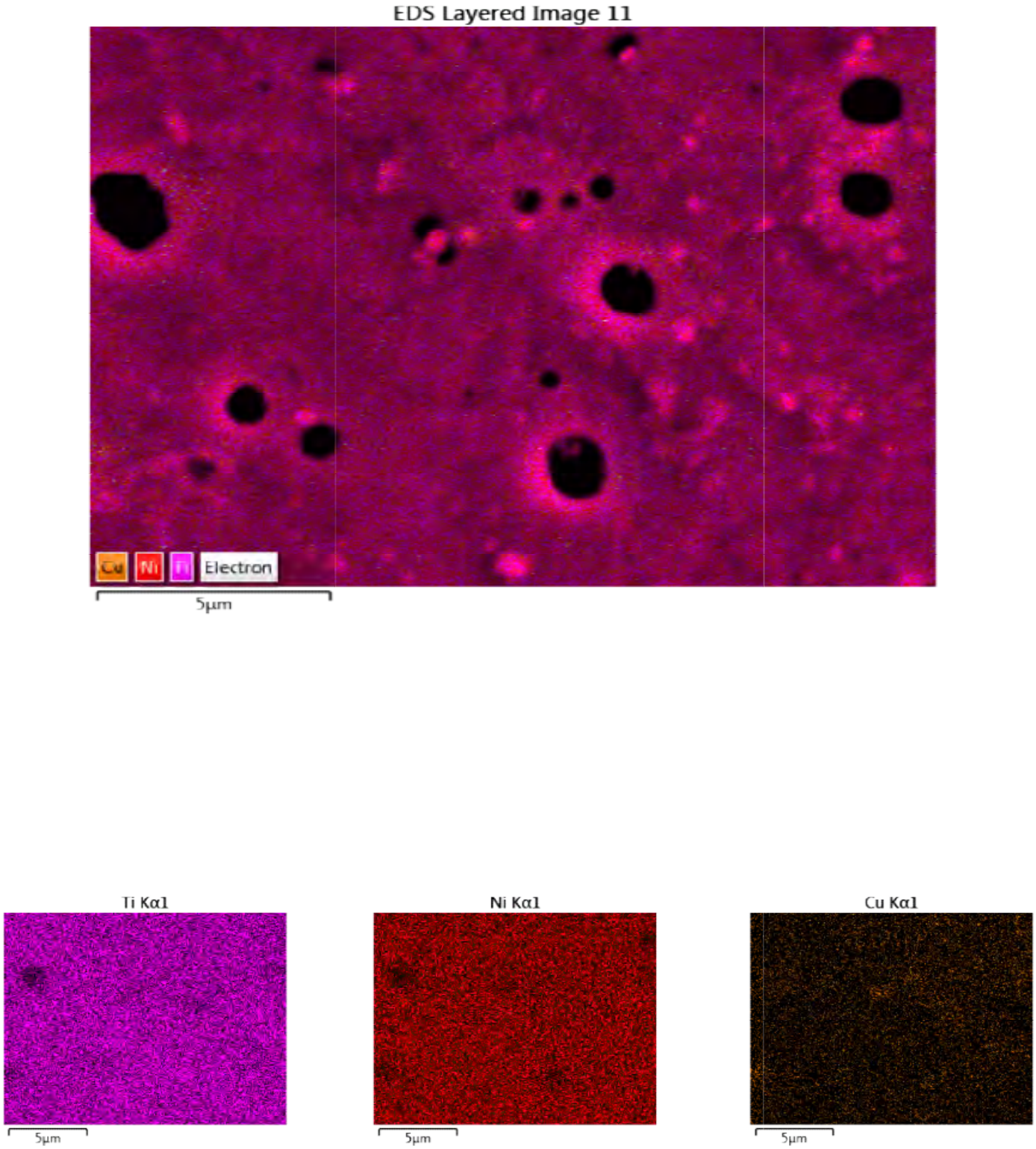

Fig.4.21. X-ray mapping of Fig.4.20

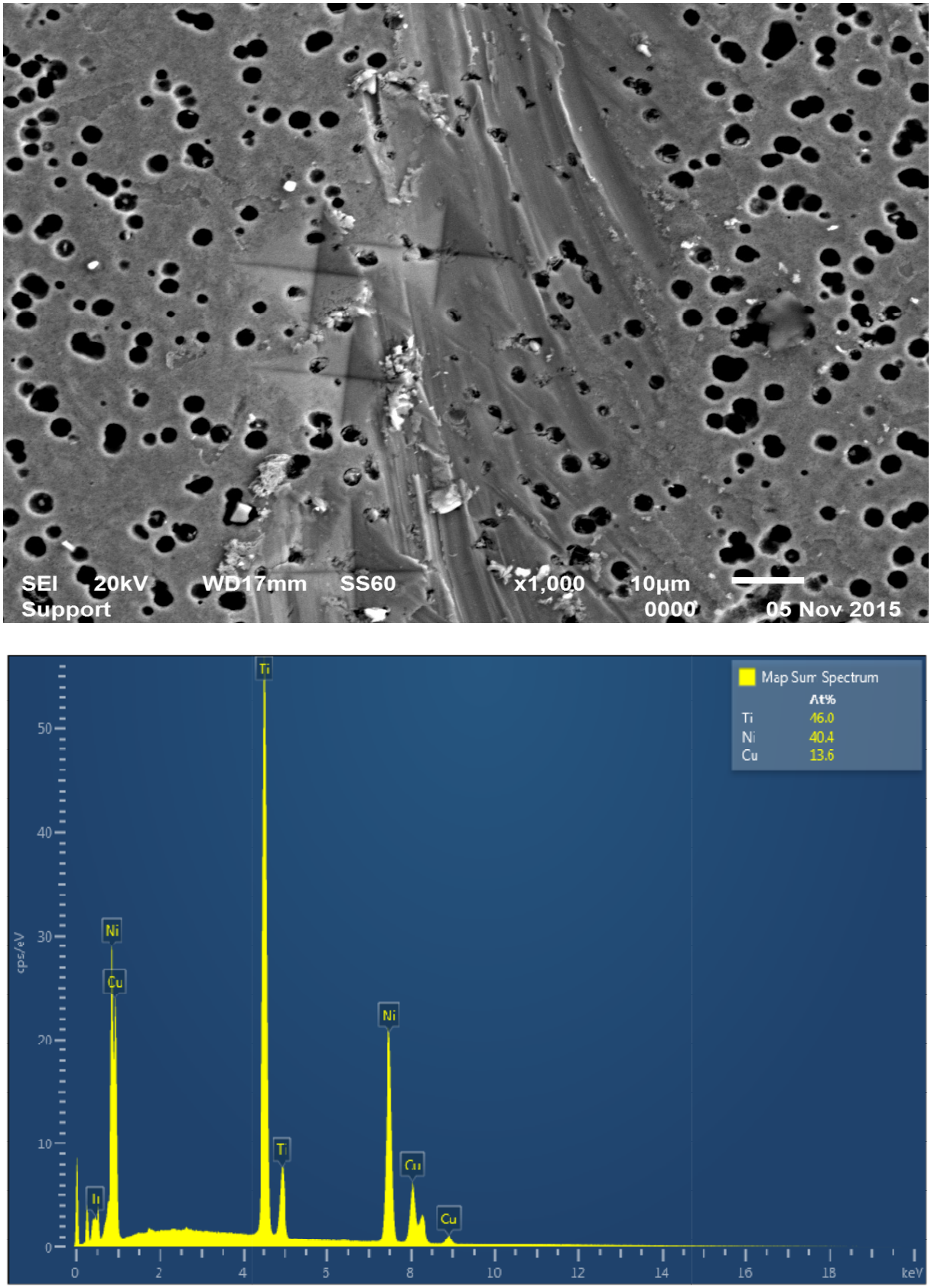

Fig.4.22. Microstructure of needle shape phase. The Vickers imprints are at the center of the image.

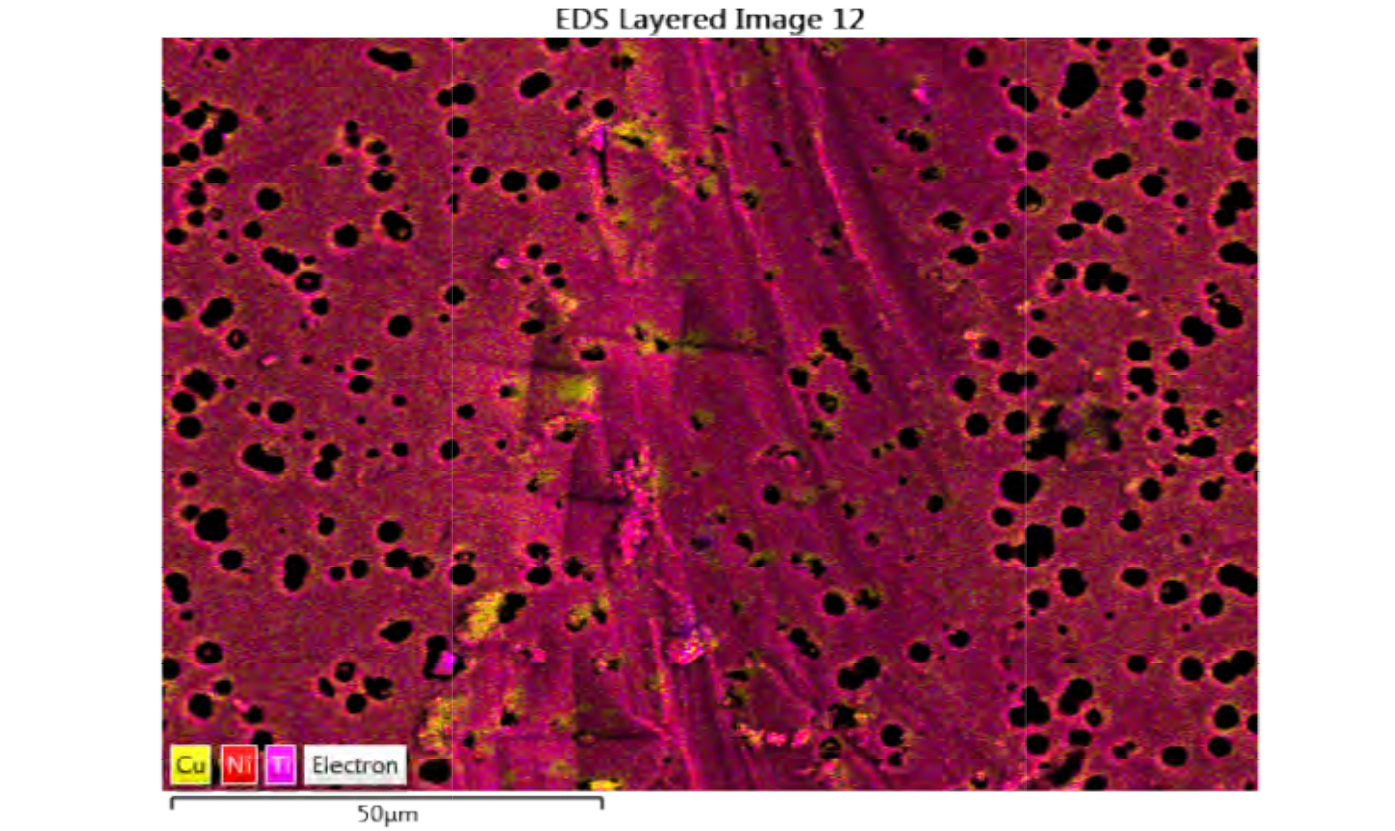

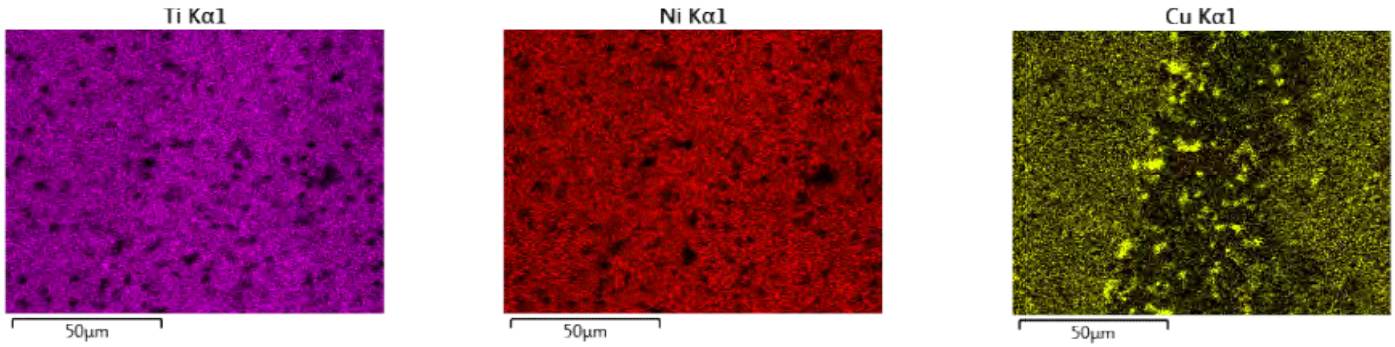

Fig.4.23. X-ray mapping of Fig.4.22

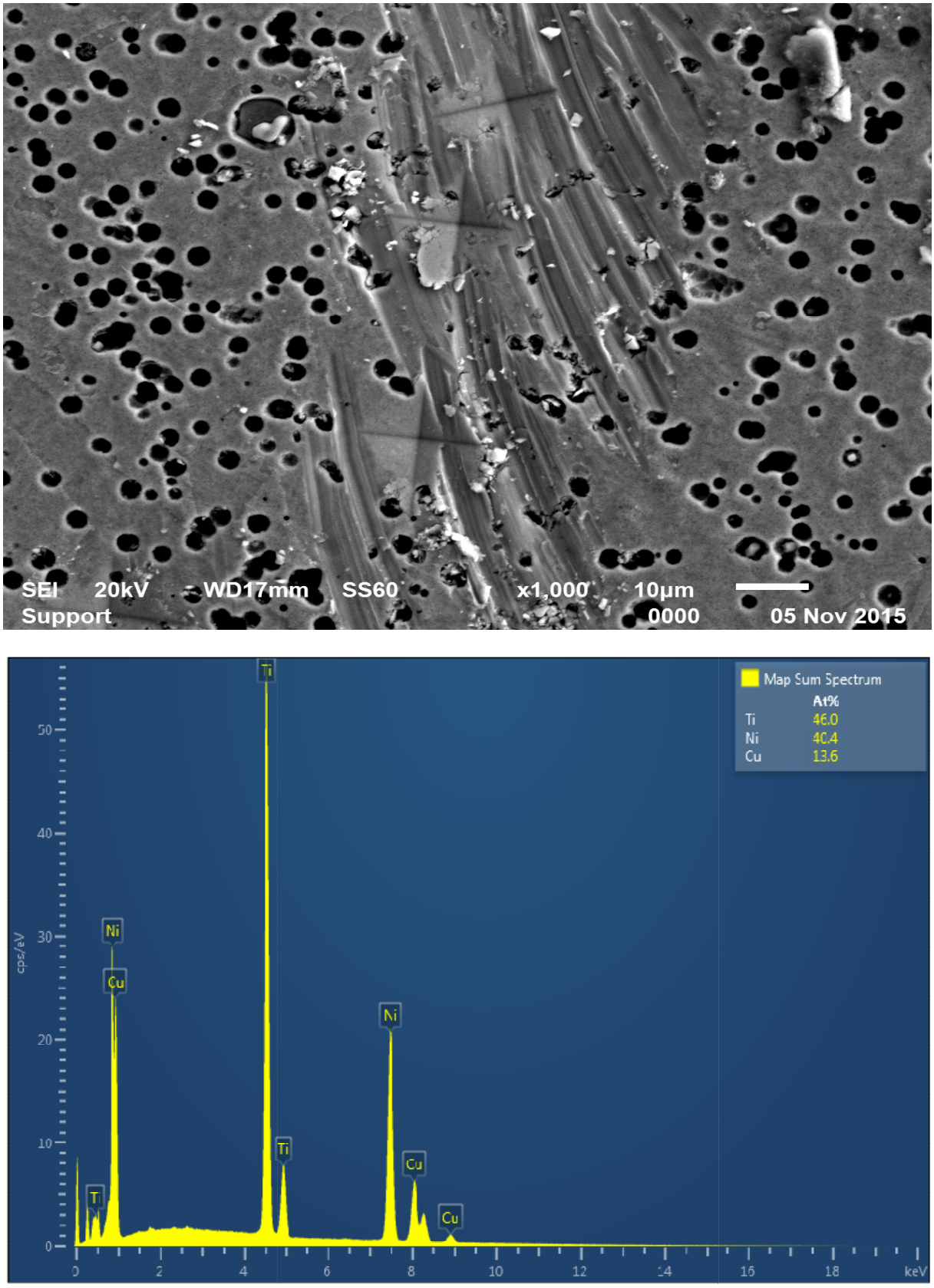

Fig.4.24. Microstructure of needle shape phase. Image similar to that of Fig. 4.22

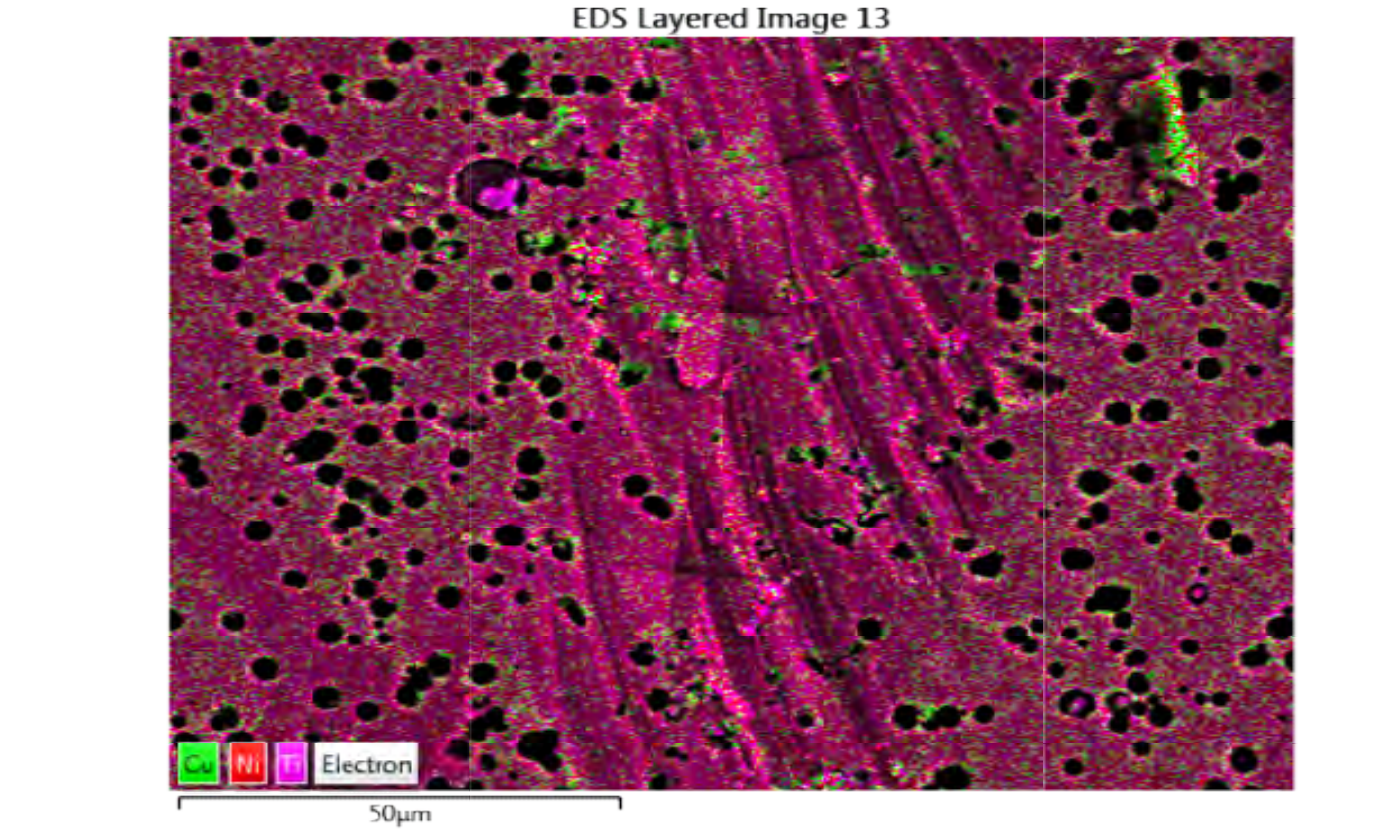

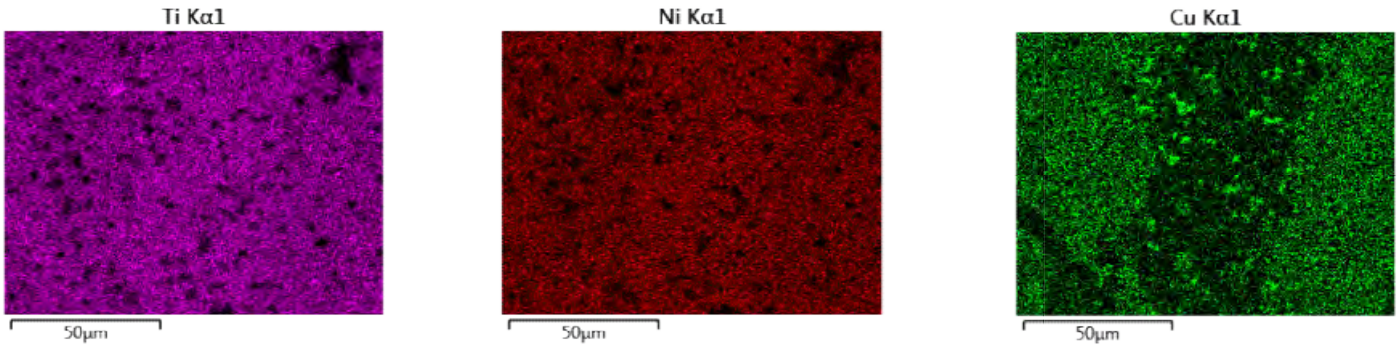

Fig.4.25. X-ray mapping of Fig.4.24

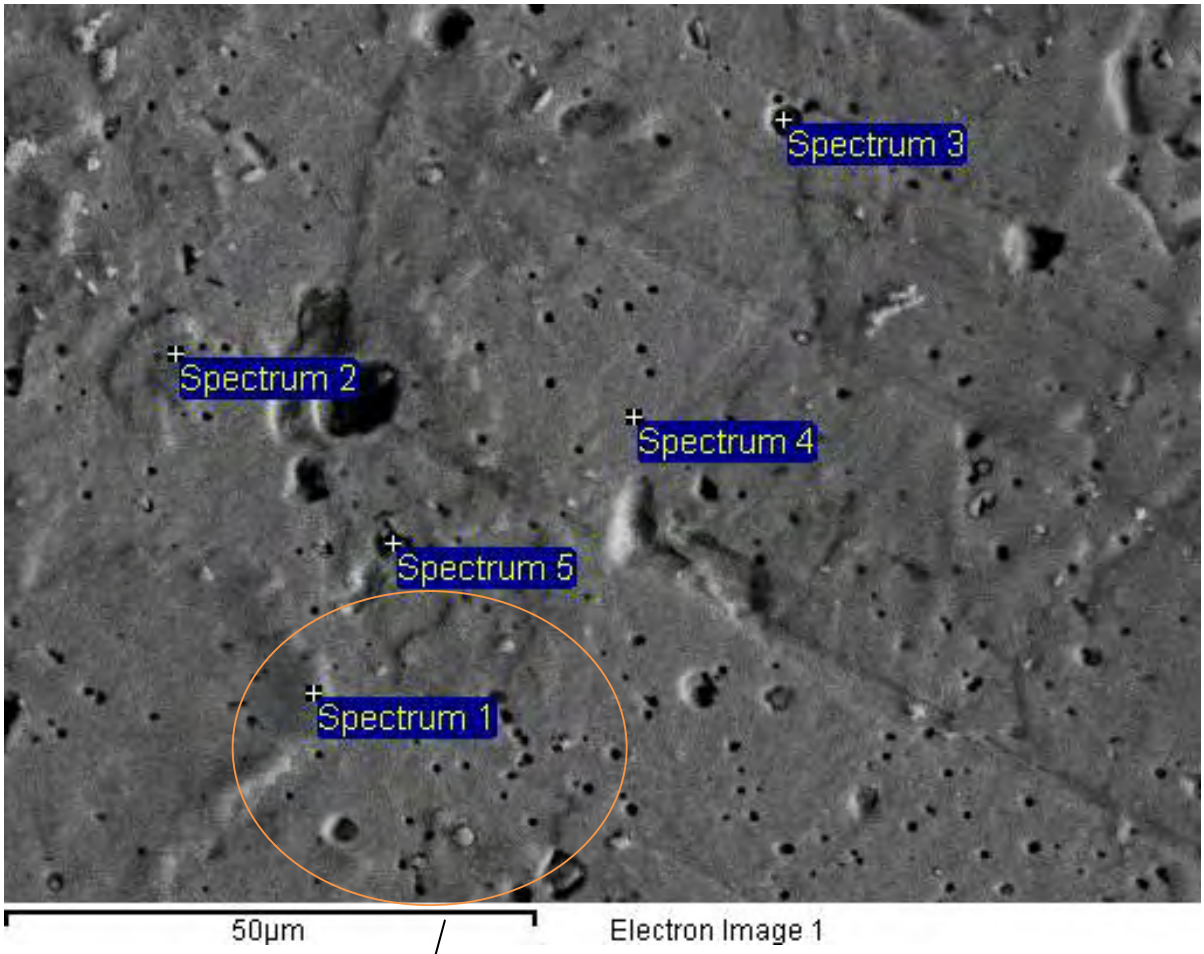

Spectrum	In stats.	Ti	Ni	Cu
Spectrum 1	Yes	46.93	44.20	8.87
Spectrum 2	Yes	50.66	45.35	3.99
Spectrum 3	Yes	49.27	41.45	9.29
Spectrum 4	Yes	48.45	41.92	9.62
Spectrum 5	Yes	53.29	38.84	7.87

Fig.4.26. Secondary Electron image, relevant quantitative EDX analysis

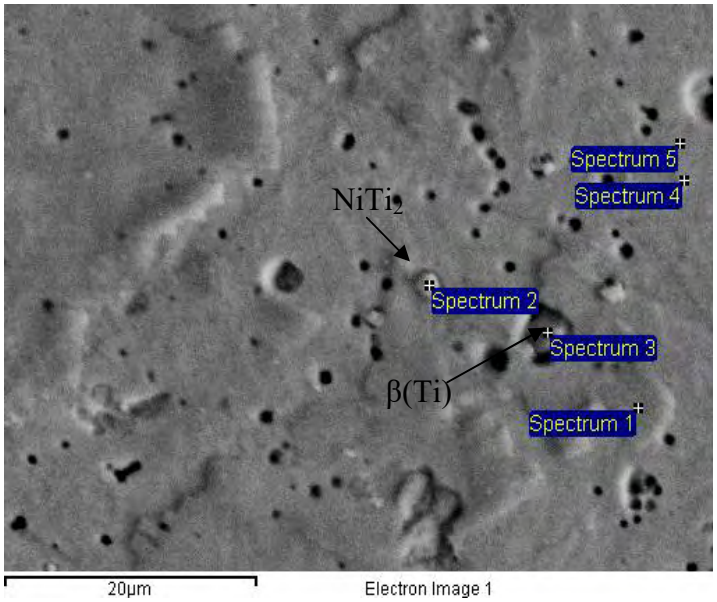

Spectrum	In stats.	Ti	Ni	Cu
Spectrum 1	Yes	50.26	45.40	4.33
Spectrum 2	Yes	59.43	32.52	8.05
Spectrum 3	Yes	82.61	10.89	6.50
Spectrum 4	Yes	47.13	42.71	10.16
Spectrum 5	Yes	49.62	39.99	10.39

Fig.4.27. Secondary Electron image associated with quantitative EDX analysis

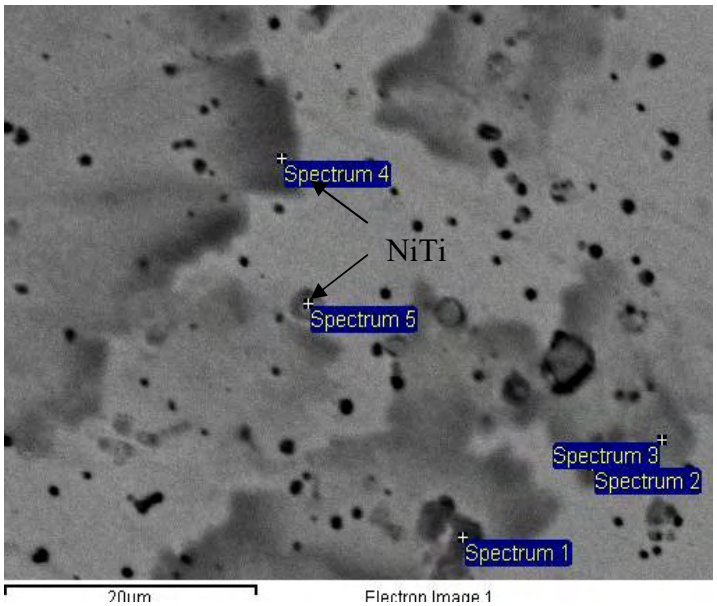

Spectrum	In stats.	Si	Ti	Ni	Cu
Spectrum 1	Yes	61.95	19.06	12.97	6.02
Spectrum 2	Yes	0.06	52.63	42.79	4.52
Spectrum 3	Yes	0.37	50.80	44.48	4.36
Spectrum 4	Yes	0.27	49.94	41.26	8.54
Spectrum 5	Yes	-0.07	47.97	40.93	11.17

Fig.4.28.Backscattered Electron image associated with EDX analysis on selected spots

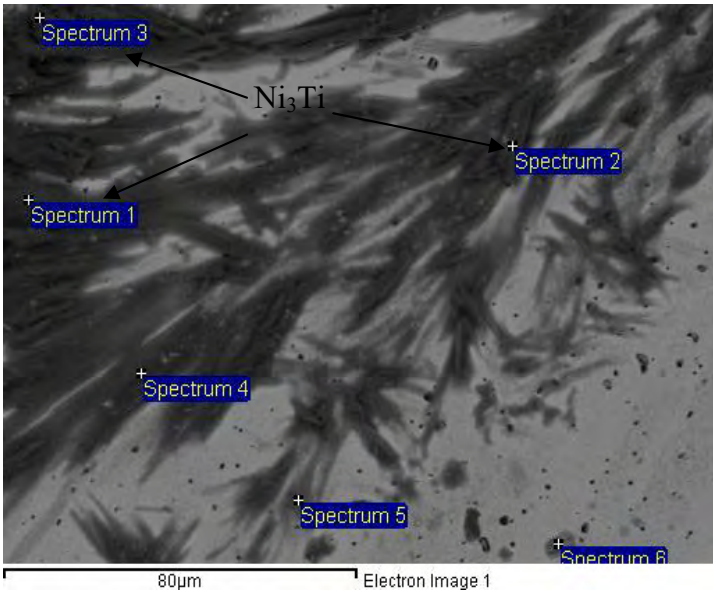

Spectrum	In stats.	Ti	Ni	Cu
Spectrum 1	Yes	25.35	73.26	1.38
Spectrum 2	Yes	16.13	78.15	5.72
Spectrum 3	Yes	10.57	87.45	1.99
Spectrum 4	Yes	38.35	57.78	3.87
Spectrum 5	Yes	40.13	48.18	11.69
Spectrum 6	Yes	35.27	29.08	35.64

Fig.4.29. Electron image – Element analysis

Phase		Molecular Weight	at % Ti	at % Ni	at % Cu	Composition Range
Bcc_B2, NiTi		106.4	44.9	55	-	Dissolves 43-50.5 at%Ti
$NiTi_2$	$(Cu_xNi_{1-x})Ti_2$, x=0	154.2	62	38	-	x=0-0.15, dissolves ~6%atCu
	$(Cu_xNi_{1-x})Ti_2$, x=0.15	155	61.6	32	6	
β(Ti)		47,8	100	-	-	dissolves, ~14at%Cu, ~10at%Ni
Ni_3Ti		223.6	21.3	78.6	-	Dissolves ~5%atCu

Table.3: The Ni-Ti-Cu solid phases considered in this work for specimen 2. [14]

4.3Microhardness Testing

4.3.1 Vickers Microhardness-Specimen 1: “Spring” shape

The Vickers method was conducted with a load of 200g. The results are represented in the following figures:

Specimen 1 (“spring” shape – longitudinal)

N°	HV 0.2
1	238
2	224
3	219
4	213
5	244
6	245
7	211
8	233
9	227
10	224
11	240
12	275
13	230
14	228
15	231

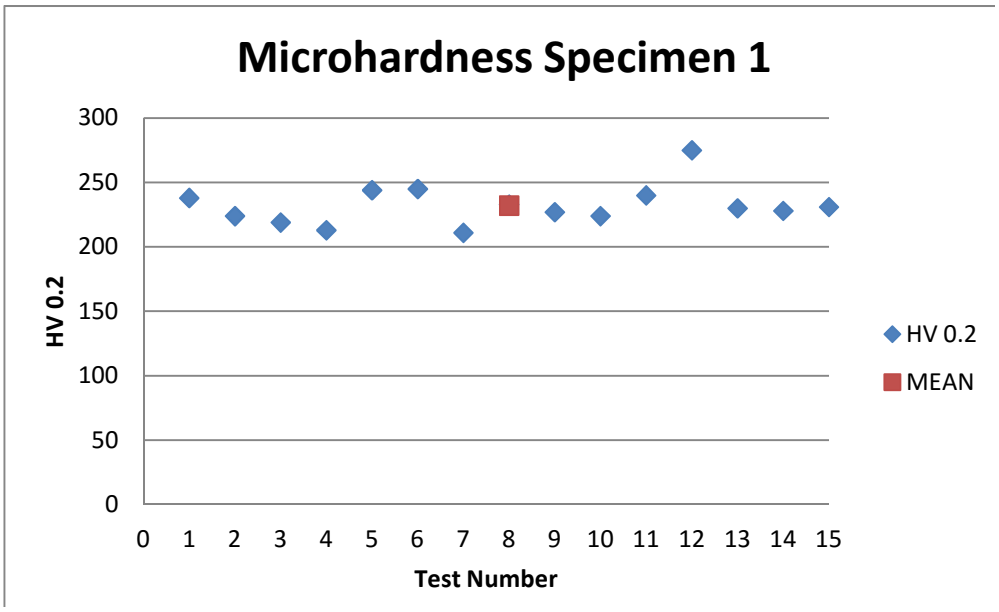

Fig.4.30: Microhardness results for specimen 1 “spring”

Mean: 232 Stdev: 15

Specimen 1γ ("spring" shape – transverse)

N°	HV 0.2
1	188
2	200
3	206
4	211
5	220
6	214
7	206
8	210
9	205
10	205
11	218
12	226
13	208
14	217
15	222

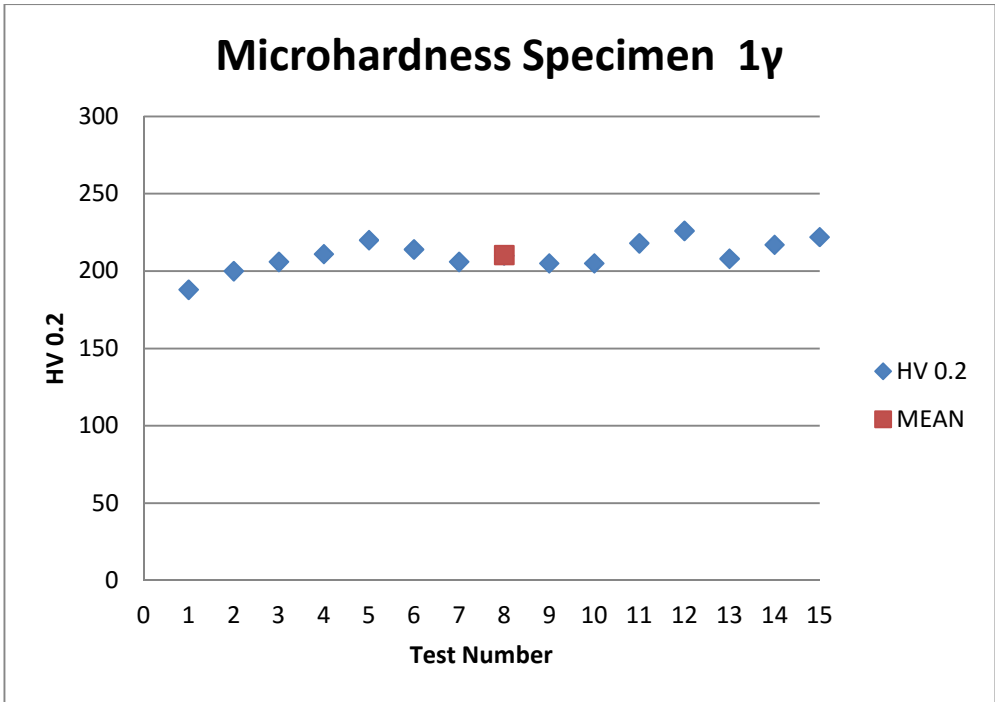

Fig.4.31: Microhardness results for specimen 1 "spring" Mean:210 Stdev: 9,62

4.3.2 Vickers Microhardness-Specimen 2: “Wire” shape

Specimen 2 (“wire” shape – longitudinal)

N°	HV 0.2
1	251
2	234
3	239
4	225
5	220
6	219
7	205
8	218
9	203
10	209
11	241
12	235
13	245
14	271
15	236

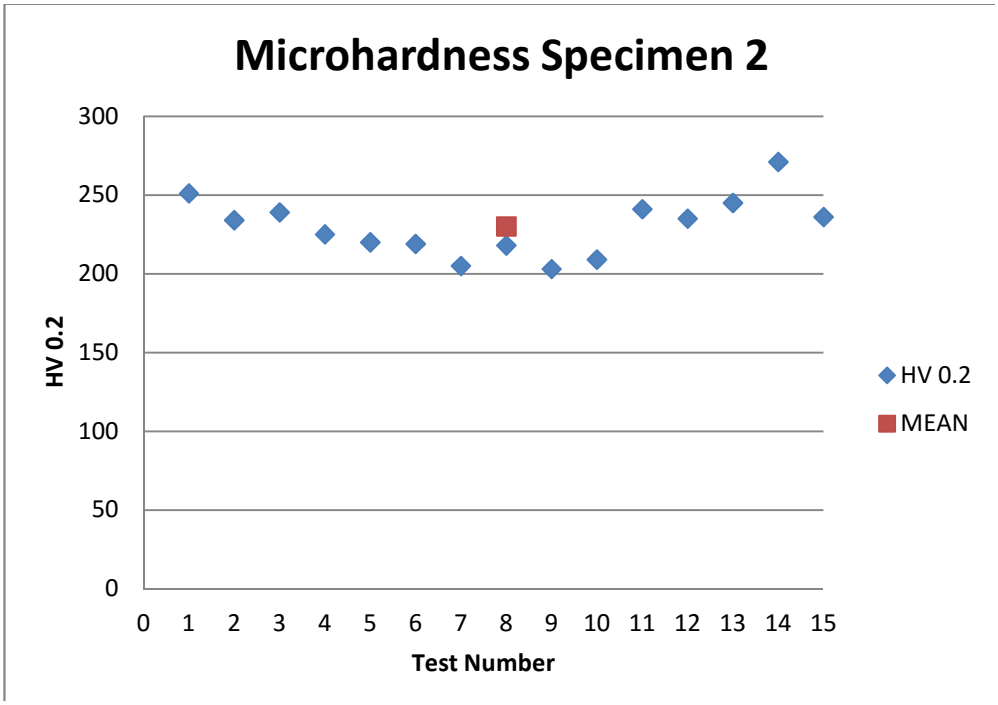

Fig.4.32: Microhardness results for specimen 2 “wire” Mean: 230 Stdev: 18, 53

Specimen 2α ("wire" shape – transverse)

N°	HV0,2
1	205
2	196
3	197
4	191
5	207
6	191
7	195
8	230
9	234
10	211
11	241
12	213
13	201
14	203
15	201

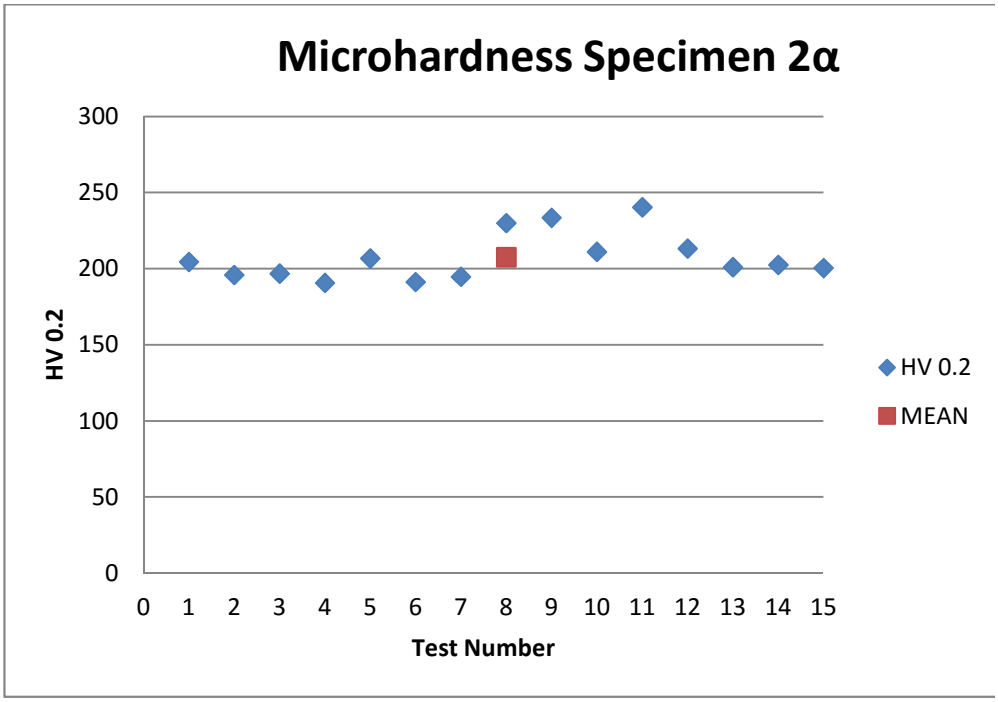

Fig.4.33: Microhardness results for specimen 2 "wire" Mean: 207 Stdev: 15,64

In addition microhardness measurements were carried out on selected areas of specimen #2, where differences were observed during the metallographic evaluation **(Figs.4.9, 4.10)**

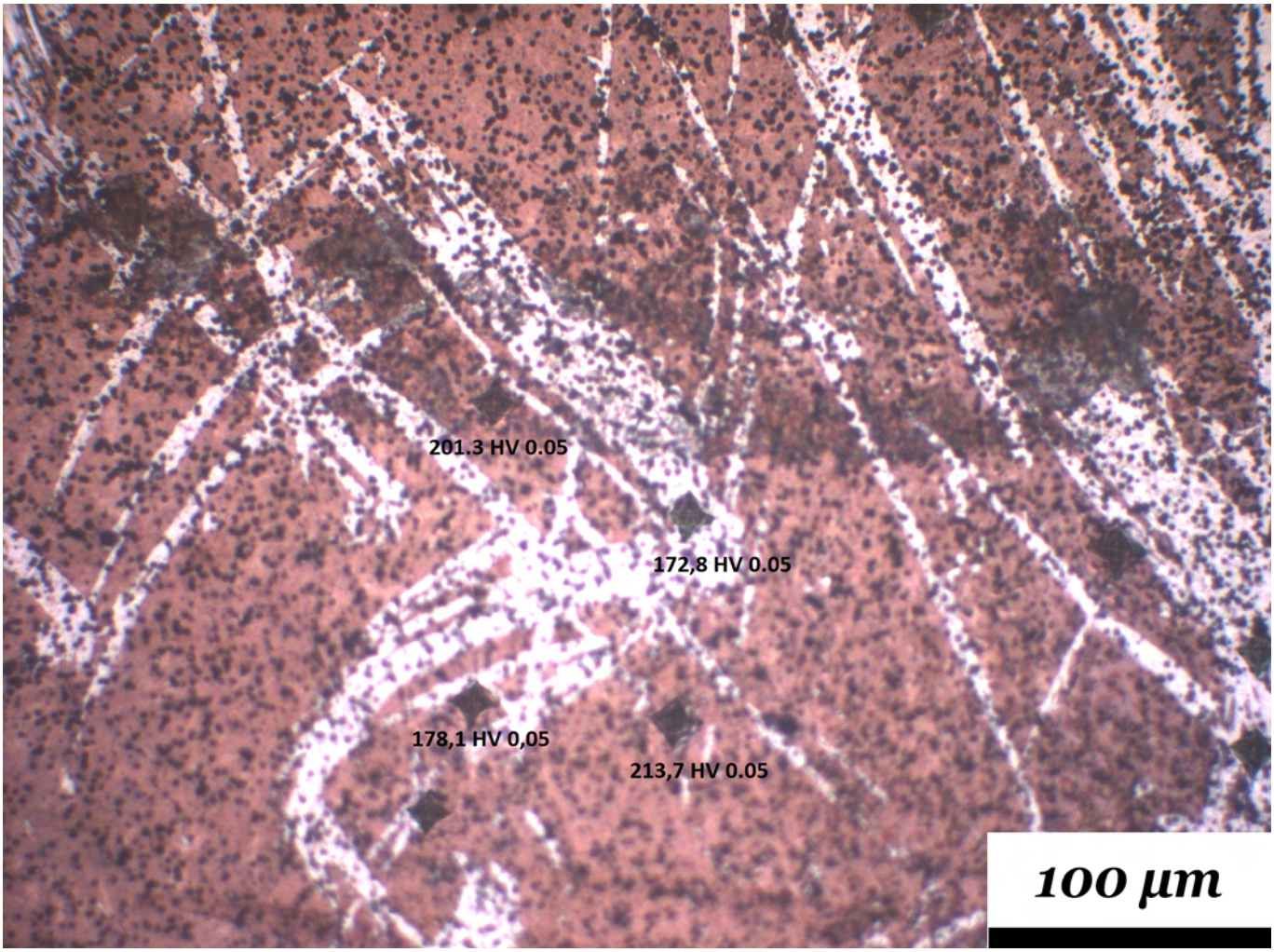

Fig.4.34: Microhardness imprints

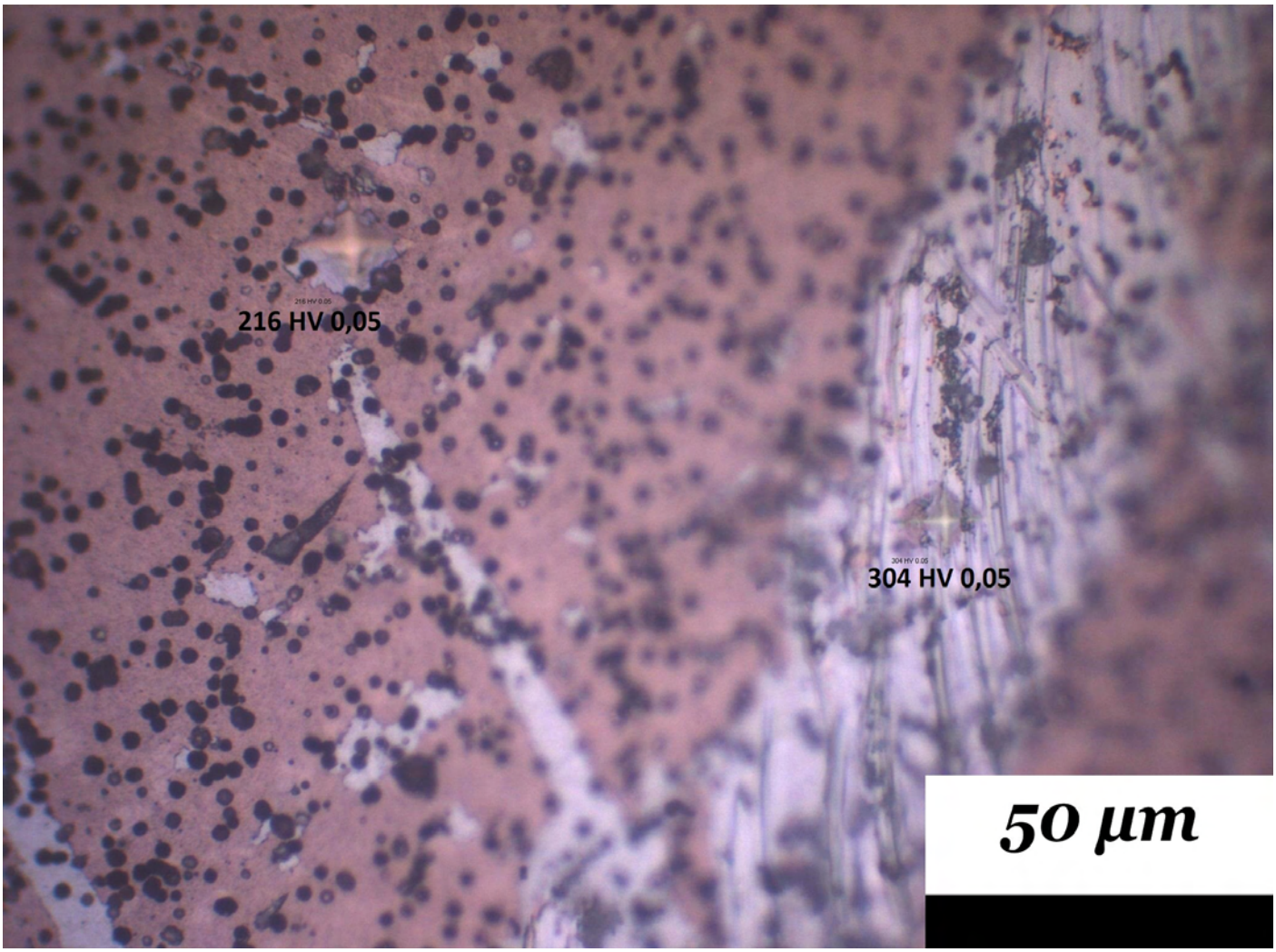

Fig.4.35: Microhardness imprints on the needles

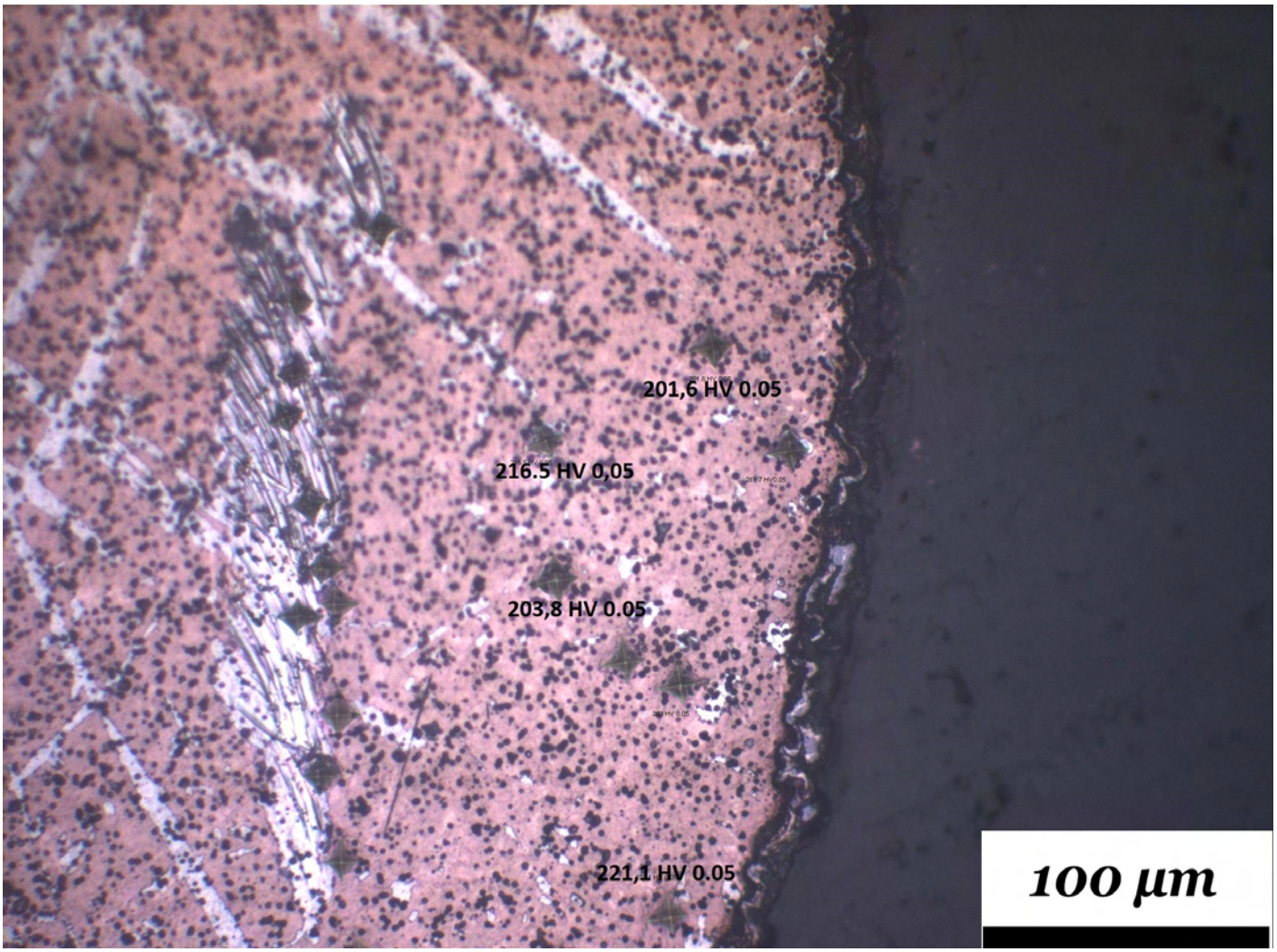

Fig.4.36: Microhardness imprints close to the surface of specimen #2 (wire)

4.4Knoop Microhardness – Modulus of Elasticity

Knoop microhardness measurements were conducted with a load of 50, 200 and 500g on both specimens and the results are given hereinafter:

4.4.1 Knoop Microhardness Specimen #1 “spring” shape

Table.4: Knoop measurements on specimen #1 “spring” shape

Load	Section	Number	HK (kgf)	HK* (GPa)
50g	*Longitudinal*	1	215	2,1
		2	220	2,2
		3	173	1,7
		4	141	1,4
		5	153	1,5
		6	228	2,2
		7	187	1,8
		8	157	1,5
		9	176	1,7
		10	167	1,6
	Transverse	1	215	2,1
		2	211	2,1
		3	208	2
		4	203	2
		5	200	2
		6	176	1,7
		7	168	1,7
		8	159	1,6
		9	170	1,7
		10	226	2,2
200g	*Longitudinal*	1	167	1,6
		2	153	1,5
		3	143	1,4
		4	163	1,6
		5	158	1,5
		6	193	1,9
		7	159	1,6
		8	136	1,3
		9	228	2,2
		10	163	1,6
	Transverse	1	217	2,1
		2	215	2,1
		3	254	2,5
		4	155	1,5
		5	146	1,4
		6	214	2,1
		7	237	2,3
		8	152	1,5
		9	136	1,3
		10	162	1,6

500g	*Longitudinal*	1	152	1,5
		2	134	1,3
		3	168	1,7
		4	135	1,3
		5	145	1,4
		6	143	1,4
		7	129	1,3
		8	112	1,1
		9	163	1,6
		10	136	1,3
	Transverse	1	135	1,3
		2	14,	1,4
		3	116	1,1
		4	129	1,3
		5	135	1,3
		6	131	1,3
		7	126	1,2
		8	126	1,2
		9	131	1,3
		10	137	1,3

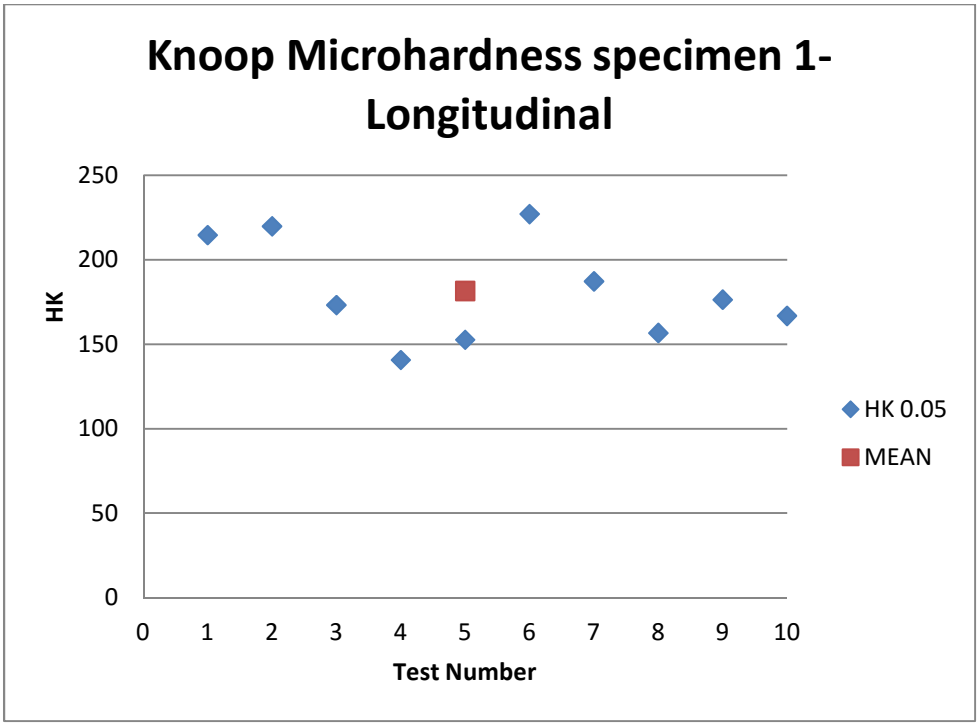

Fig.4.37:Knoop Microhardness results for specimen 1 "spring shape", also given in Table.4

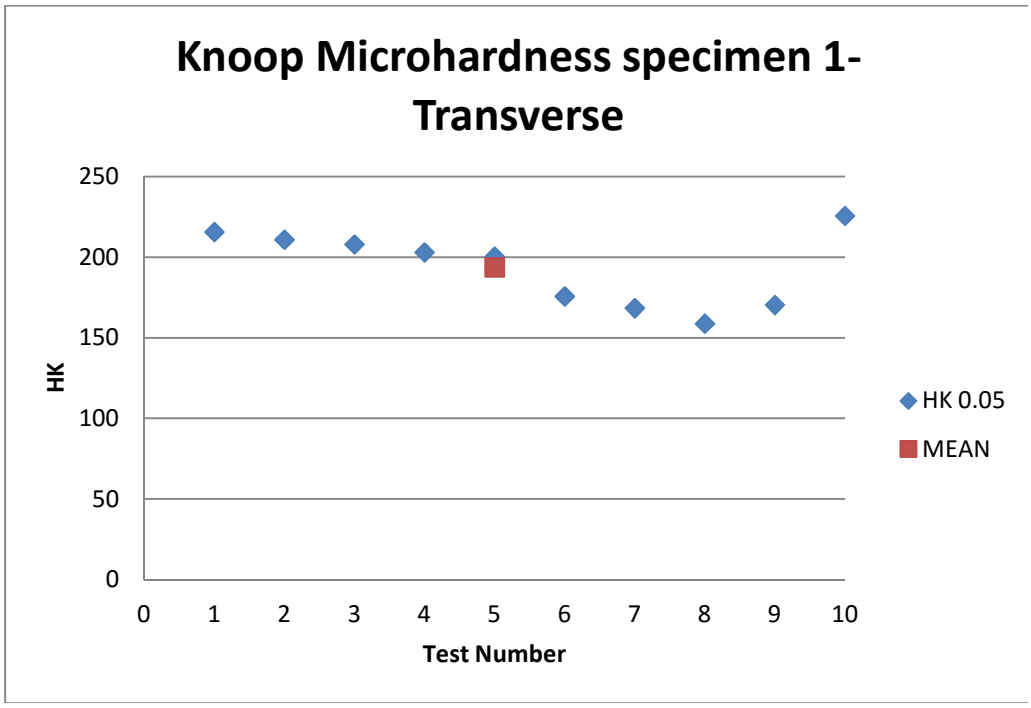

Fig.4.38:Knoop Microhardness results for specimen 1 "spring shape", also given in Table.4

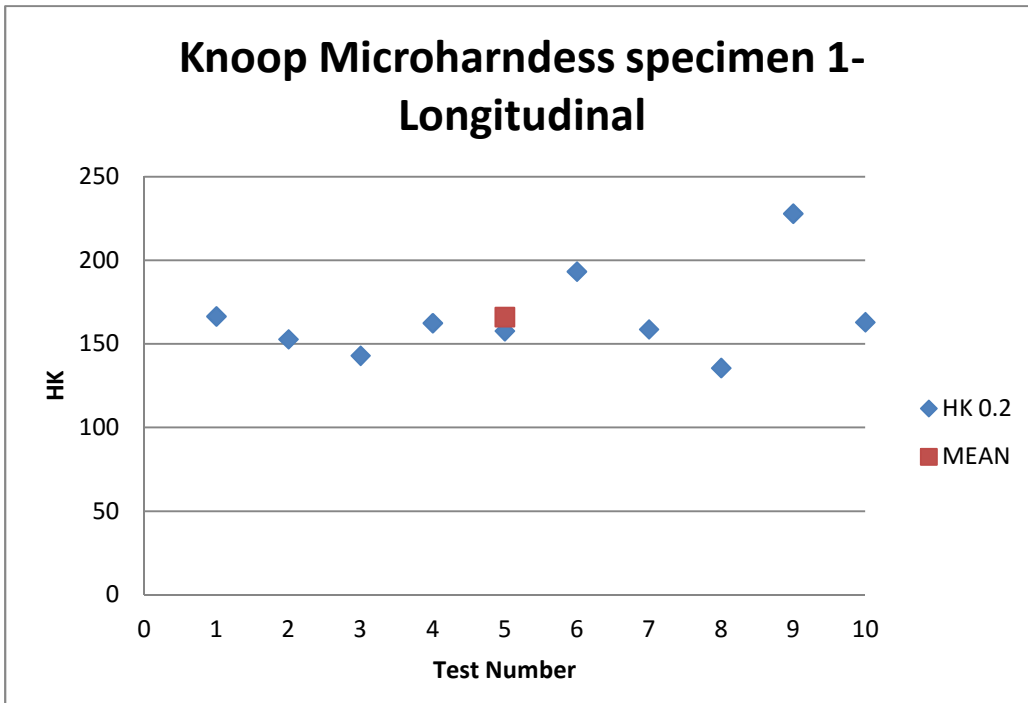

Fig.4.39:Knoop Microhardness results for specimen 1 "spring shape", also given in Table.4

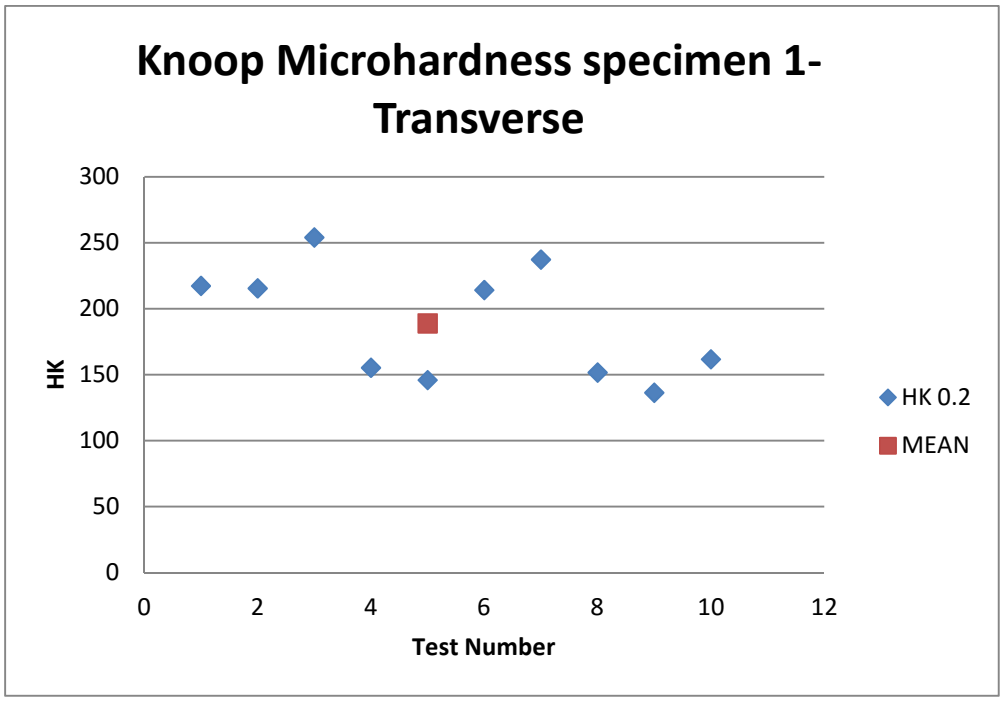

Fig.4.40:Knoop Microhardness results for specimen 1 "spring shape", also given in Table.4

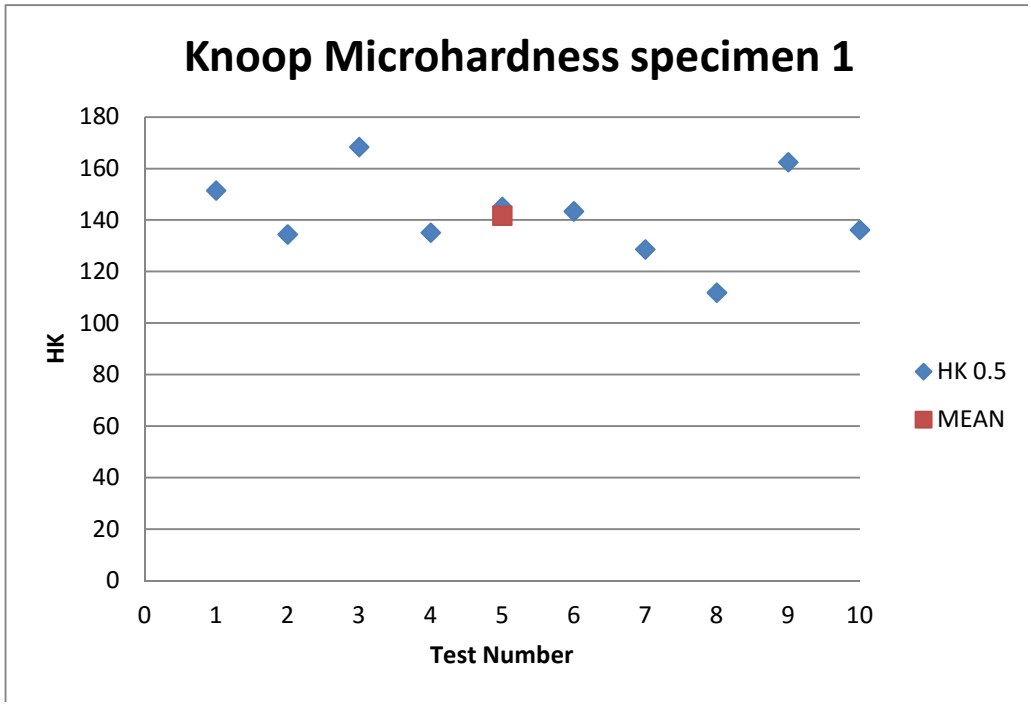

Fig.4.41:Knoop Microhardness results for specimen 1 "spring shape", also given in Table.4

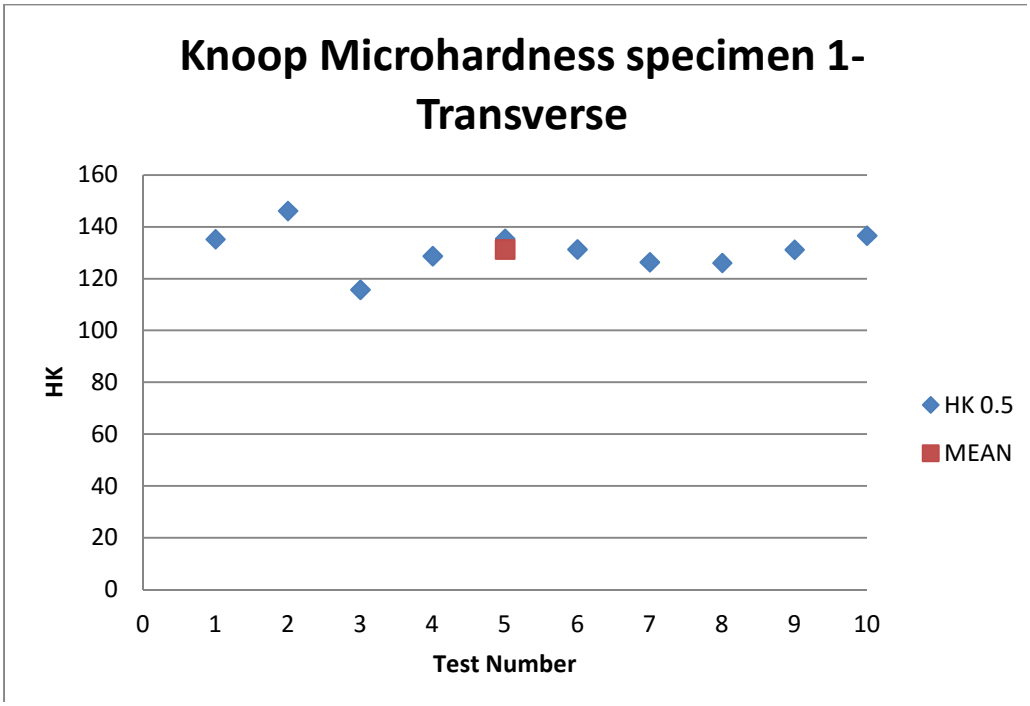

Fig.4.42:Knoop Microhardness results for specimen 1 "spring shape", also given in Table.4

4.4.2 Modulus of Elasticity Specimen #1 “spring” shape

Table.5: Modulus of Elasticity specimen #1 “spring” shape

Load	Section	Number	Modulus of Elasticity		
			E1 (a=0.34)	***E2 (a=0.45)***	***E3 (a=1.5)***
50g	*Longitudinal*	1	39,9	52,8	176,2
		2	25,1	33,2	110,8
		3	45,1	59,7	199,3
		4	16,2	21,5	71,8
		5	63,8	84,5	281,8
		6	34,7	45,9	153
	Transverse	1	59,4	78,6	262,1
		2	119,4	158	526,8
		3	30,3	40,1	133,6
200g	*Longitudinal*	1	9	12	40
		2	10,8	14,4	48
		3	13,3	17,6	58,9
		4	23,7	31,4	104,8
		5	21,4	28,3	94,5
		6	18,2	24,1	80,3
		7	7,4	9,8	32,8
		8	37,9	50,1	167,2
		9	16	21,2	70,7
	Transverse	1	65,5	86,7	289,1
		2	34,3	45,4	151,6
500g	*Longitudinal*	1	22,1	29,3	97,7
		2	7,6	10,1	33,7
		3	30,8	40,8	136
		4	9,4	12,5	41,6
		5	12,8	16,9	56,5
		6	10,1	13,4	44,8
		7	9,1	12	40,2
		8	5,9	7,8	26,1
		9	16,4	21,7	72,4
		10	11	14,6	48,7
	Transverse	1	33,6	44,5	148,5
		2	47,1	62,4	208,1
		3	7,1	9,4	31,6
		4	7,6	10,1	33,9
		5	8,8	11,7	39
		6	8,1	10,7	35,8
		7	8,1	10,7	35,9
		8	7,8	10,3	34,4
		9	10	13,3	44,4
		10	10,3	13,7	45,8

4.4.3 Knoop Microhardness Specimen #2 “wire” shape

Table.6: Knoop measurements on specimen #2 “wire” shape

Load	Section	Number	HK (kgf)	HK* (GPa)
50g	*Longitudinal*	1	154	1,5
		2	153	1,5
		3	144	1,4
		4	154	1,5
		5	176	1,7
		6	169	1,7
		7	195	1,9
		8	194	1,9
		9	213	2,9
		10	192	1,9
	Transverse	1	162	1,6
		2	157	1,5
		3	142	1,4
		4	164	1,6
		5	163	1,6
		6	127	1,2
		7	153	1,5
		8	176	1,7
		9	125	1,2
		10	148	1,5
200g	*Longitudinal*	1	134	1,3
		2	170	1,7
		3	114	1,1
		4	98	1
		5	126	1,2
		6	113	1,1
		7	134	1,3
		8	141	1,4
		9	174	1,7
		10	122	1,2
	Transverse	1	124	1,2
		2	113	1,1
		3	120	1,8
		4	135	1,3
		5	126	1,2
		6	134	1,3
		7	202	2
		8	137	1,3
		9	131,	1,3
		10	170	1,7

500g	*Longitudinal*	1	383	3,8
		2	151	1,5
		3	144	1,4
		4	133	1,3
		5	136	1,3
		6	129	1,3
		7	135	1,3
		8	141	1,4
		9	204	2
		10	262	2,6
	Transverse	1	148	1,5
		2	117	1,2
		3	154	1,2
		4	154	1,2
		5	120	1,2
		6	154	1,5
		7	147	1,4
		8	132	1,3
		9	132	1,3
		10	133	1,3

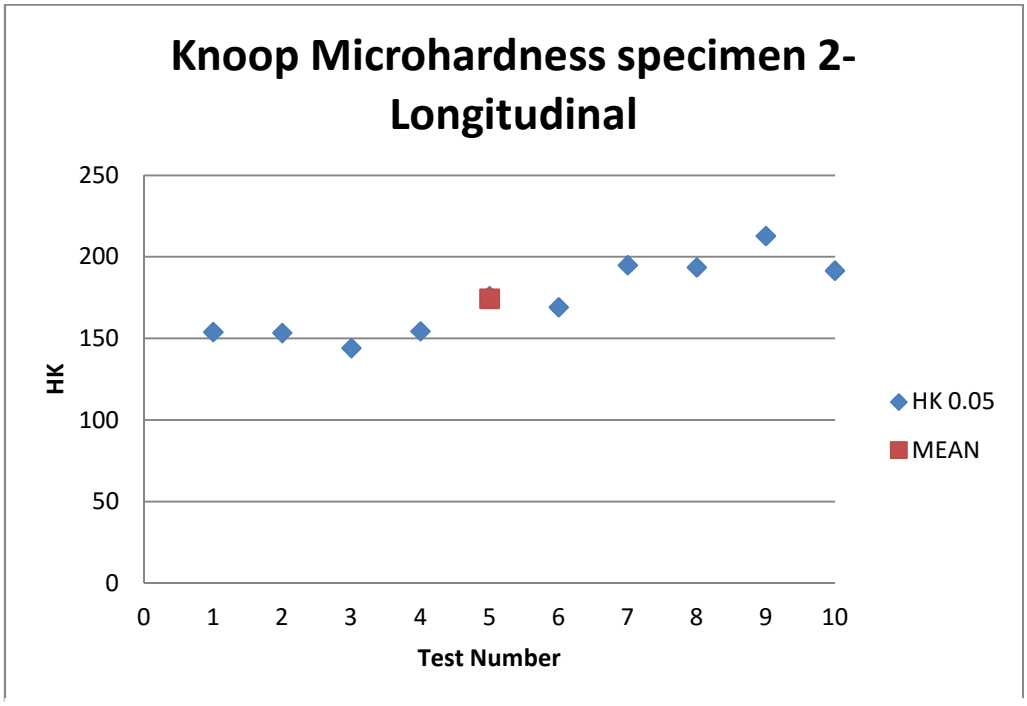

Fig.4.43:Knoop Microhardness results for specimen 2 "wire shape", also given in Table.6

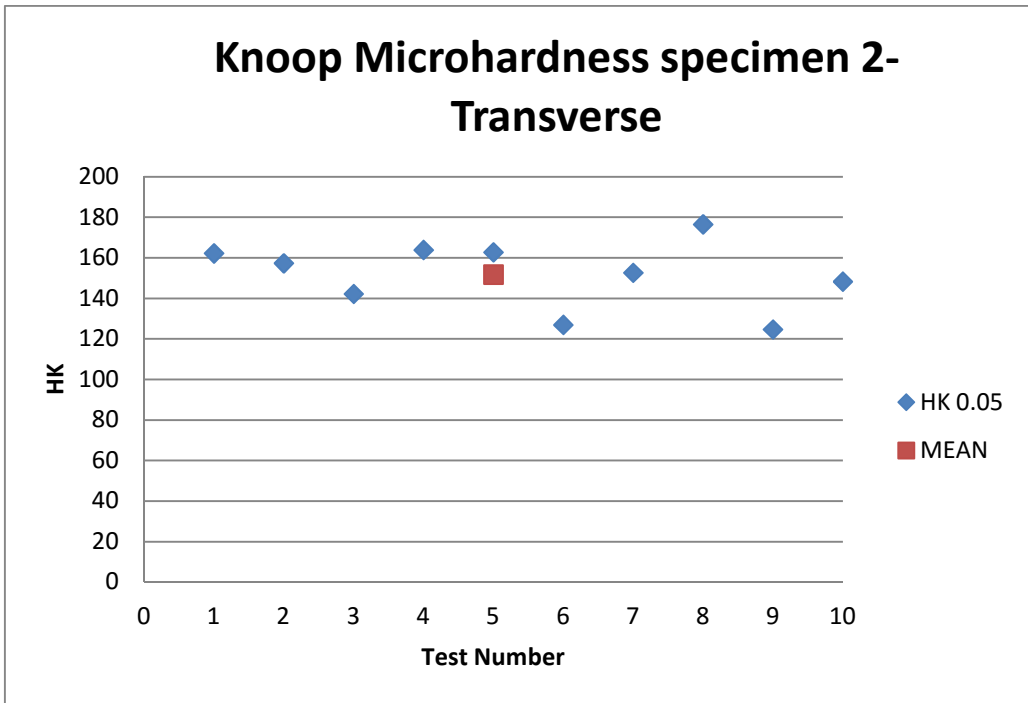

Fig.4.44:Knoop Microhardness results for specimen 2 "wire shape", also given in Table.4

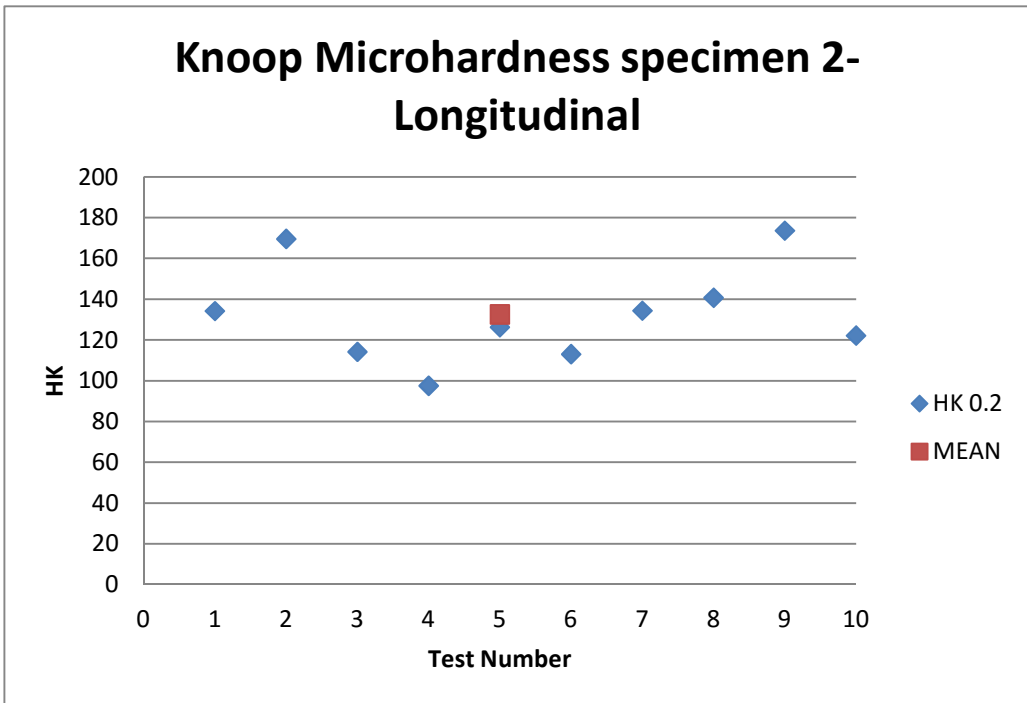

Fig.4.45:Knoop Microhardness results for specimen 2 "wire shape", also given in Table.4

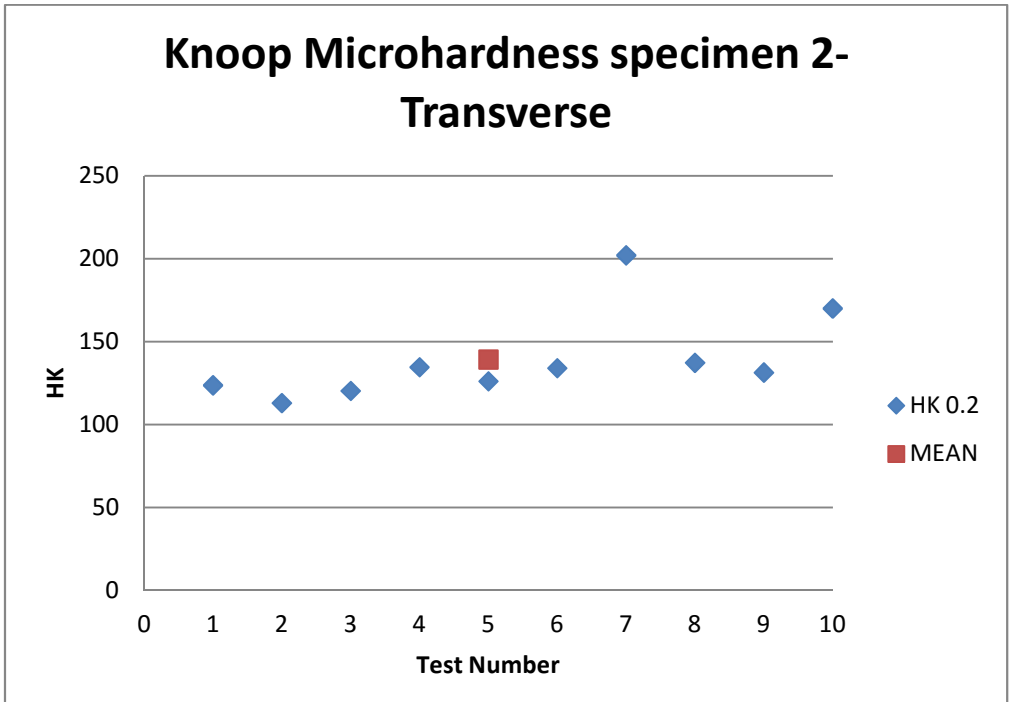

Fig.4.46:Knoop Microhardness results for specimen 2 "wire shape", also given in Table.4

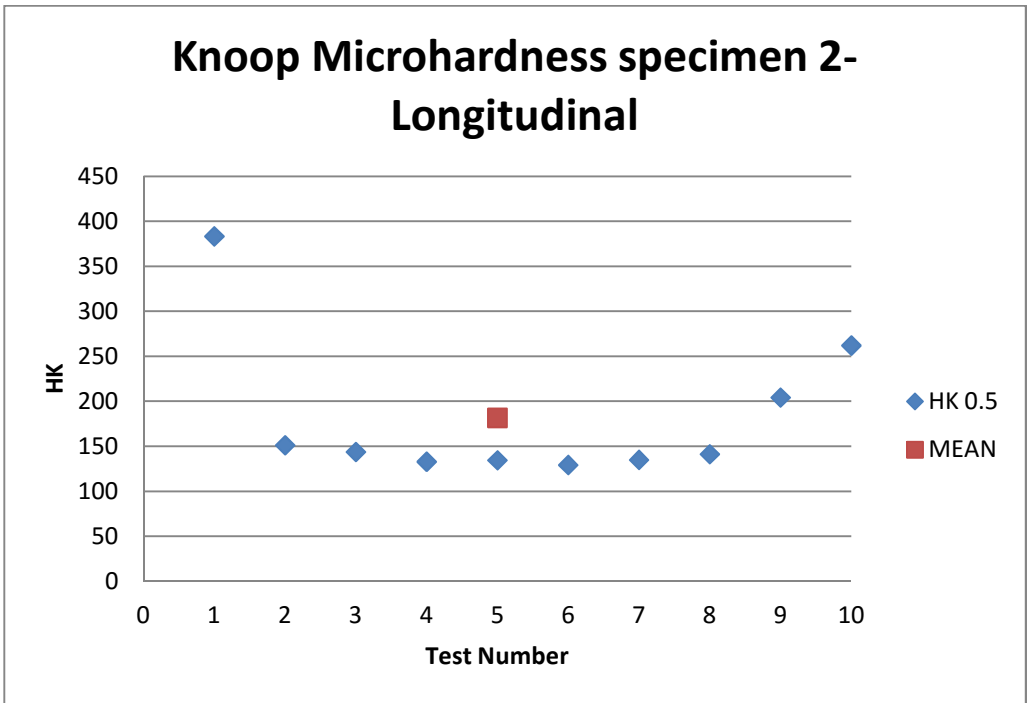

Fig.4.47:Knoop Microhardness results for specimen 2 "wire shape", also given in Table.4

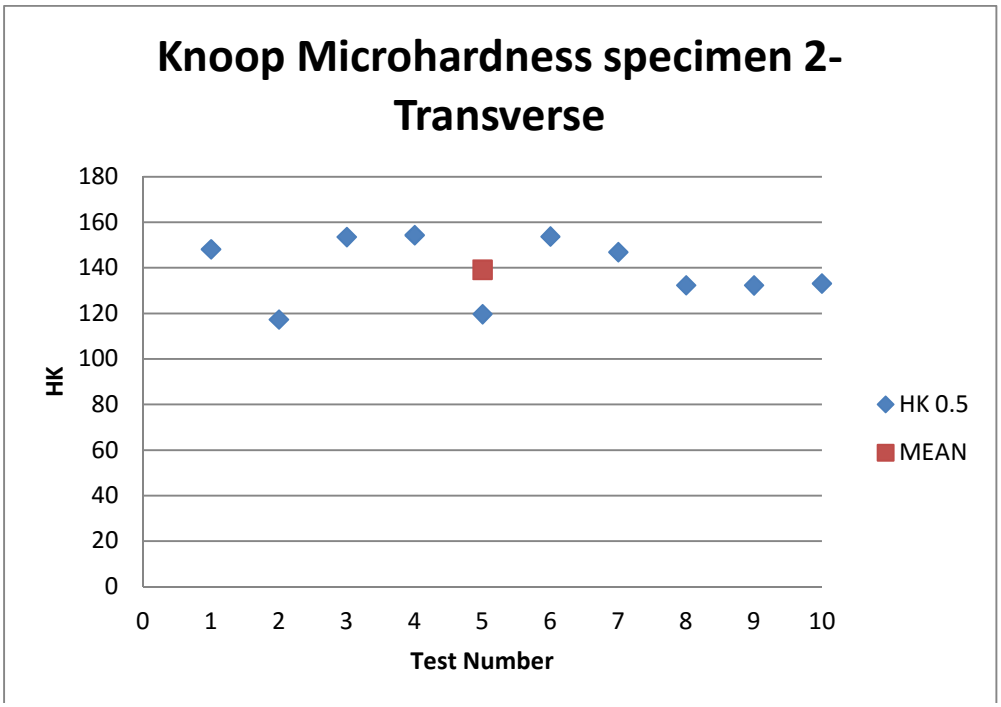

Fig.4.48:Knoop Microhardness results for specimen 2 "wire shape", also given in Table.4

4.4.4 Modulus of Elasticity Specimen #2 “wire” shape

Table.7: Modulus of Elasticity specimen #2 “wire” shape

Load	Section	Number	Modulus of Elasticity		
			E1(a=0.34)	***E2(a=0.45)***	***E3(a=1.5)***
50g	*Transverse*	1	15,1	20	66,8
		2	29,7	39,3	131,2
		3	18,9	25	83,5
		4	22,3	29,5	98,5
		5	32,9	43,6	145,5
		6	13,9	18,4	61,3
		7	19,8	26,2	87,5
200g	*Longitudinal*	1	10,3	13,6	45,5
		2	17,4	23,1	77,1
		3	6,1	8,1	27
		4	4	5,2	17,6
		5	9,4	12,5	41,8
		6	8,2	10,9	36,5
		7	11,7	15,5	51,7
		8	12	15,9	53
		9	18,1	24	80
		10	7	9,2	30,9
	Transverse	1	12,2	16,1	53,9
		2	15,4	20,5	68,3
		3	16	21,2	70,8
		4	102,7	135,9	453,2
		5	15,1	20	66,6
		6	56,5	74,8	249,6
		7	22,8	30,1	100,6
		8	22,3	29,6	98,8
500g	*Longitudinal*	1	321,8	88	1419,8
		2	17,2	42,5	76,3
		3	27,6	36,5	121,9
		4	15,2	37,3	67,2
		5	13,2	39,5	58,3
		6	9,7	42	42,9
		7	11,9	41,1	52,7
		8	13	42,3	57,7
		9	66,6	49,1	294
		10	182,3	60,5	804,3
	Transverse	1	17,1	22,6	75,4
		2	40,3	53,3	177,8
		3	48,4	64,1	213,7
		4	42,7	56,5	188,4
		5	54,1	71,6	238,8

4.5Differential Scanning Calorimetry

In both samples DSC measurements were performed in order to determine the critical temperatures i.e.:

- As : Austenite start temperature
- Af: Austenite finish temperature
- Ms: Martenstite start temperature
- Mf: Martenstite finish temperature

The results from specimen #1 "spring" shape are depicted in **Fig.4.37,** while the results from specimen #2 "wire" shape are given in **Fig.4.38.** A comparative plot of both samples is provided in **Fig.4.39.** The results for each specimen are summarized in **Table.8**

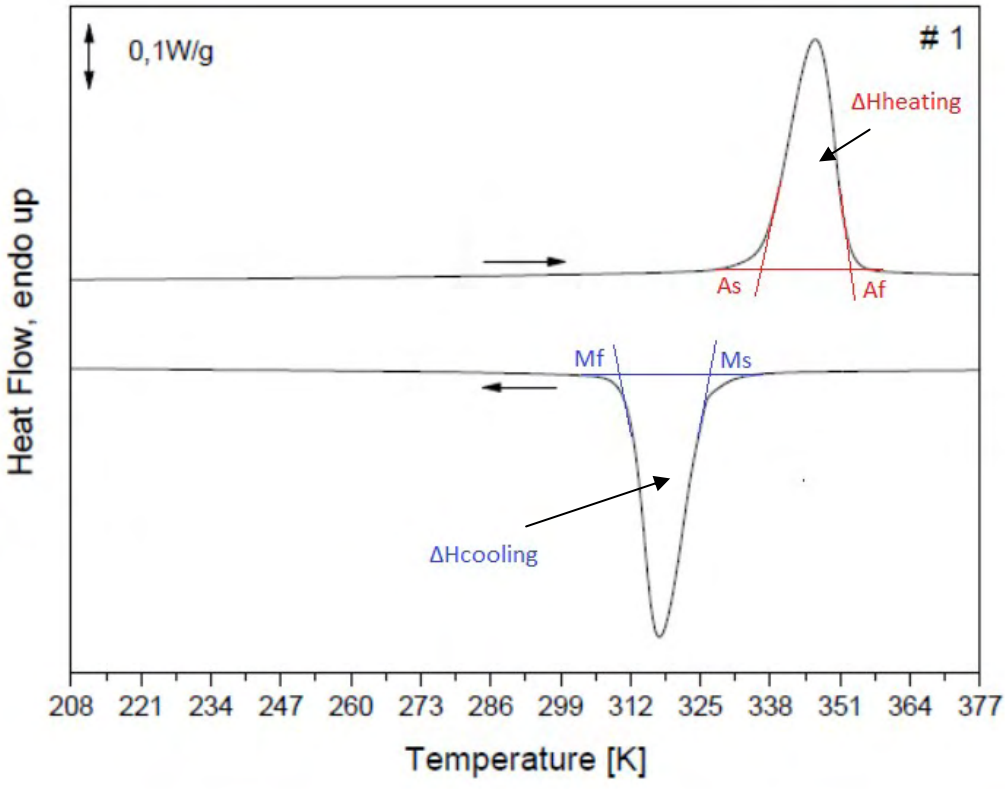

Fig.4.49: Heat flow as a function of temperature during cooling and heating with a rate of 10K/min for the sample #1.

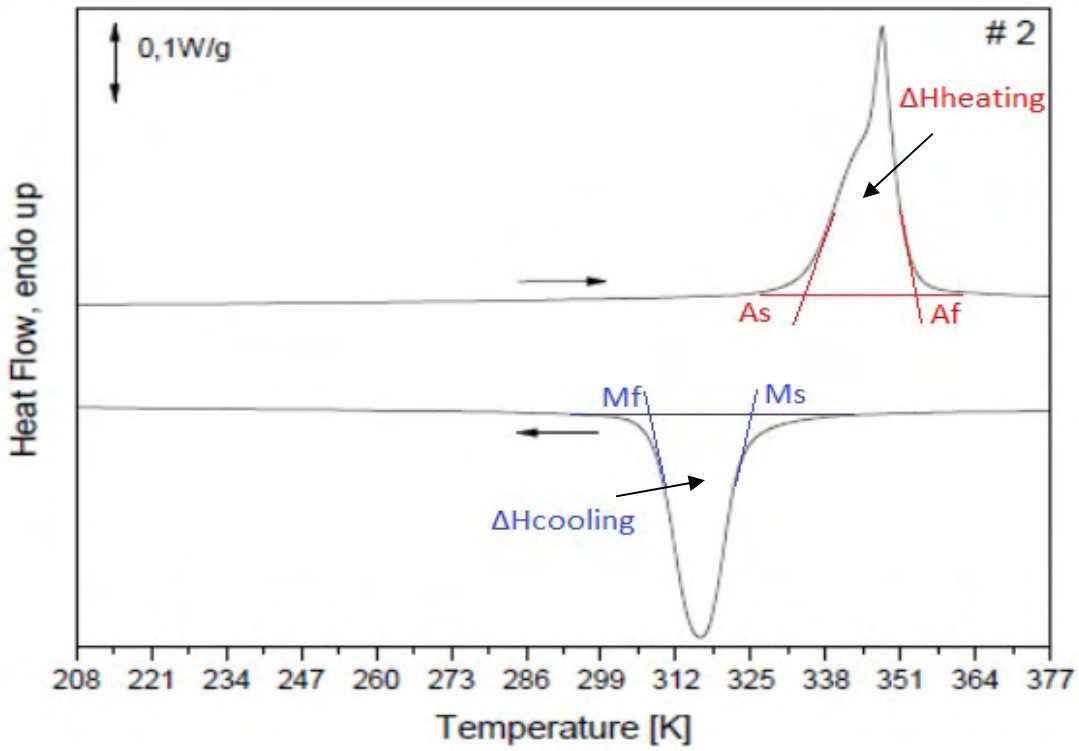

Fig.4.50: Heat flow as a function of temperature during cooling and heating with a rate of 10K/min for the sample #2.

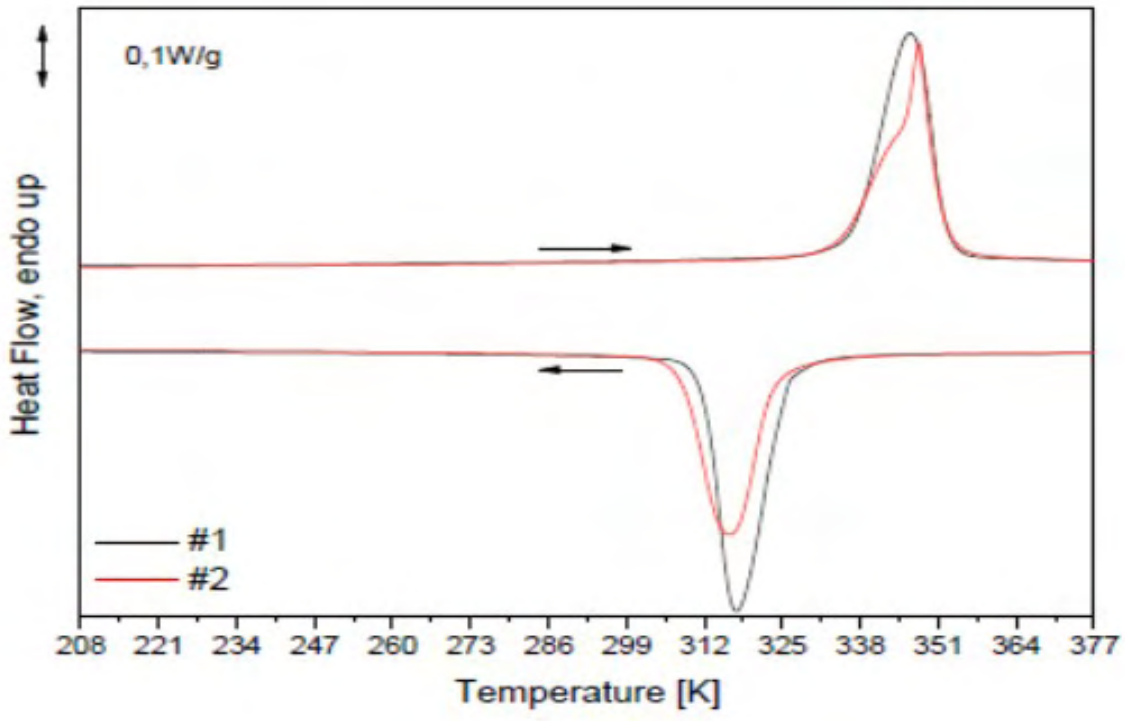

Fig.4.51: Comparative plot of heat flow as a function of temperature during cooling and heating with a rate of 10K/min for both samples.

Table.8: Temperatures and enthalpy of transformation calculated during cooling (Tc, ΔHc) and of melting calculated during heating (T_H, ΔH_H) for samples # 1 and #2

Sample	As(^{o}C)	Af(^{o}C)	Ms(^{o}C)	Mf(^{o}C)	Tc(^{o}C)	ΔHc(J/g)	T_H(^{o}C)	ΔH_H(J/g)
#1	58	84	55	33	44	23.8	73	23.9
#2	58	84	52	27	43	19.5	75	20.0

Chapter 5 Conclusions

The SMA actuator was a NiTiCu alloy contained 49%Ni, 44% Ti, 7%Cu. The main conclusions came out of the experimental work are summarized as follows

- The time of etching (270s) despite the references, was too long resulting in holes around the Cu rich phase of the specimens. This effect is clearly seen both in the metallography as well ass in the SEM images
- In specimen 1 "spring" shape the phases NiTi, τ1 , $NiTi_2$ were identified
- In specimen #2 "wire shape were identified i.e.
    - A rich in Cu area 11-14at% with an average microhardness of 175 $HV_{0.05}$
    - A martenstitic area with 13at% Cu with a microhardness of 304 $HV_{0.05}$
    - An area with low Cu ~6.3at% with an average microhardness of 210 $HV_{0.05}$
    - The pahses identified were the NiTi, β(Ti), $NiTi_2$, Ni_3Ti and probably the τ1.
- The results from the DSC provided the temperatures of transformation and the enthalpies of and are represented in the following table

Sample	A_s(°C)	A_f(°C)	M_s(°C)	M_f(°C)	T_c(°C)	ΔH_c(J/g)	T_H(°C)	ΔH_H(J/g)
#1	58	84	55	33	44	23.8	73	23.9
#2	58	84	52	27	43	19.5	75	20.0

Both specimens exhibit the same A_s and A_f temperatures and differ slightly regarding the M_s and M_f.

- The average results from Vickers microhardness tests with a load of 200g are represented in the following table:

Specimen 1	HV 0.2
Longitudinal	232
Transverse	210
Specimen 2	**HV 0.2**
Longitudinal	230
Transverse	207

These results are similar enough to the results of other researchers [15]

- Selected results concerning the modulus of Elasticity are provided in the following tables for a=0.45. It seems that the results are load dependent, with high scattering. More measurements are required in the future.

Specimen 1	E_2 (a=0.45) GPa		
Load	***50g***	***200g***	***500g***
Longitudinal	33-59	12-31	10-29
Transverse	40-78	45-86	10-44

Specimen 2	E_2 (a=0.45) GPa		
Load	***50g***	***200g***	***500g***
Longitudinal	-	9-23	37-60
Transverse	20-39	20-30	53-64

Chapter 6: Future Work

Based on the experience gained during this thesis the following steps may be proposed as future work in the field:

- Transmission Electron microscopy for studying the microstructure in the nano scale

- XRD for phase identification

- NanoHardness measurements for comparison with the Marshall method

References

[1] Ashwin Rao, A.R Srinivasa, J.N. Reddy. *Design Of Shape Memory Alloy (SMA) Actuators,* Springer.

[2] Dimitris C. Lagoudas, *Shape Memory Alloys Modeling and Engineering Applications,* Springer.

[3] W. J. Buehler, J. V. Gilfrich, R. C. Wiley, *Effects of low-temperature phase changes on the mechanical properties of alloys near composition TiNi*, Journal of Applied Physics 34 (1963) 1475.

[4] C. M. Jackson, H. J. Wagner, R. J. Wasilewski, *55-Nitinol−The alloy with a memory: Its physical metallurgy, properties and applications*, Tech. Rep. NASA SP-5110, NASA Technology Utilization Office, Washington, D.C. (1972).

[5] Weimin Huang *, Shape Memory Alloys and their Application to Actuators for Deployable Structures* , University of Cambridge , Department of Engineering (1998).

[6] Mel Schwatz , *Encyclopedia Of Smart Materials Volume 1 and Volume 2 ,* A Wiley- Interscience Publication , John Wiley & Sons, Inc.

[7] Ming H. Wu & L. McD. Schetky*, INDUSTRIAL APPLICATIONS FOR SHAPE MEMORY ALLOYS*, Proceedings of the International Conference on Shape Memory and Superelastic Technolgies, Pacific Grove, California, P.171-182 (2000).

[8] Peter Malatin – Miroslav Spišák , AIRCRAFT NOISE AND ITS SUPPRESSION , ACTA AVIONICA , Number 28 Volume XV (2013), ISSN 1335-9479, EV 4867/13 , Faculty of Aeronautics Technical University of Košice.

[9] G. Song, N. Ma, H. – N. Li, *Applications of shape memory alloys in civil structures ,* Engineering Structures 28 (2006) 1266–1274.

[10] Scott Wade Robertson, *On the Mechanical Properties and Microstructure of Nitinol for Biomedical Stent Applications,* UNIVERSITY OF CALIFRONIA, BERKELEY Fall 2006 .

[13] D. B. Marshall, Tatsuo Noma, and A. G. Evans, *A Simple Method for Determining Elastic-Modulus-to-Hardness Ratios using Knoop Indentation Measurements,* Department of Materials Science and Mineral Engineering, University of California, Berkeley California 94720.

[14]W.J. Zhu a,b, L.I. Duarte a, C. Leinenbach, Experimental study and thermodynamic assessment of the Cu–Ni–Ti system, CALPHAD · DECEMBER 2014

[15] Antonio Aristófanes da Cruz Gomes et al. , FABRICATION OF SHAPE MEMORY ALLOYS USING THE PLASMA SKULL PUSH-PULL PROCESS , 19th International Congress of Mechanical Engineering November 5-9, 2007, Brasília, DF

Websites

[11] https://www.labtesting.com/services/materials-testing/metallurgical-testing/microhardness-testing/

[12] http://www.gordonengland.co.uk/hardness/microhardness.htm